TECHNICAL REVIEW

2001 NO. 13

MITSUBISHI MOTORS CORPORATION
TOKYO, JAPAN

• Cover Photograph

The cover photograph shows a conceptual image of the Multi-Eye System used in a Mitsubishi ASV-2 (second-stage Advanced Safety Vehicle) passenger car. Employing radio-frequency radar, infrared cameras, charge-coupled-device cameras and other devices, this system monitors the road environment, provides the driver with information in audible and visible forms, and helps the driver take action to avoid hazards.

Driver-support technologies such as the Multi-Eye System have been realized through efforts to give vehicles a degree of artificial intelligence. By dramatically improving safety and comfort, they are likely to play a valuable role in the 21st century.

Published by Editorial Committee for the Technical Review
c/o Environmental & Technical Affairs Department
Car Research & Development Office (Tamachi Branch)
MITSUBISHI MOTORS CORPORATION,
33-8, Shiba 5-chome, Minato-ku, Tokyo 108-8410, Japan
Phone: +81-3-5232-7643
Fax: +81-3-5232-7770

MITSUBISHI

Technical Review 2001

13

Previous page (top)
Jutta Kleinschmidt of Germany drove a Mitsubishi PAJERO and achieved an all-round victory in the 2001 Paris-Dakar Rally, covering the total distance of 10,739 km from Paris to Dakar in 70 hours, 42 minutes, and six seconds. Kleinschmidt is the first woman to win the Paris-Dakar Rally. Her victory is the sixth one achieved by Mitsubishi Motors since the company began its Paris-Dakar participation in 1983. The photograph shows the celebration at the finish.

Previous page (bottom)
In the 2001 Rallye Monte Carlo (the first leg of this year's FIA World Rally Championship), the Mitsubishi LANCER EVOLUTION of Finnish driver Tommi Makinen covered the total distance of 284.42 km in four hours, 38 minutes, and three seconds, earning Makinen his third consecutive Monte Carlo victory. The photograph shows the celebration at the finish.

MITSUBISHI MOTORS TECHNICAL REVIEW 2001 NO. 13

Contents

At This Juncture of the Turn of the Century

Yuhiko KIYOTA
Representative Director

I am filled with a sense of pride to announce the publication of Technical Review NO. 13 in the first year of the 21st century. Approximately 110 years have elapsed since automobiles propelled by gasoline engines first ran on the roads and the 20th century will certainly be recognized in history as one of great advancements in automotive technologies. Although this advancement has brought about affluent society, problems from environmental and safety perspectives still remain. At this juncture of the turn of the century, I would like to express my opinion about what people carrying motor vehicle development forward should consider and do in mind.

First of all, the need for accommodating coexistence with human society, preservation of the global environment and conservation of energy are issues which are growing evermore larger. Since 1960s we, a group of people participating in the development work of the motor vehicles, have been engaging in the solution of many problems related to motor vehicles, such as reduction of exhaust gas emission, improvements in fuel economy, occupant protection, pedestrian protection, preventive safety, recycling technology etc. By exploiting our intelligence and experience as well as combining our mutual efforts in technological research and studies. We must continue our challenge with a firm determination for fulfillment of the needs of society which are being intensified day by day.

Second, the IT society, a generation in which information technology is being avidly and extensively explored, is growing at a speed far exceeding our expectation. Under such circumstances, we must expedite the research and development of new technological fields that will become a mainstream for vehicles in the 21st century like technologies that bilaterally exchange data between vehicle information and information outside the vehicle.

Third, we must endeavor to amalgamate our technologies into a product which will fully satisfy the needs of our customers. Development of new technologies and unceasing evolution of vehicles must be pursued continuously. However, it is also essential to review constantly whether such technologies will bring real benefits to customers and gain their satisfaction and whether a product to be produced by employing such technologies will be worthwhile for sale or not.

Fourth, even though it is in a slow and steady pace, we should carry out fundamental research and development far in advance. Since the resources for research and development are always limited and efforts tend to be more centered on today's and tomorrow's profits rather than the day after tomorrow's ones, it is important not to neglect but advance fundamental research and prior development that foresee the future. Therefore, it is very important not to be lazy about carrying out fundamental research far in advance by retain-

ing a sharp insight into expected future trends and needs. Such action will surely play a major role in retaining and enhancing the latent physical strength of an enterprise and its products.

Fifth, we must continue to keep high spirits in challenging an objective which is set at a highly elevated position. If an objective is set at a position beyond the scope normally resulting from common sense, it may cause the birth of an entirely new concept. A story about the development of the Walkman, the smallest portable tape player in the world, was related in last year's Japan Society of Mechanical Engineering magazine by a person from Sony Corporation, who participated in the project. Explaining their basic philosophy of development, he said "It was our unanimously accepted rule that an objective of a project should be set without giving a serious consideration whether it could be accomplished or not. If a preliminary investigation is carried out for achievability, an objective eventually set up by this method would be obliged to include a safe margin for the elimination of risks. Therefore, we did not discuss the appropriateness of an objective but concentrated our full efforts to find a way to accomplish such an objective".

In development, it is essential to cultivate a custom that no excuse be made for failure but instead full efforts be concentrated to find a way leading to success.

Sixth is the succession of acquired technologies to younger generations. When a development project is carried out by human beings, the possibility of error always exists. However, the technological knowhow acquired in the course of development is of precious value and the knowhow accumulated in such a manner should be surely handed down to younger generations engaged in various development projects so that they will be given an opportunity to develop a method of design and experiment which will be free from flaws.

In conclusion, people participating in the development of motor vehicles must not be afraid of failures but gallantly face the assigned job by harboring an unyielding spirit of challenge deep in their mind. The execution of job without compromise will eventually bring forth the accomplishment of a difficult objective by employing mistakes and failures as a springboard to success. It is my earnest hope that we shall be able to continuously report success stories related to advanced research work in future editions of MITSUBISHI MOTORS TECHNICAL REVIEW.

TECHNICAL PERSPECTIVE

Innovations in Manufacturing Information Technology

Shinichi OKI* Masaru MASUDA**

Abstract

Information technology (IT), which is based on computer and network technologies, has accomplished rapid progress and automotive development has changed extensively through the application of this technology. Four years ago, our company began upgrading of the IT environment – including the sharing of product information – in order that IT may be applied fully and practically to all stages from production through development. As a follow-on to TECHNICAL REVIEW 1999 NO. 11, this paper describes the current condition of the application of IT in the manufacturing process of digital assemblies and the like. Furthermore, it details both how IT has changed manufacturing as we know it and how manufacturing is currently under change.

Key words: *IT, Digital Assembly, Digital Mockup, Digital Factory, Product Geometry Assurance, Robot Simulation, Engineering System, Bill of Process, Virtual Factory*

1. Introduction

In an effort to offer products that meet the market's needs at competitive prices and in a timely manner, automobile manufacturers have rapidly expanded their use of IT in the development of new models. The specific benefits of IT include the ability to share information with all relevant companies and individuals on a global scale irrespective of time and distance (thus enabling various studies to be conducted simultaneously) and the ability to complete all necessary studies of objects – even those that do not yet physically exist – in a virtual-reality environment (thus eliminating the need for reworking and other forms of trial and error when production begins). These benefits translate into increased efficiency and consistency in new-model development.

With a view to creating a global development and production environment appropriate for its 21st-century needs, MMC established in April 1996 a body known as the New Engineering Systems Office. This body has worked on the development of a so-called New Engineering System – a collection of technologies that centralize computer-aided-design (CAD) functions, parts lists, and other data – and has begun establishing a digital infrastructure. Computer technologies used in key areas of automobile development are shown in **Fig. 1**.

Studies related to product design and production engineering are major factors determining the efficiency of automobile development and production, so the application of IT to these areas has a significant effect on the overall efficiency with which new models are created. As a follow-up to the Technical Perspective paper in Mitsubishi Motors TECHNICAL REVIEW NO. 11 (1999), this paper describes how IT is currently used in these and other areas of manufacturing, and it outlines likely future developments.

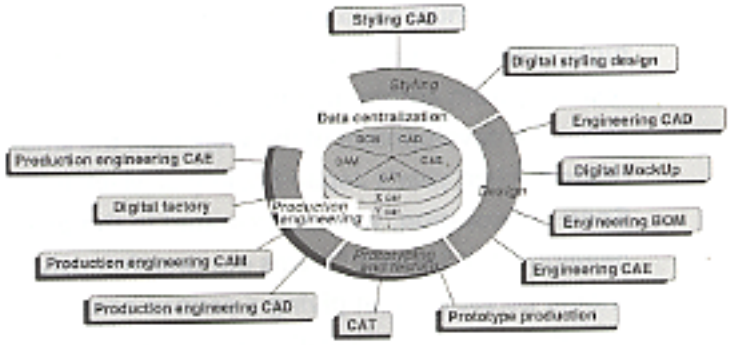

Fig. 1 Engineering systems used in automobile development

2. Use of IT in automobile development

The use of IT in automobile development allows the creation of a flow within the corporate group of information on proprietary technologies amassed in the CAD, CAE, CAT, CAM, BOM, and infrastructure fields. Sharing of this flow of information by factories, suppliers, and all other relevant domestic and overseas parties revolutionizes all automobile development processes from planning to production.

Information on the shapes, mounting structures, and all other shape-related aspects of products and parts are digitized as surface- and solid-model CAD data, allowing automobiles to be assembled in a virtual-reality environment as digital mockup (DMU). Releasing necessary parts of the data to relevant departments of the corporation and to relevant outside companies (including those overseas) allows personnel to simultaneously subject a single, common set of data to engineering and production studies using CAD, CAE,

* Engineering Information Technology Dept., Car Production Headquarters

** Car Production Headquarters, Nagoya Plant

and other systems before the objects being studied physically exist. Before this arrangement was established, it was often impossible to detect structural problems in an automobile without physically building a prototype. Now, however, any structural problems can be detected at an early stage of the development program, allowing the structure study meeting to promptly agree on design change and reflect the revisions in drawings. A further benefit is that engineering work necessary to reflect design revisions after the start of production preparations can be minimized. Thus, production preparations can be made quickly and efficiently and in a manner that ensures high product quality. Examples of DMUs are shown in **Fig. 2**, and the benefits in terms of improved quality and shorter development periods are illustrated in **Fig. 3**.

Fig. 2 Passenger-car DMUs

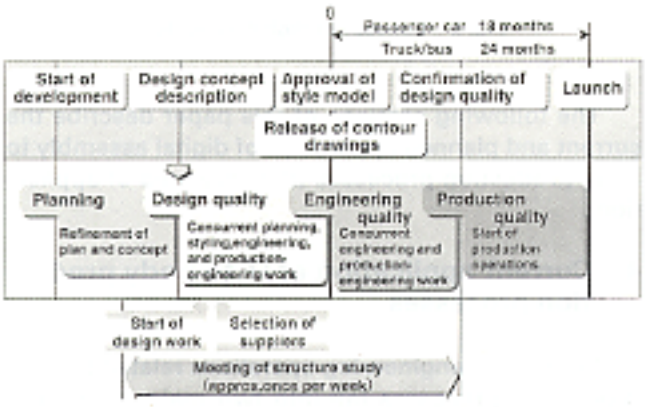

Fig. 3 Improved quality and shorter development periods

Drawings, engineering order (EO), and other engineering information issued separately by engineering departments have been replaced with digital parts data, whose format consists of three-dimensional geometric-shape data; shape-supplemental data (for example, dimensional tolerances and accuracies) that cannot be expressed as geometry data; and part-characteristics data such as names, materials, masses, and configurations. With this arrangement, approval for EO is given using electronic signatures rather than handwritten ones and approved EO are sent to relevant parties by electronic mail in the form of computer data. In line with this new approach to the handling of drawings, the original mainframe-based BOM system (known as the Engineering Information and Control System (ENICS)) was replaced with a server/client system that allows shape data and BOM data to be controlled and provided in conjunction with each other. The new approach to the handling of drawings and EOs is illustrated in **Fig. 4**.

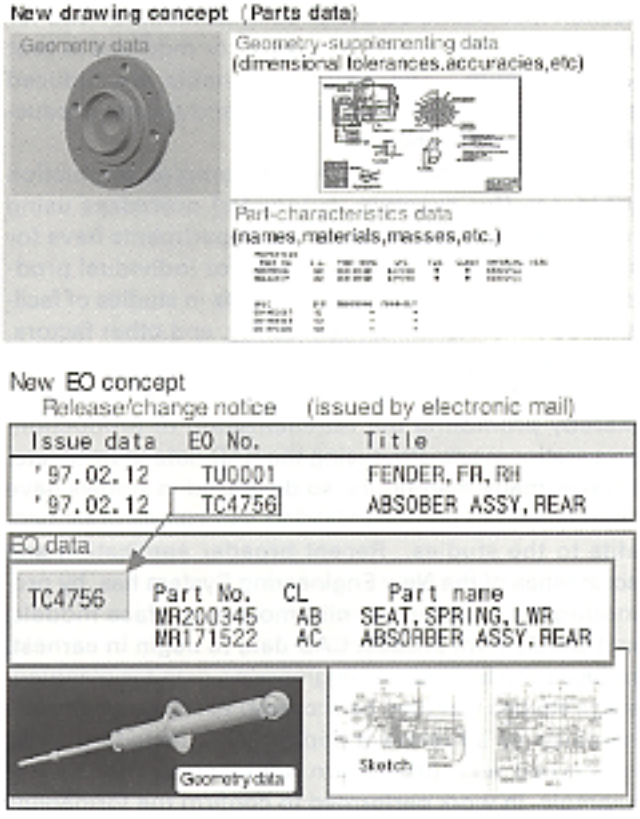

Fig. 4 New concept for component drawing (parts data) and related EO

Before digital processes were adopted, it took four to five days to distribute drawings and EOs domestically and up to 21 days to distribute them internationally. It now takes only one day to distribute them domestically and internationally. The digital processes thus enable shorter development periods and contribute to globalization.

3. Use of IT in production processes

The use of IT in production processes is focused on digital assembly, a procedure that brings together DMUs and digital factories and allows all processes from development to production to be represented and checked in the form of digital information. With digital assembly, all aspects of the creation of prototype and production vehicles can be shown on a computer screen, allowing all necessary studies to be completed before any object is physically produced.

Previously, it was necessary to conduct studies (mainly on paper) at an early stage of the development program. Since digitization has allowed objects to be displayed on computer screens in a form almost identical to the form they would take if produced physically, however, it is now possible for anyone to visualize and understand complex shapes quickly and easily. As a result, information on product structures that facilitate easy production and high quality can be fed back into the product-engineering process before objects are physically produced. This information also allows production facilities to be designed such that the need for equipment to be newly introduced or modified is kept to a minimum. The resulting benefits are reduced investment on production facilities and shorter production-preparation schedules.

For verification of important, complex production processes (for example, automated processes using robots), production-engineering departments have for several years produced CAD data for individual products and facilities and used these data in studies of facilities' common usability, operability, and other factors. Production-engineering departments also employ these data directly in robot teaching and other activities, thereby promoting the rationalization of production-preparation work. Producing the CAD data unfortunately takes many man-hours, so data used in studies have been limited to portions yielding particularly great benefits to the studies. Recent broader application and acceptance of the New Engineering System has, by promoting the creation of solid models, surface models, and DMUs from product CAD data to begin in earnest, reduced the limitations; engineering data for planning-stage studies can now be accessed easily as a common resource by all relevant departments including those concerned with production engineering. By way of example, in work performed to confirm the formability of pressed parts the use of a CAE system capable of performing analyses directly from product CAD data has enabled product shapes with superior formability to be proposed to engineering personnel (Fig. 5).

Improvements in the usability of CAD data thus allow the studies based on digital data to be improved in terms of both quality and quantity, resulting in a stronger base on which to promote digital assembly.

Practical adoption of digital assembly requires three groups of information. One group is information on the planned product. The second group is information on the resources (equipment and personnel) required for production. The third group is information on work procedures, movement paths, restrictions, and other aspects of the production process. (The third category serves to link the first two categories.) All three categories of information must be produced and appropriately linked before adequate studies are possible, so MMC intends to produce them in a planned manner so that they can be used in various studies. Fig. 6 illustrates the concept of digital assembly by showing the relationships between the three categories of information and their contents.

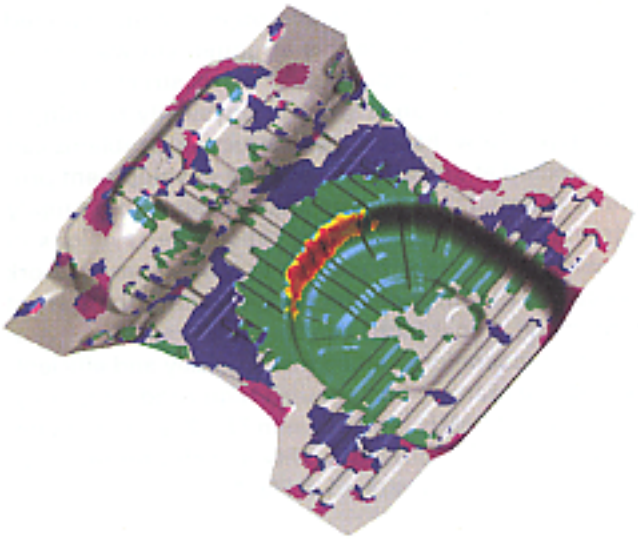

Fig. 5 Press-forming simulation using CAE technology

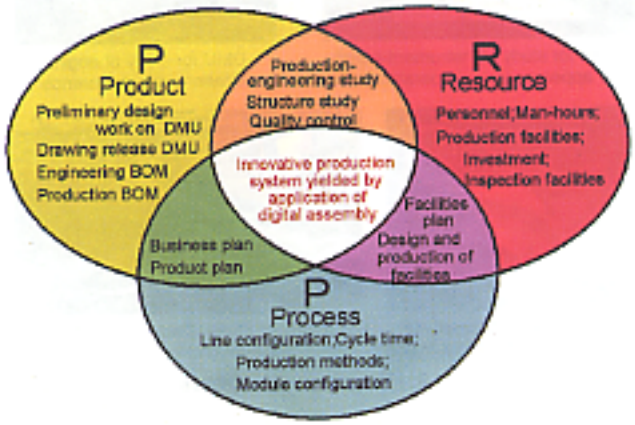

Fig. 6 Concept of digital assembly

The following sections of this paper describe the current and planned application of digital assembly to body production processes (the core area of application).

4. Current application of IT to body production processes

Production-engineering operations related to body production processes fall into two main categories: (1) studies of production-engineering structures; and

(2) production-preparation operations. In the former category, IT is currently used mainly in productivity studies, production-method studies, and production-method planning. In the latter category, IT is currently used mainly in the engineering of facilities and jigs and in the teaching of robots. Details are given in the following sections of this paper.

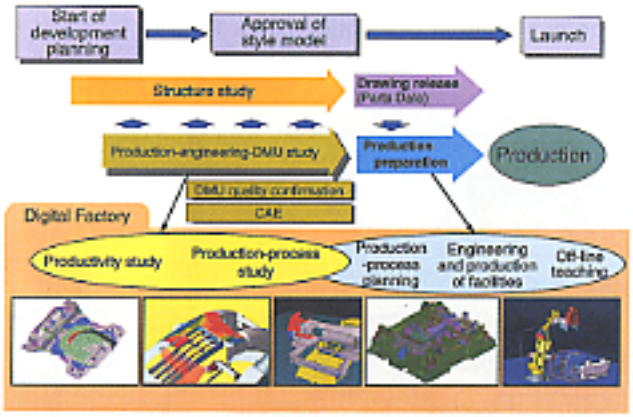

Fig. 7 Production engineering: job flow and IT application

4.1 Studies of production-engineering structures

(1) Three-dimensional models of factory facilities

At the initial stage of body development, various production-related factors (these include limitations on the size and other aspects of vehicles that can be produced on existing lines; automated processes; and work sequences) are checked and, in accordance with the findings, proposals (including those for the elimination of items that cannot be produced) are made for body structures that allow expenditure to be minimized. The first items necessary for this work are models of facilities that represent restrictions upon production (for example, conveyors, body supports, trim-assembling tools, and automated equipment).

These facilities models are controlled by a shared server such that they can be used also by engineering departments, and details of data (for example, models and utilized parts) are posted on an intranet such that they can be used as a common resource for engineering and production-engineering purposes. Important data needed by engineers who use this resource include those showing what tools should be used in what locations and those showing whether required ranges of movement are satisfied. However, the range of available data does not currently include all necessary items. Measures to make the range of data more comprehensive are required.

(2) Studies of line passableness

Each of MMC's production lines is used to produce multiple vehicle models. The introduction of any new model is therefore predicated upon the use of facilities that are used to produce existing models. Further, any greater-than-planned variation in production volume makes it necessary to consider revisions to the allocation of particular models to particular factories. For these reasons, the basic dimensions (length, width, and height), body locating holes, and side-sill shape of any new model's body must permit the use of handling equipment that is used for existing bodies. Any need for significant modification of body-handling equipment to accommodate a new model would not only increase expenditure; it would also have a likely impact on models currently being produced. To ensure that new models can be produced using existing facilities, it is essential to perform adequate studies at an early stage and to reflect the findings in the new model's body design such that the unwanted effects of the new model's introduction are minimized. To this end, effective use is made of three-dimensional models to maximize accuracy in studies A facilities model for a study of line passableness is shown in Fig. 8.

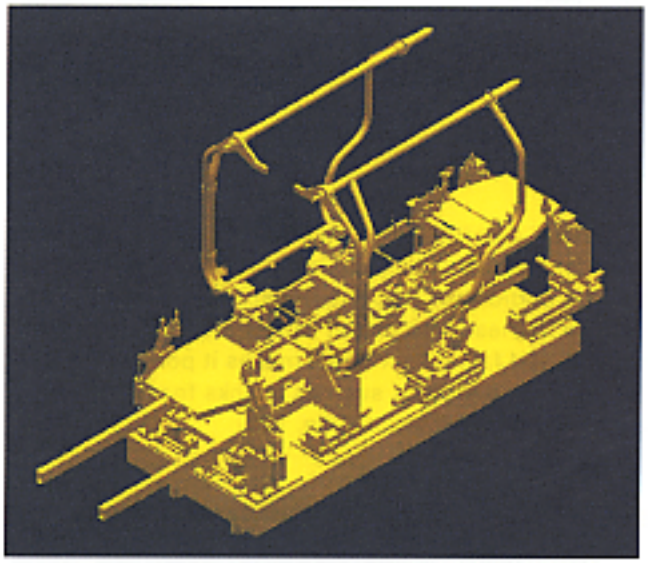

Fig. 8 Facilities model for study of line passableness

(3) Production-method studies

Before the introduction of digital assembly, a study of production methods for a new vehicle model could not be performed until a prototype vehicle had been produced. The study was performed using actual tools and cardboard or wooden models of welding guns, and any problems identified were fed back into the product-engineering process. Unfortunately, the product-engineering process was already well advanced by this time. To overcome these problems, MMC created a system that allows product CAD data to be freely incorporated into DMU data for use in production-engineering studies from the beginning of any engineering-study process. With this system, any specified body part or all of the parts in a specified body area can be called up on a CAD-system screen and combined with data on equipment and tools to allow early studies of a kind that were previously performed using a physical vehicle. Revisions to die designs are extremely difficult to implement after the beginning of die production. By contrast, revisions implemented at an earlier stage represent a

lighter burden; modifications to dies and jigs are less significant, the financial cost is lower, and less time is required. **Fig. 9** shows the tree structure that permits engineering models and facilities models to be combined in DMUs.

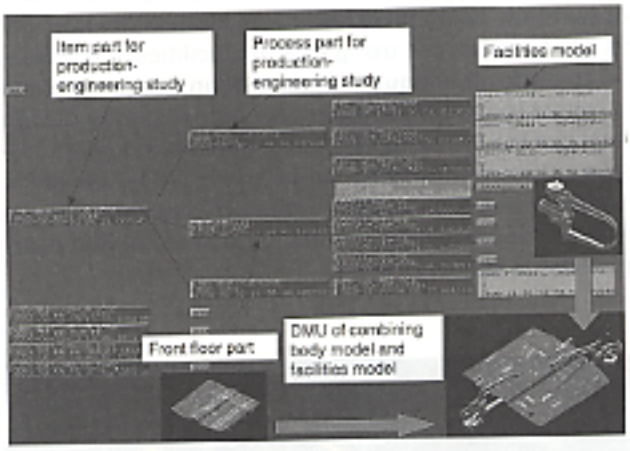

Fig. 9 Shared DMU tree structure

In trim-assembling processes, automatic equipment used for tasks such as installation of heavy items inside vehicle bodies can impose physical conditions on the vehicle bodies. The use of DMUs that combine body models and facilities models makes it possible to perform detailed studies such as checks for interference along paths of movement (**Fig. 10**).

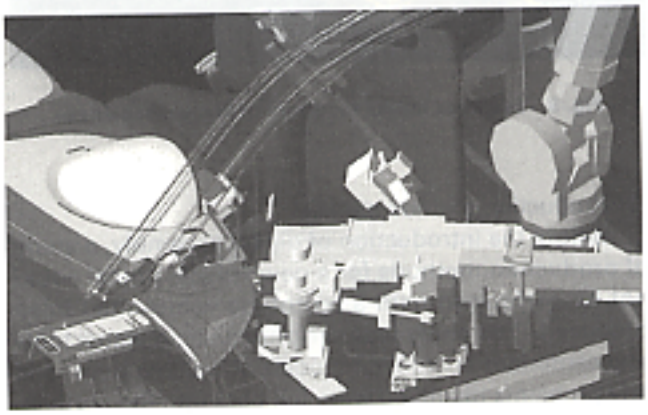

Fig. 10 Seat-installation simulation

In electrodeposition processes performed to make vehicle bodies rust-resistant, it was formerly impossible to determine final coating thicknesses without using an actual body. Now, however, it is possible to perform CAE analyses based on body CAD data, so electrodeposition improvements yielded by revisions to hole shapes can be reflected in product designs at an early stage.

Since three-dimensional models allow bodies to be visualized easily, they allow appearances to be verified and thus allow early proposals for design improvements. For example, it is possible to implement a proposal to conceal a ridge by creating a slight difference in height between mating parts, thus eliminating the need for precise alignment.

To permit production-engineering, quality-control, and assembly personnel to meet and hold discussions, MMC has established digital assembly rooms, each equipped with an engineering workstation and a projector, in a number of locations (**Fig. 11**).

Fig. 11 Digital assembly room

(4) DMU quality confirmation meetings

Structure studies are performed separately for a vehicle body's various areas. To prevent problems (for example, incorrectly located holes for installation of parts; insufficient space for installation of harnesses; and obstructions that prevent parts from being installed) when a prototype is subsequently built, the structure studies must be properly coordinated such that no important factors are overlooked. Before any physical construction begins, therefore, assembly is performed digitally in the sequence of the actual production processes to enable confirmation of the DMUs' quality.

4.2 Rationalization of production preparations

(1) Production-method planning

On a production line, which consists of many processes, the time available for each process is limited by the production volume, making it necessary to plan the amount of work to match the production volume. If any operation takes longer than the fixed, permitted length of time, the process becomes a bottleneck, preventing the line from operating at its full production capacity. To prevent this problem, it is necessary to revise the distribution of operations and verify the benefits of speeding up the equipment. The length of time required for each operation in each process is verified using simulation tools. For processes employing robots, simulations are performed to establish ranges of robot movement, making it easy to check whether robot-mounted tools can reach necessary positions. Production-method plans can thus be produced with a

high degree of accuracy. A welding-robot simulation is shown in **Fig. 12**.

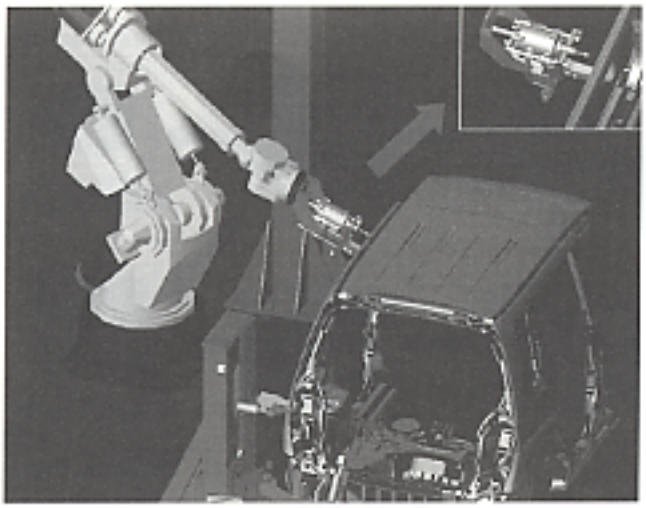

Fig. 12 Welding-robot simulation

(2) Facilities and jig design

Three-dimensional visualization has been adopted also in the design of facilities and jigs to be used for production (**Fig. 13**).

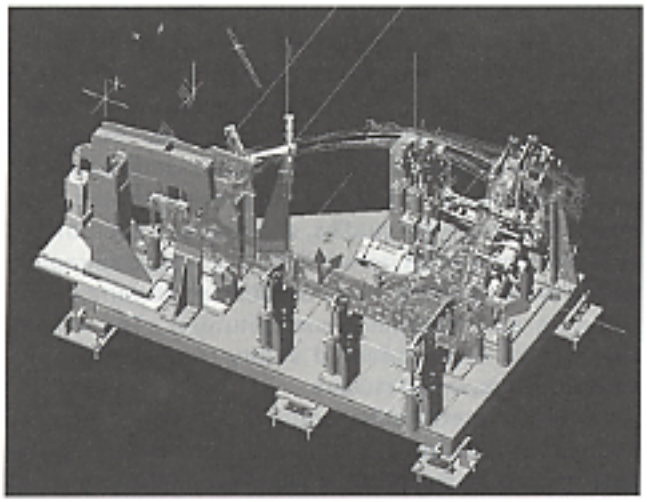

Fig. 13 Welding-jig design

Three-dimensional jig design is attractive in several respects: As with vehicle-body design, it allows adequate checking for interference before objects are physically produced. It affords ease of visualization that allows engineers to notice important factors that they might miss with two-dimensional drawings. It allows personnel to gather in digital-assembly rooms and conduct thorough design reviews. And it allows parametric functions to be used to produce standardized parts and templates, thus shortening the time required to produce models. Nevertheless, construction of facilities and jigs designed using this technology still depends upon two-dimensional drawings, necessitating time-consuming conversion of three-dimensional images to two-dimensional drawings. A solution to this problem must be found.

(3) Robot teaching

With an automated process employing robots, it is necessary to teach the robots about the relevant vehicle body. Previously, the teaching was performed on weekends and public holidays using an actual body. Now, however, simulations performed for verification of robot movement during the planning of production methods serve as a source of teaching data that can be supplied directly to the robots. Teaching can thus be completed before physical production begins. The configuration of a teaching system is shown in **Fig. 14**.

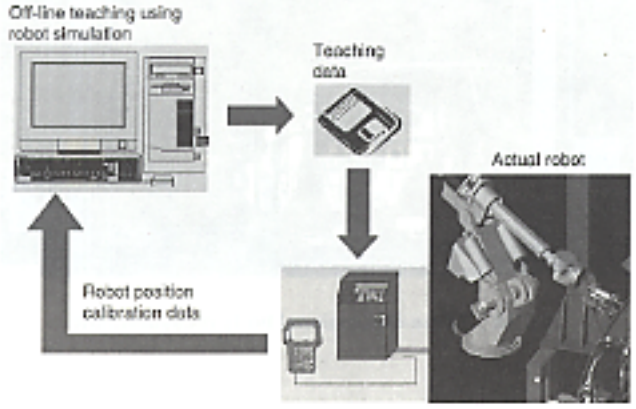

Fig. 14 Off-line robot teaching using simulation

This type of teaching is particularly beneficial with paint robots: A paint robot must be taught such that the spray gun remains at a specified distance from the vehicle body at all times, and a process of trial and error was formerly necessary to achieve the correct paint-film thickness. Now, however, paint-film simulations (**Fig 15**) can be performed, allowing the thickness to be checked graphically. Since any areas of excessively thick or thin paint can be identified easily, it is possible to produce teaching data that prevent paint-film inconsistency.

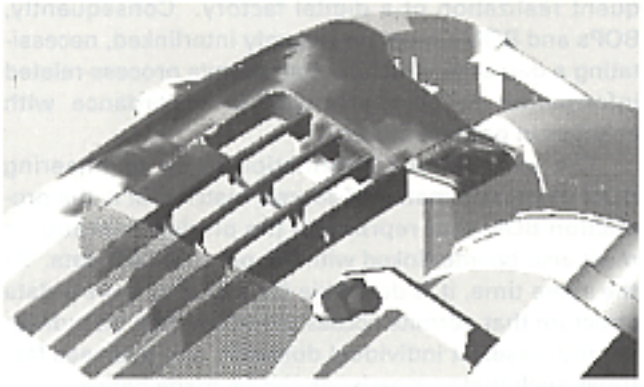

Fig. 15 Paint-film simulation

(4) Inspection

Three-dimensional measuring systems are used to measure discrepancies between the designed and actual dimensions of bodies on production lines (**Fig. 16**). Before the systems can start taking measurements, they must be taught the positions of holes, sections, and other items. This work was formerly performed by hand and involved significant time and effort. Now, however, teaching can be performed with a simulator using DMU data, thereby reducing the time and effort necessary for teaching on the shop floor.

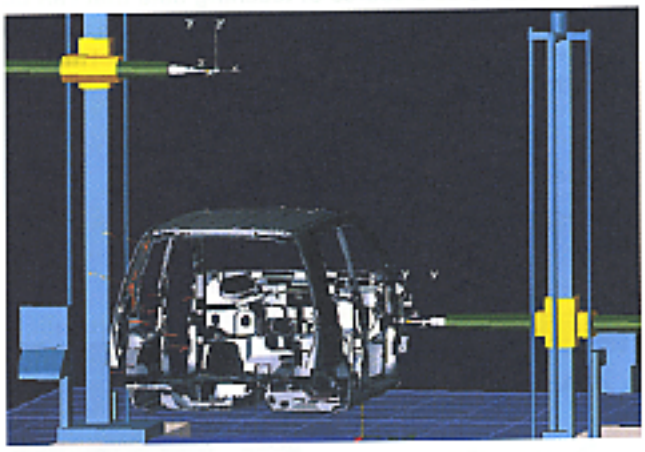

Fig. 16 Three-dimensional body measurement

5. Future developments

5.1 Construction of bill of process (BOP)

Just as a BOM is a database containing information on the makeup of a product, a BOP is a database containing detailed information on the makeup of processes. With today's mixed-flow production lines, it is essential to control data on a model-by-model basis. Similarly, it is essential to employ information on production processes' resources (for example, personnel, man-hours, production facilities, and investment) and information on actual processes (for example, line configurations, cycle times, and production methods) on a product-by-product basis. The ability to access resource- and process-related information in accordance with changes in products is the key to subsequent realization of a digital factory. Consequently, BOPs and BOMs must be strongly interlinked, necessitating a database structure that permits process-related information to be rearranged in accordance with changes in product makeup.

The parts-related information in an engineering BOM must, as a matter of course, match that in the production BOM that represents the product makeup. It must also be interlinked with the product CAD data. At the same time, it is desirable for a BOP to have a data structure that permits access to information on individual processes at individual domestic and overseas factories such that comparisons can be made between factories. The information in the BOP must also be interlinked with CAD models of facilities and personnel.

Fig. 17 shows the relationship between other databases and the BOP that MMC plans to develop.

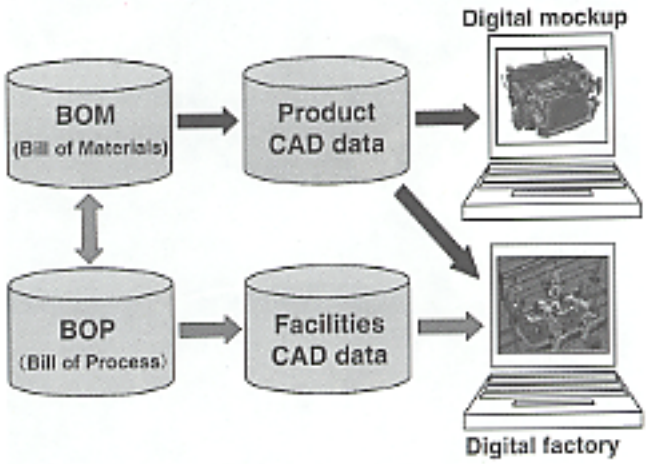

Fig. 17 BOP concept

5.2 Seamless use of process-study information

Once an environment in which BOMs, BOPs, product CAD data, facilities CAD data, and production-engineering simulations can be accessed in a linked manner is established, all processes can be reproduced using a CAD system, allowing a single body of data to be used for production-engineering studies, for the production of off-line teaching data, and for other production-preparation operations. Constructing an environment that permits seamless use of the single body of data in various areas permits a dramatic increase in the efficiency of production-engineering studies. Further, it permits the construction of a database that gives instant access to product-, resource-, and process-related information necessary for studies, allowing any department, via a company-wide network, to begin studies rapidly and to draw upon the study capabilities of parts manufacturers and facilities manufacturers. The overall result is an unprecedented ability to perform multifaceted and repeated studies.

A further predictable benefit is a dramatic increase in the speed and quality of production-related studies necessitated by design changes of product and process additions during production. The range of instantly available information will rapidly expand to include factors such as the extent of the influences of design changes of product, the extent of necessary modifications to facilities, and the extent of changes in production costs.

5.3 Ergonomic studies

Technologies on which MMC plans to focus with a view to making process studies more comprehensive include those for the simulation of human movements. This type of simulation will allow verification of the ease with which planned operations can be performed and of the physical burden imposed on workers. Although it will be necessary to program computers with infor-

mation on movements and working postures in processes to be studied, improved simulation technologies for prevention of interference, optimization of lines of movement, and other purposes will likely reduce the amount of work involved in defining movements. With the results of simulations applied to all processes, it will be possible to completely prevent ergonomic problems when production of new vehicle models begins and to eliminate superfluous movement within processes. Also, it will be possible to use the simulations in studies related to optimization of process configurations. As a further benefit, it will be possible to convert finished process data into animated instructions that can be transmitted in real time to workers on the shop floor or used as training videos.

5.4 Maximizing quality within processes

Small shape differences between digital information and the actual objects that they represent are inevitable. In theory, such discrepancies in CAD data are not significant enough to represent a problem. In actual production, however, errors in the shapes and installation of individual parts can translate into cumulative errors that are significant enough to hinder assembly. It is necessary to consider an approach to quality assurance whereby measurement of accuracy in finished vehicles is superseded by measurement of accuracy on a subassembly-by-subassembly basis in each process. Preassembly prediction of errors in subassemblies based on aggregates of individual tolerances can be translated into improvements in assembly structures and production methods. To make related work easy to understand and perform, MMC intends to switch from its current drawing-based study process to a computerized, graphics-based arrangement. MMC further intends to combine this arrangement with accumulated data from three-dimensional measurement of body frames and from non-contact three-dimensional measurement of individual parts with a view to enabling data-based product geometry assurance (**Fig. 18**).

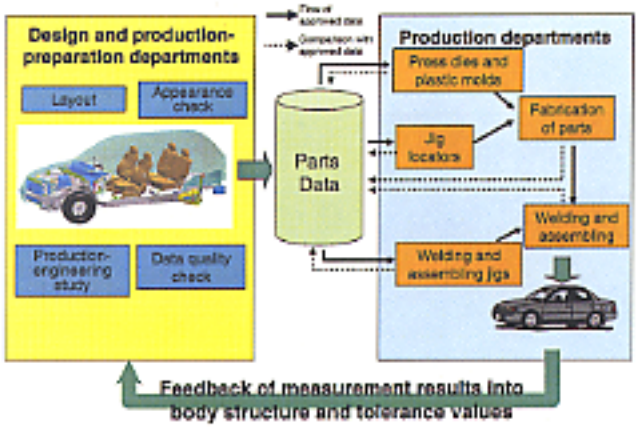

Fig. 18 Concept of product geometry assurance

5.5 Process simulation

It is necessary not only to study individual welding and assembling processes, painting processes, and final-assembling processes using related shape information (in the form of product CAD data and facilities CAD data) but also to verify production-method conditions affecting the productivity and quality yielded by the processes. (This work necessitates interlinking of information on part installation sequences, production methods, standard work durations, robot teaching, and other items in the processes.) The first step toward enabling relevant studies is to establish a system that allows required data to be taken from BOMs and BOPs for detailed studies of individual processes. The next step is to establish definitions for the entire line's process configuration, distribution, and process synchronization and to perform line-balance studies and distribution simulations (**Fig. 19**) with a view to optimizing the factory's overall productivity.

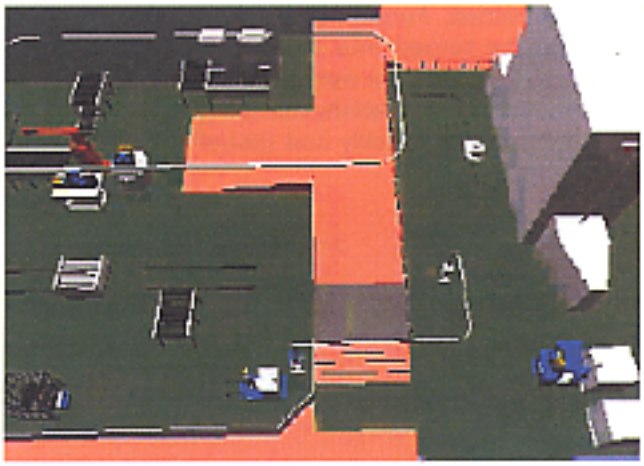

Fig. 19 Distribution simulations

It is likely that Japanese automobile manufacturers including MMC will perform much of the planning and fabrication of their line facilities in-house, maximizing accuracy in their plans by actively employing process simulations. An example of a virtual factory (a three-dimensional model of a factory layout) is shown in **Fig. 20**.

Fig. 20 Virtual factory (bumper production line in Okazaki plant)

6. Summary

An automobile manufacturer with digital-factory capability benefits in terms of ability to accommodate the production of new models and in terms of ability to implement subsequent running changes. And since it possesses all necessary production-related information, the manufacturer is able to perform investment studies and cost comparisons accurately and quickly when it begins planning the development of subsequent new models and evaluating their commercial viability. Scope for application of digital-factory technologies is not limited to projects involving the construction of new factories; it also encompasses reallocation of models among factories, expansion of production from domestic to overseas factories, and all other activities that today's automobile manufacturers must accommodate in their business plans. Concomitantly great benefits can be expected. Further, production-process simulations can be turned into videos and other training resources for shop-floor workers and service personnel. The benefits of IT (especially the ability to transmit digitized information quickly and globally) have created unprecedented opportunities for automobile manufacturers to improve efficiency in all of their production-related activities.

With a view to enabling all parts and processes to be checked digitally in a systematic manner before objects are physically produced, MMC is moving forward with the construction of systems that provide clear visual representations of factories and allow computerized data to be employed in a wide range of activities. As a result, MMC's factories will continue to evolve toward their ideal future form.


Shinichi OKI


Masaru MASUDA

Development of New Technologies for Exhaust-Emission Control Catalysts and Advanced Catalytic-Reaction Controls for Gasoline Direct-Injection Engines

Keisuke TASHIRO* Kazuo KOGA* Kinichi IWACHIDO*
Yasuki TAMURA* Hiroyuki NAKAJIMA*

Abstract

An optimum combination of catalyst and an advanced catalytic-reaction control method has been realized by the design – based on the principle of catalytic reaction – of a NOx absorber catalyst system for a gasoline direct-injection engine. Through this achievement, Mitsubishi now provides a gasoline direct-injection engine with exhaust-emission control technologies which will meet the exhaust-emission regulations scheduled in 2005 and the following years in Japan and Europe.

A new concept of potassium-capture which improves thermal stability of potassium is incorporated in washcoat design to enhance NOx adsorbability at high temperature. Furthermore, a new TWC with a dual-layer coat has been developed based on the effective utilization of platinum (Pt), and this will enhance HC reduction efficiency in lean burn operations. The new catalytic-reaction control technologies that have been developed include the following: a stratified slight-lean-burn control process which accelerates earlier catalyst activation; enhancement of NOx-reduction efficiency using NOx purge pulse injection; oxygen storage control for provision of an optimum catalyzing condition through the detection of variations in the output of an oxygen sensor; and assisted temperature-rise control process that accelerates sulfur desorption with minimized deterioration of fuel consumption. Full and thorough application of catalytic performance has been made possible as a result of these new developments.

Key words: *Catalyst, Emission, Gasoline Direct-Injection Engine*

1. Introduction

Development of lean-NOx catalysts (catalysts that reduce emissions of nitrogen oxides during lean operation) is essential for wider adoption of gasoline direct-injection (GDI) engines. Mitsubishi Motors Corporation (MMC) has pursued relevant developments on two fronts: For Europe, where gasoline with a relatively high sulfur (S) content is used, MMC has based its efforts on selective reduction type lean-NOx catalysts, which are highly resistant to sulfur poisoning. And for Japan, where gasoline with a relatively low sulfur content is used, MMC has based its efforts on NOx-trap catalysts, which offer relatively high NOx-reduction efficiency.

In Europe, a decision was made to steadily reduce the sulfur content of gasoline from 2000, paving the way toward an environment more conducive to the use of NOx-trap catalysts.

However, conventional NOx-trap catalysts are problematic in terms of limited reduction efficiency during high-temperature operation and heat resistance. They are thus unsuitable for use in Europe, where high-speed driving is frequent and catalysts become consequently hot. These factors have delayed the adoption of direct gasoline injection engines by European automobile manufacturers.

To address the above mentioned problems, MMC recently developed a group of technologies centered on a new high-temperature lean-NOx catalyst that offers superior reduction efficiency at high temperatures, superior resistance to heat, and superior resistance to sulfur poisoning. MMC's new catalyst system is shown in Fig. 1.

2. High-temperature NOx-trap catalyst

2.1 Obstacles to improvement of NOx adsorption at high temperatures

NOx adsorption takes place under lean-burn conditions. The process is believed to entail a reaction in which nitrogen monoxide (NO) in the exhaust gases is converted into nitrogen dioxide (NO_2) by a precious metal, after which the NO_2 is trapped by an adsorbent in the form of a nitrate. Materials that can be used as adsorbents include the alkali metals and alkaline-earth

* Power Train Research Dept., Car Research & Dev. Office

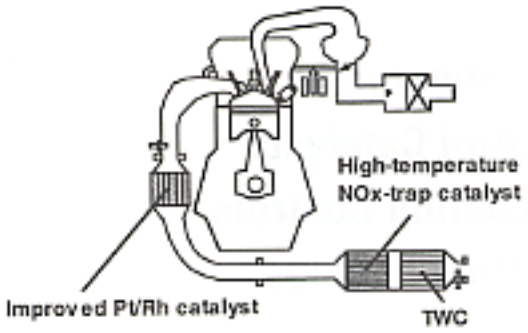

Fig. 1 Catalyst system

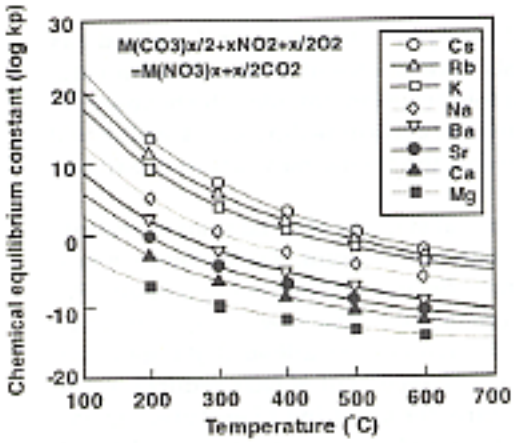

Fig. 2 Chemical equilibrium constant for NOx adsorption reaction

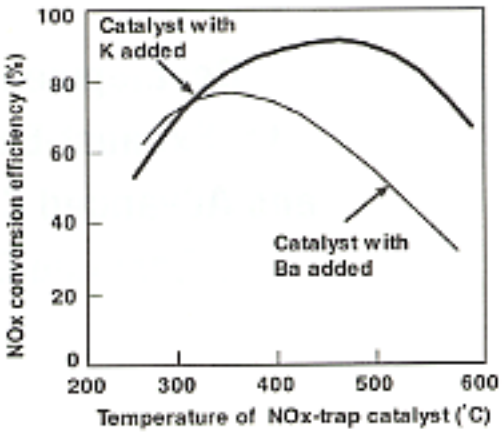

Fig. 3 Characteristics of NOx-trap catalyst

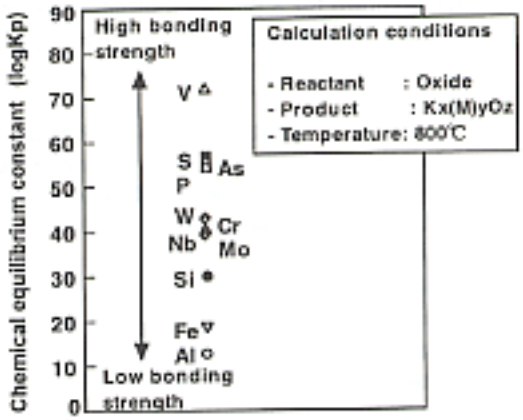

Fig. 4 Generation reaction of K compound

metals whose respective chemical equilibrium constants for the aforementioned reaction are shown in **Fig. 2**. The results of experiments in which a precious metal was actually used as a catalyst showed that potassium (K) and barium (Ba) offered superior performance as adsorbents and that the performance of K was, as shown in **Fig. 3**, better than that of Ba at high temperatures. However, Ba has thus far been used as the main adsorbent in NOx-trap catalysts because K is problematic in the following respects:

(1) Penetration of K into the substrate

K adsorbent carried in the washcoat penetrates in the substrate and tends to combine with cordierite in the substrate, thus (a) detracting from NOx-adsorbing performance and (b) weakening the substrate by making its coefficient of thermal expansion inconsistent.

(2) Outpouring of K

As the catalyst's temperature increases, the K adsorbent carried in the washcoat is increasingly outpoured, leading to a reduction in NOx-adsorbing performance.

2.2 Minimizing the penetration and outpouring of K

To utilize the high-temperature characteristics of K, it is necessary to minimize movement of the K such that the K exists in the catalyst layer in an optimally stable condition. In this regard, K's basicity was focused on and retaining the K using an acidic material was considered. The results of a study conducted by means of chemical-equilibrium calculations are shown in **Fig. 4**.

These results showed that excessively strong affinity detracted from K's reactivity and that, conversely, excessively weak affinity detracted from K's retaining power. Therefore a silicon (Si)-based material was selected, which had optimum affinity with K plus a high melting point. Added to the washcoat was a zeolite whose affinity was slightly suppressed. Also, the substrate's surface was coated with a Si oxide whose bonding strength was greater than that of the zeolite. As shown by the post-aging K-concentration distributions shown in **Fig. 5**, these two new technologies minimized penetration of the carrier by K and outpouring of K, thus improving NOx-adsorbing performance and solving the substrate-strength problem.

2.3 Effects of high-temperature NOx-trap catalyst

(1) Improvement of high-temperature NOx-reduction performance

As shown in **Fig. 6**, the addition of the Si-based material enabled high NOx-reduction performance up to a catalyst temperature of 550 °C, making it possible to expand the range of lean operation. And as shown in **Fig. 7**, heat resistance also benefited, making it possible to significantly improve high-speed fuel economy in Europe.

(2) Prevention of sulfur poisoning

Sulfur in the fuel becomes SO_2 as a result of com-

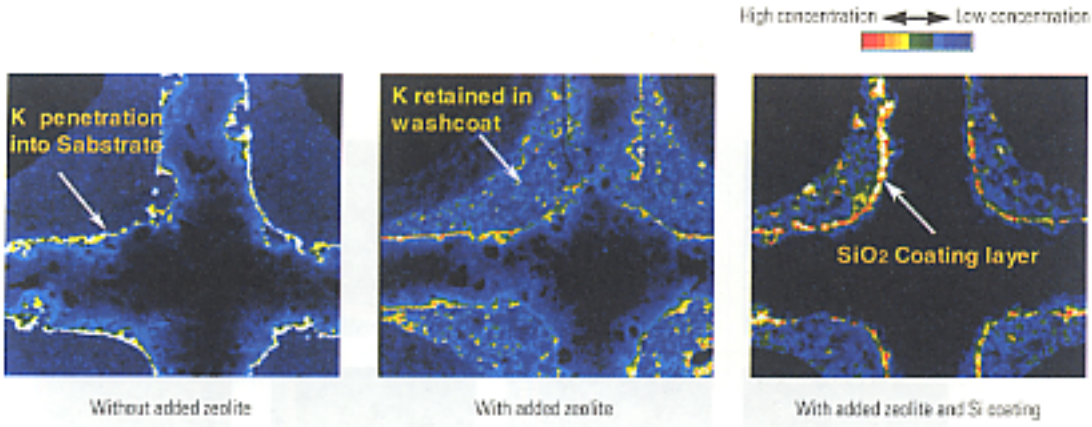

Fig. 5 K distribution in washcoat after lean/rich 32-hour aging at 850 °C (EPMA analysis)

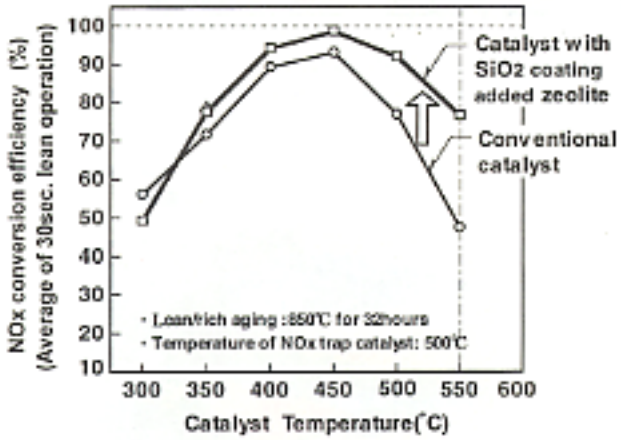

Fig. 6 NOx storage performance

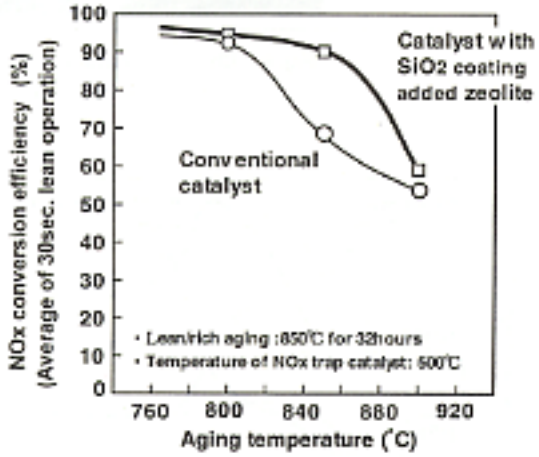

Fig. 7 NOx storage performance

bustion, but during lean operation it is converted by the precious metal into SO_3, which displays the same behavior as NOx and is trapped by the adsorbent in the form of a sulfate. Whereas NOx trapped by the adsorbent is easily displaced from the adsorbent by CO during rich operation, sulfur is not prone to such displacement by CO. Over time, therefore, the adsorbent's active points are decreased and NOx storage performance deteriorates consequently. To compare sulfur desorption characteristics, a catalyst carrying K and a catalyst carrying Ba were subjected to lean/rich aging using high-sulfur fuel and subsequently the catalyst layers were observed. **Fig. 8** shows the results of analyses performed using an electron probe microanalyzer (EPMA) before and after regeneration sulfur desorption. After regeneration the sulfur and Ba distributions were, as shown, approximately equal, but hardly any sulfur was detected in the layer that carried K. These results indicate that K is superior to Ba in terms of sulfur desorption and that it is inherently resistant to sulfur poisoning. Further, adding a titanium (Ti)-based material to the base material to increase its acidity had, as shown in **Fig. 9**, the effect of lowering the temperature at which sulfur purging began. As reflected in the EPMA-analysis results shown in **Fig. 10**, sulfur poisoning was reduced eventually.

As a result, a NOx-trap catalyst with sufficient durability for use with fuel containing approximately 50 ppm of sulfur was realized. This catalyst had the additional merit of recovering its performance when the fuel's sulfur content was returned to 50 ppm or lower after temporary use of fuel with a sulfur content exceeding 50 ppm. **Fig. 11** shows how the NOx-trap catalyst regenerated itself after being sulfur-poisoned by high-sulfur fuel. The catalyst's ability to regenerate itself is a prerequisite for the introduction of NOx-trap systems in the European market, where the sulfur content of gasoline varies from country to country.

3. New dual-layer-coat Pt/Rh TWC

3.1 Problems with TWCs for GDI engines

A TWC used with a GDI engine, which operates with a lean mixture, must provide high hydrocarbon (HC)-reduction performance during lean operation. A palladium (Pd)/rhodium (Rh) TWC is effective for this purpose. Since emissions-reducing technologies employing large amounts of Pd offer better low-temperature HC-reduction performance than other technologies, however, demand for Pd has grown rapidly and Pd has become costly. Pt is relatively inexpensive, by contrast, but conventional Pt/Rh TWCs suffer from a deteriora-

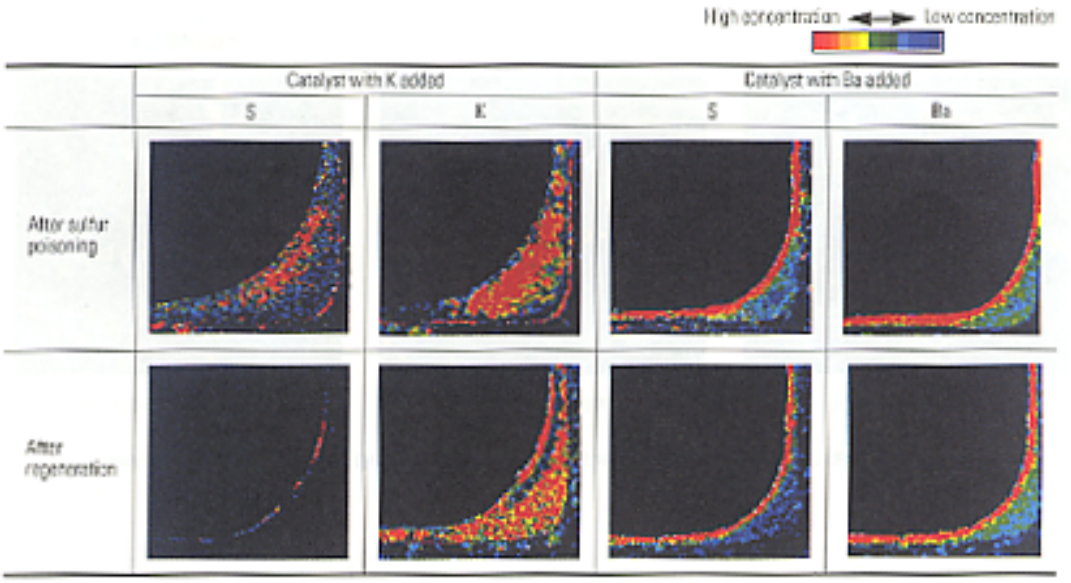

Fig. 8 Characteristics of sulfur poisoning and regeneration (EPMA analysis) after seven hours of lean/rich aging at 550 °C (with fuel sulfur content of 300 ppm-wt)

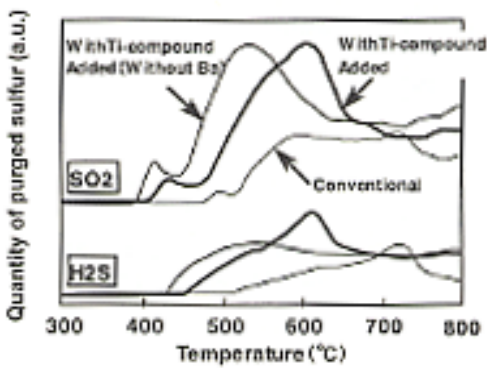

Fig. 9 Effect of addition of Ti compound on sulfur purge characteristics

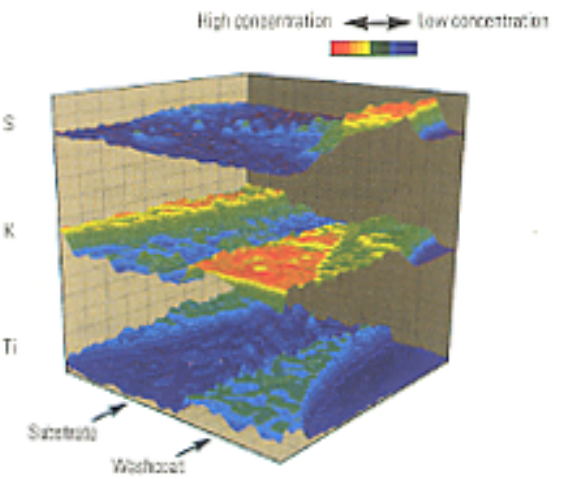

Fig. 10 Sulfur poisoning characteristics of catalyst with zeolite and Ti comound (EPMA analysis)

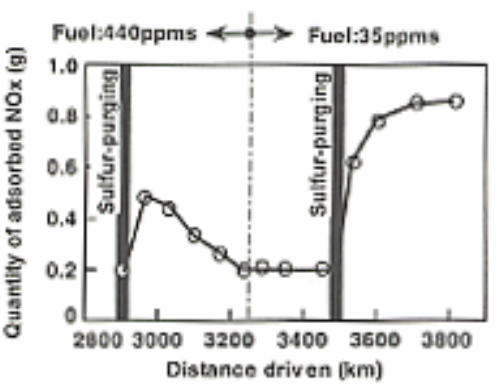

Fig. 11 Sulfur-purge performance of sulfur-poisoned catalyst

tion in HC-reduction performance when exposed to an oxygen-rich atmosphere at high temperatures during lean operation. Noting that Pt itself is known to offer high performance during lean-burn operation, the authors used energy-dispersive X-ray diffraction and transmission electron microscopy to investigate the reasons for the abovementioned deterioration in the HC-reduction performance of conventional Pt/Rh TWCs. It was found that oxidized Rh covered the Pt surface, causing the active points decrease so that performance deteriorated.

3.2 New dual-layer-coat Pt/Rh TWC

With conventional Pt/Rh TWCs, effective use of the Rh, which has superior exhaust-emissions-reduction characteristics with a stoichiometric or near-stoichiometric air/fuel ratio, is enabled by the addition of Pt to the same layer; the hydrogen-producing properties of the Pt are used to minimize oxidative deterioration of the Rh.

With the new dual-layer-coat Pt/Rh TWC, by contrast, we conceived that the Pt and Rh should be carried separately in respective layers to minimize the decrease of the active point. As shown in **Fig. 12**, the Pt is carried in the outside layer for optimum HC-reduction perfor-

mance during lean operation and the Rh, which performs a three-way reduction function with a stoichiometric or near-stoichiometric air/fuel ratio, is carried in the inside layer. Further, Pt was added to the inside layer as a promoter to minimize Rh oxidation. This layer structure assures adequate HC-reduction performance during lean operation, and since it has the Rh, which is prone to oxidative deterioration, in the inside layer it minimizes oxidative deterioration and thus also assures adequate performance with a stoichiometric air/fuel mixture. Further, lantanoids were added to the Pt-carrying layer to optimize thermal stability. As shown in **Fig. 13**, the resulting TWC has oxidation performance equivalent or superior to that of a Pd catalyst during lean operation.

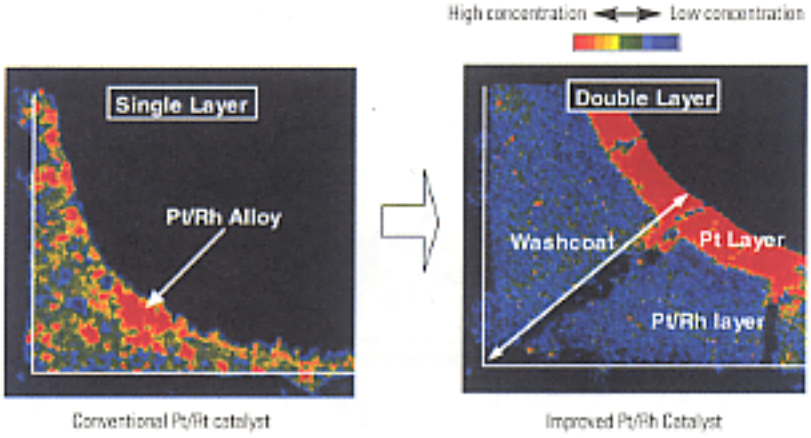

Fig. 12 Layering of improved Pt/Rh catalyst (EPMA analysis)

4. Technologies for control of catalytic reaction

To optimize engine operating conditions to match the complex reaction mechanism of a NOx-trap catalyst and enable a TWC to be used effectively to realize clean exhaust emissions, it is necessary to take an approach based on the concept of designing the catalytic reaction. To achieve the best possible catalyst performance, therefore, we developed combustion technologies for control of the catalytic reaction.

4.1 Stratified slight-lean combustion

Rapid catalyst activation is essential for minimization of exhaust emissions while the engine is cold immediately after startup. With GDI engines, MMC ensures rapid catalyst warmup using two-stage combustion[2], a unique technology that takes advantage of the freedom in mixture-preparation. With two-stage combustion, additional fuel is, as shown in **Fig. 14**, injected in the late stage of the expansion stroke into the hot, burned gases containing a large quantity of excess oxygen that result from ultra-lean stratified combustion (**Fig. 14**). This fuel ignites and burns in the cylinder, raising the exhaust-gas temperature to approximately 700 °C such that the catalyst warms up in a short time. Unfortunately, most of the fuel injected during the expansion stroke is consumed only for the increase in exhaust-gas temperature; its consumption does not yield torque. A shorter period of two-stage combustion is thus desirable for improved fuel efficiency. To overcome this obstacle, we developed a catalyst-warm up technology that keeps the two-stage-combustion period optimally short by making effective use of the catalytic reaction. This technology is one that controls stratified slight-lean combustion[3].

(1) Mechanism of stratified slight-lean combustion

Fuel injection during the compression stroke creates a heterogeneous mixture pattern in which rich areas are unevenly distributed within lean mixture. If ignition and combustion are subsequently caused with the average

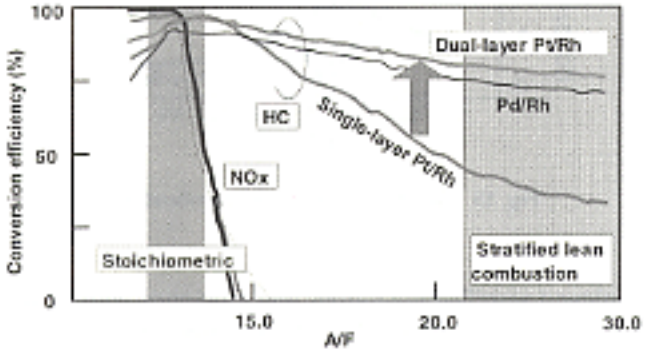

Fig. 13 Performance of improved Pt/Rh catalyst and conventional catalysts during lean operation

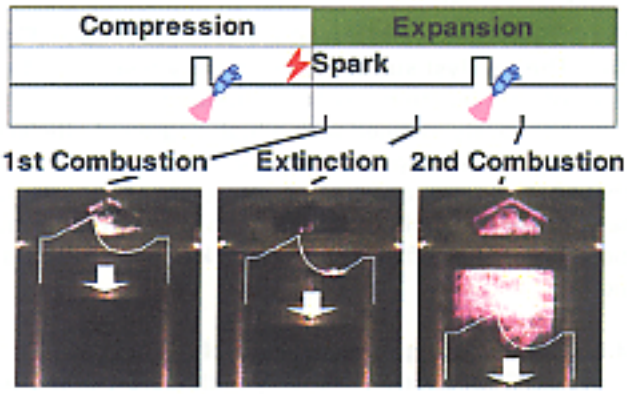

Fig. 14 Two-stage combustion

air/fuel ratio slightly on the lean side of stoichiometric, carbon monoxide (CO) is produced in the rich areas and oxygen exists in the lean areas. As shown in **Fig. 15**, the resulting exhaust emissions contain sufficient quantities of both CO and oxygen to cause an oxidation reaction on the surface of the catalyst. The abovementioned type of combustion is known as "stratified slight-lean combustion". Owing to its heterogeneous nature, it is accompanied by a deterioration in combustion efficiency. However, the detrimental effect is small; we

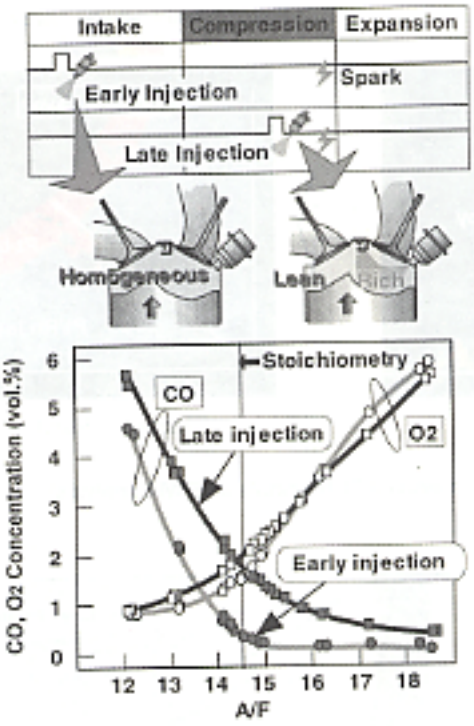

Fig. 15 Stratified slight-lean combustion

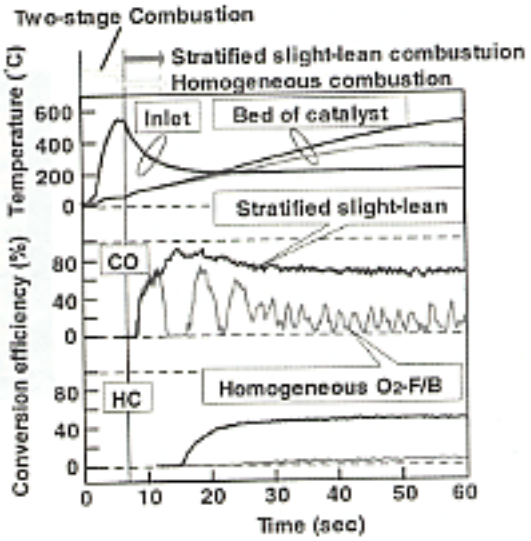

Fig. 16 Catalyst temperature after cold start

achieved significantly higher fuel efficiency with stratified slight-lean combustion than is possible with two-stage combustion.

(2) Mechanism and effects of catalytic reactions

To heat the catalyst to the lowest temperature at which the CO-oxidation reaction is possible, two-stage combustion is performed for several seconds following a cold start. The engine then switches to stratified slight-lean combustion, causing an immediate start in the CO-oxidation reaction on the catalyst surface (Fig. 16). The catalyst surface is selectively heated by the heat of this reaction, so an HC-oxidation reaction is simultaneously induced with a high degree of efficiency. With this arrangement, we significantly shortened the required duration of two-stage combustion (several tens of seconds with earlier technology) and realized both higher fuel efficiency and quicker catalyst activation.

4.2 Oxygen storage support control

A TWC functions effectively with a stoichiometric air/fuel ratio. With air/fuel-ratio control employing an oxygen sensor, however, the air/fuel ratio varies on either side of the stoichiometric point, meaning that the storage/release function of the oxygen storage component (OSC) in the catalyst plays an extremely important role. When the air/fuel mixture is rich, oxygen stored in the OSC is released and oxidizes excess CO and HCs and simultaneously protects the catalyst's metal surface from CO poisoning, thus facilitating the NOx-reduction reaction. Conversely, when the air/fuel mixture is lean the OSC absorbs excess oxygen, thus preventing it from hindering NOx reduction. Once the OSC's active points have become decreased with deterioration of the catalyst, however, NOx emissions are, as shown in part A of Fig. 17, seen to increase sharply after a certain period of stoichiometric operation. If the catalyst is briefly given a lean spike at this time, it immediately recovers its earlier performance. This phenomenon suggests that the OSC's oxygen storage/release function depends greatly on the state of oxidation of the OSC itself. Further, calibration performed for compliance with regulations shifts air/fuel-ratio control slightly to the rich side; this presumably reduces the extent of oxidation of the OSC during stoichiometric operation with the air/fuel ratio control. To minimize NOx emissions, therefore, it is necessary to create a balance between

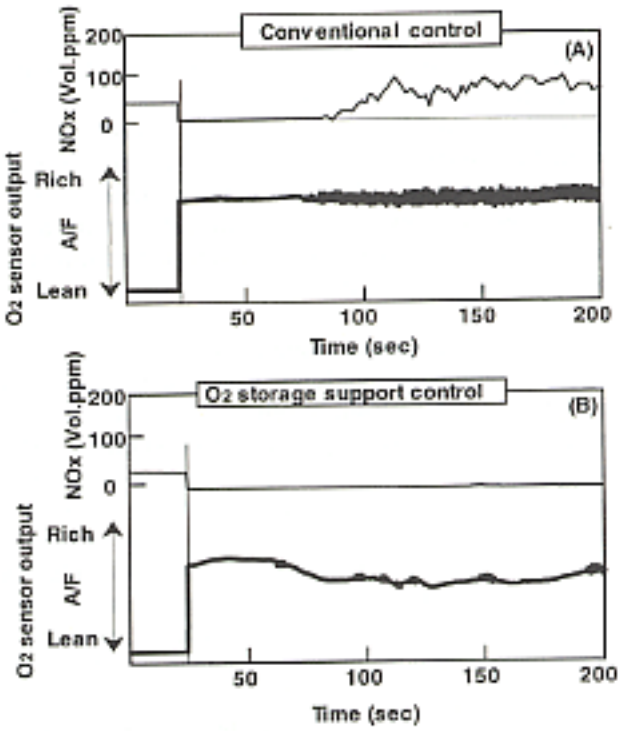

Fig. 17 O_2 storage support control

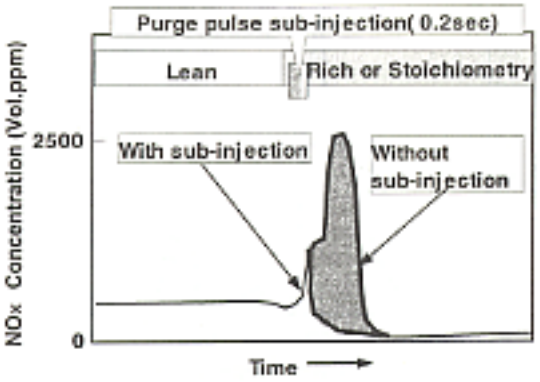

Fig. 18 Purge pulse sub-injection control

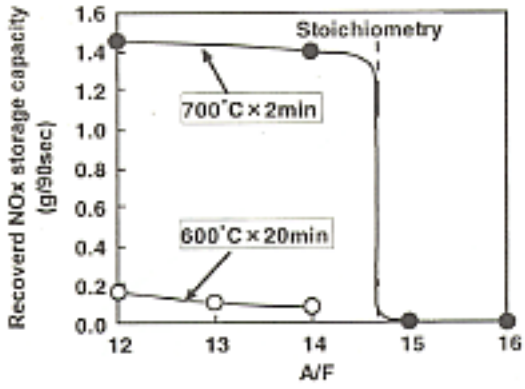

Fig. 19 Effect of air/fuel ratio on sulfur-purge level

conventional stoichiometric air/fuel-ratio control and a new form of air/fuel-ratio control intended to maintain the OSC's state of oxidation. The appropriateness of the control balance is reflected in the air/fuel ratio of exhaust emissions downstream of the catalyst. If the control balance is inappropriate, the oxygen sensor's output amplitude increases as shown in part A of **Fig. 17**. Utilizing this correlation between the oxygen sensor's output amplitude and the OSC's state of oxidation, the authors developed an oxygen storage support control technology for minimization of NOx emissions (see part B of **Fig. 17**). With this technology, an increase in the output amplitude of the oxygen sensor downstream of the catalyst is taken to indicate a decrease in the OSC's oxygen storage/release functionality. In response, the air/fuel ratio is made lean to restore the OSC's state of oxidation. Performing this oxygen storage support control enabled NOx emissions caused by variation of the air/fuel ratio during stoichiometric operation were minimized.

4.3 NOx purge pulse sub-injection

The NOx-reduction process with the NOx-trap catalyst consist of with NOx storage and release (yielded by nitrate/carbonate displacement) and a reduction reaction of the released NOx undergoing in the downstream TWC. At the begining of rich operation, most of the CO (the reducing agent) is consumed by carbonate formation at this time, so the reducing agent becomes insufficient for reduction of the released NOx and a large amount of NOx is temporarily emitted. If the air/fuel mixture is made richer to increase the CO as a countermeasure, the amount of NOx released as a result of the displacement reaction increases further, making it impossible to reduce NOx emissions sufficiently. We thus considered supplying HCs as a reducing agent whose effect on NOx release is small. Supplying HCs to the TWC by additional fuel injection for an extremely short period during the expansion stroke had the effects shown in **Fig. 18**. These effects were apparently yielded as follows: K held in the NOx-trap catalyst and π electrons in the HCs repelled each other such that adsorption of HCs by the precious metal was restricted. The proportion of the HCs that was thus not eliminated was supplied to the TWC, where it was converted into CO and H_2, which reduced the NOx. By effecting momentary fuel injection purged in this way, we made significant reductions in NOx emissions possible.

4.4 Assisted temperature-rise control

The new NOx-trap catalyst, which uses K as an adsorbent and has an added Ti compound, is inherently less subject to sulfur poisoning. Yet it needs the purging of sulfur, however, sulfur accumulated during a prolonged operation.

An index reflecting the extent of sulfur-poisoning damage is necessary for the creation of a sulfur-purging algorithm. One possible index is the quantity of accumulated sulfur. Another is the extent to which sulfur has been purged, i.e., the catalyst's degree of cleanliness. The usability of both of these indices was studied.

In principle, the quantity of accumulated sulfur can be inferred by means of analysis taking into account the concentration of sulfur in the fuel, the active point of the adsorbent, the quantity of fuel consumed, the frequency of lean operation, and the catalyst temperature. However, the concentration of sulfur in the fuel varies according to the type of fuel and detection of the active point of the adsorbent is affected by the extent of thermal degradation, which is difficult to ascertain. It was thus determined that the quantity of accumulated sulfur could not be determined with sufficiently high accuracy.

By contrast, the catalyst's degree of cleanliness can be defined with sufficient accuracy by means of detection and analysis of the frequencies of catalyst temperatures corresponding to stoichiometric and rich operation. **Fig. 19** shows the influence of the air/fuel ratio on the sulfur-purge speed, and **Fig. 20** shows the influence of the catalyst temperature on the sulfur-purge speed. As shown, when the air/fuel mixture is not lean the sulfur-purge speed increases logarithmically with respect to the catalyst temperature. For practical purposes, therefore, it can be inferred that the sulfur-purge speed depends on the catalyst temperature only. Thus, it is possible to infer the catalyst's possible degree of cleanliness from the catalyst temperature hysteresis.

To obtain catalyst cleanliness indices from the cata-

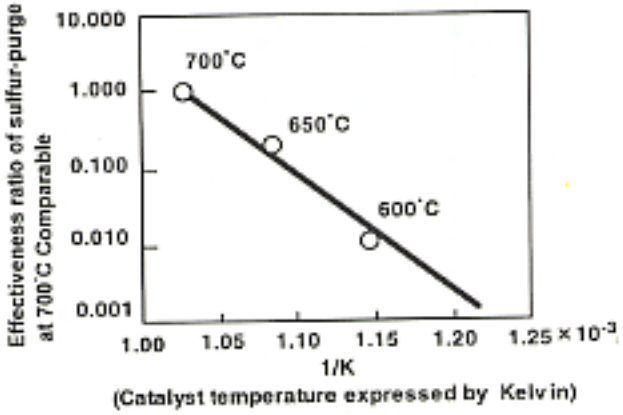

Fig. 20 Sulfur-purge level as function of catalyst temperature

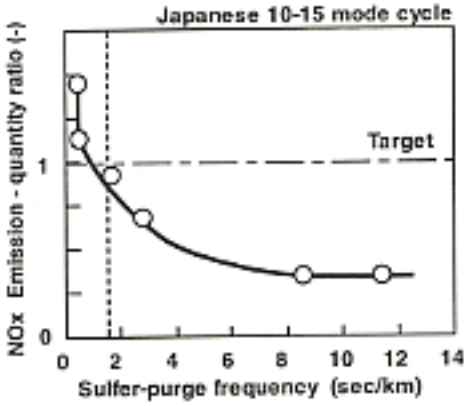

Fig. 21 Dependence of NOx emissions on sulfur-purge frequency

lyst temperature hysteresis, the authors used the equations shown below after working out the reaction speed at various temperatures using that at 700 °C (obtained from the relationship shown in Fig. 20) as a base and assigning as weight the residence time to the speed corresponding to each temperature. The result of the calculation was defined as "sulfur purge frequency".

$$\text{S-purge frequency} = \{\int k(T)/k(700 + 273)dt\}/L \text{ (sec/km)}$$

$ds(T)/dt = A \cdot \exp(-\Delta E/RT) \cdot (S\ trap)$ Purge reaction speed

$k(T) = A \cdot \exp(-\Delta E/RT)$ Reaction speed constant

where

S	:	Purged sulfur
A	:	Frequency factor
ΔE	:	Activation energy
R	:	Gas constant
T	:	Catalyst temperature (K)
(S trap)	:	Trapped sulfur
t	:	Time (sec)
L	:	Total distance driven (km)

Fig. 21 shows the relationship between the sulfur-purge frequency and the quantity of NOx emissions in Japanese 10-15-mode test cycle. The clear correlation

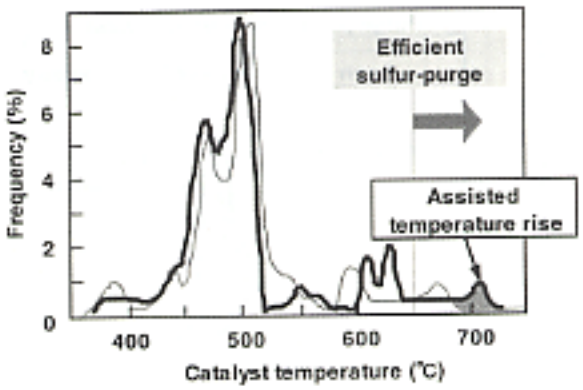

Fig. 22 Effect of assisted temperature-rise control

suggests that it is possible to minimize sulfur poisoning by controlling the sulfur-purge frequency.

To minimize sulfur poisoning during actual vehicle operation, it is necessary to control the catalyst temperature such that the sulfur-purge frequency does not drop below a certain target level. Adopted as a means of controlling the catalyst temperature was a temperature-rise control process utilizing ignition-timing retardation, because of the good control ability of the process. Additional fuel consumption required by the temperature-rise control process is kept to a minimum by actively assisting increases in temperature only when the temperature approaches near to the level at which sulfur is released (for example, during acceleration, during uphill driving and so on).

Fig. 22 shows the effect of the temperature-rise control process. This control process enabled us to reduce the amount of sulfur accumulating in the NOx-trap catalyst and to significantly improve the NOx-trap catalyst's durability.

5. Summary

To more fully realize the potential of GDI engines and thus enable wider adoption of such engines, MMC developed new catalysts and related catalytic-reaction control technologies. Specifically, these items are as follows:

(1) A high-temperature NOx-trap catalyst whose catalyst layer is loaded with K, in a stabilized state which has superior charactoristics under high-temperature condition

(2) A dual-layer-structure TWC that offers superior HC-reduction characteristics during the lean operation that characterizes GDI engines.

(3) Catalytic-reaction control technologies that maximize the benefits of the catalysts'characteristics.

By developing these new catalysts and related technologies, we realized significant reductions in the exhaust emissions of GDI engines. Consequently, we expect to achieve compliance with stringent new emissions standards that are planned for introduction in Japan and Europe from 2005. We plan to pay close attention to gasoline characteristics in relevant markets and to steadily adopt NOx-trap catalysts in place of selective-reduction catalysts in line with reductions in

sulfur content.

6. Afterword

MMC has taken advantage of the freedom permitted in mixture-preparation with GDI to develop combustion-control technologies that simultaneously maximize output and fuel efficiency. Utilizing advantage of GDI's excellent controllability, it has also developed the GDI SIGMA series of technologies, which includes automatic stop-and-go integrated control with a continuously variable transmission; and turbocharging. With these and other developments, MMC has created a trend toward adoption of GDI engines.

The catalyst technologies and catalytic-reaction control technologies described in this paper represent a third wave of technological advances. We are confident that they will enable even wider adoption of GDI engines.

In closing, we wish to express our gratitude to ICT Co., Ltd. and NGK Insulators, Co. Ltd., which both cooperated extensively in our development program.

References

(1) Masao Hori et al: "Development of New Selective NOx Reduction Catalyst for Gasoline Leanburn Engine", SAE Paper 972850, 1997

(2) Nakayama: "Gasoline Direct-Injection Engines and Advances Therein", 48th JSAE lecture meeting, 1999, p. 25 – 30

(3) Shigeo Yamamoto et al: "Advanced Emission Control Technology by Utilizing Freedom of Mixing on GDI Engine", FISITA World Automotive Congress F2000A140


Keisuke TASHIRO


Kazuo KOGA


Kinichi IWACHIDO


Yasuki TAMURA


Hiroyuki NAKAJIMA

TECHNICAL PAPERS

Development of Mitsubishi Innovative Quiescent Combustion System for Low Exhaust Emissions from Diesel Engines of Heavy-Duty Trucks

Hiroshi JYOUTAKI* Kenji SAKAI* Masayuki TAKAHASHI*
Kenji KAWAI* Kazutoshi MORI**

Abstract

With the objective of achieving compatibility of low exhaust emissions with low fuel consumption in the diesel engines of heavy-duty trucks, Mitsubishi Motors Corporation undertook development based on the approach of applying combustion technology, and a new quiescent combustion system was subsequently realized. This system successfully combines an air intake port with a low swirl ratio; a combustion chamber with a large diameter; and a common-rail type, high-pressure fuel-injection system.

With the help of an EGR system, this new combustion system will ensure compatibility of both low exhaust emissions and low fuel consumption, thereby satisfying the long-term exhaust emission standard currently applicable within Japan.

Key words: *Diesel Engine, Engine Combustion, Exhaust Gas Recirculation, Quiescent Combustion System*

1. Introduction

As standards on exhaust emissions from the diesel engines of heavy-duty vehicles become increasingly stringent around the world, development efforts aimed at simultaneously reducing exhaust emissions and fuel consumption continue apace[1)2)].

As part of these efforts, we at MMC recently developed a new-generation direct-injection diesel engine. Taking a combustion-oriented approach, the designing staff employed a quiescent combustion system (QCS)[3)], which is more advantageous than the widely used swirl-supported combustion system (SSCS) with regard to simultaneous reduction of exhaust emissions and fuel consumption. The Mitsubishi Innovative Quiescent Combustion System (MIQCS) was realized by combining the QCS with a common-rail system (CRS) for fuel supply (a CRS permits a high degree of control freedom). In developing the MIQCS, the MIQCS's potential was ascertained and differences in combustion phenomena between the MIQCS and the SSCS were clarified.

Further, the possibility of further reducing exhaust emissions by combining the MIQCS with an EGR system was verified.

The MIQCS is used in the turbocharged, intercooled diesel engine of a heavy-duty truck that was launched by MMC in February 2000.

2. MIQCS development concept

2.1 Merits of the QCS

The SSCS, which is used in most diesel engines in Japanese heavy-duty vehicles, employs in-cylinder swirl and squish flows and other air flows to promote mixture of the fuel spray with the air prior to combustion.

By contrast, the QCS, which combines a low-swirl-ratio air-intake port with a large-diameter combustion bowl, does not make significant use of in-cylinder flows. Rather, it primarily employs the energy of the high-pressure fuel spray to promote mixture of the fuel spray with the air prior to combustion. The QCS is widely used in large, high-thermal-efficiency marine engines[4)].

2.2 Test engine

To ascertain the potential of the QCS, a turbocharged, intercooled engine of the type used in heavy-duty trucks was selected. The specifications of this test engine are shown in **Table 1.**

2.3 Shape of intake ports

The engine's port layout is shown in **Fig. 1.**

To ensure a sufficient air supply, each cylinder was provided with two intake valves and two exhaust valves. And to give the intake port a high flow coefficient, the intake port's shape was devised so as to minimize flow interference between the intake valves.

* Engine Research Dept., Truck & Bus Dev. Office
** Engine Testing Dept., Truck & Bus Dev. Office

Table 1 Engine specifications

Engine model	6M70TD (turbocharged and intercooled)
Bore x stroke	135 mm x 150 mm (six in-line cylinders, 12.9 L displacement)
Max. output and torque	279 kW/2200 min^{-1}, 1618 Nm/1200 min^{-1}
Fuel injection	Common-rail system

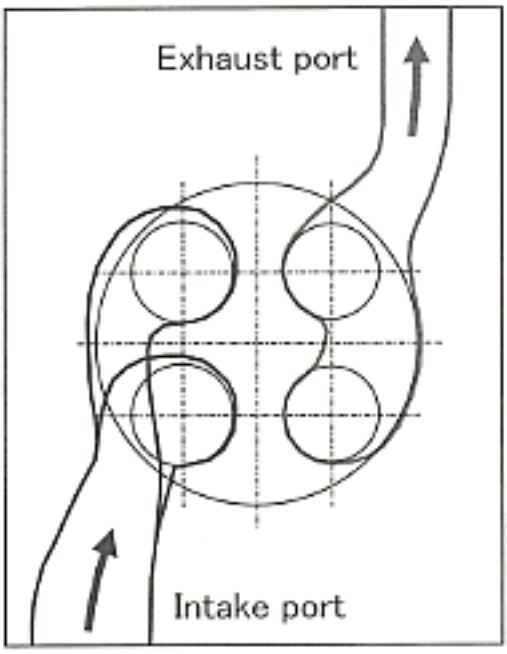

Fig. 1 Port layout

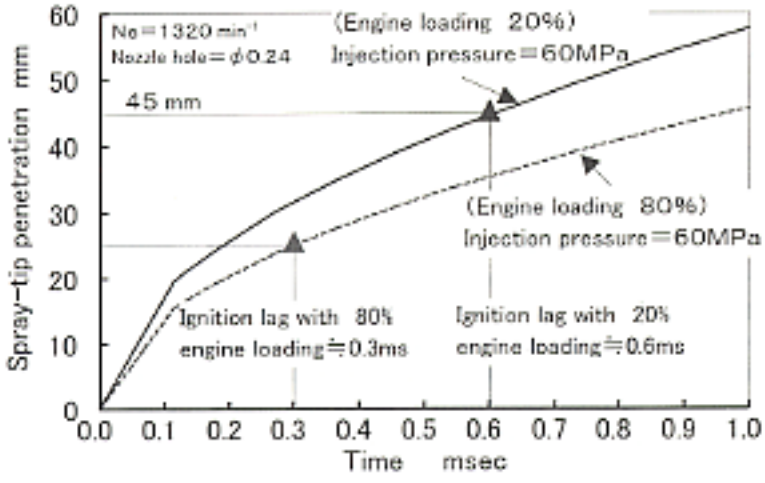

Fig. 2 Predicted spray-tip penetration

2.4 Study of combustion-bowl shape

Since the in-cylinder swirl flow is weak with the QCS, any sprayed fuel that adheres to the wall of the combustion bowl prior to combustion fails to mix with the air, resulting in significant emissions of hydrocarbons and black smoke.

To prevent this problem, the diameter of combustion bowl must be greater than the distance by which the spray tip penetrates during the ignition-lag period. Predictions of spray-tip penetration were made using the equation devised by Hiroyasu et al[5]. The results are shown in **Fig. 2**.

(1) Low-load operation

During low-load operation, the engine's ignition-lag period is approximately 0.6 ms. The spray-tip penetration during this period is approximately 45 mm.

(2) High-load operation

During high-load operation, the ignition-lag period is relatively short so the risk of adhesion of unignited fuel to the wall is negligible. However, the potential effects of the large injection amount and long injection period must be taken into account: If the diameter of the combustion bowl is too small, the weak swirl flow can allow unignited fuel to interfere with already-burned gases, resulting in significant emissions of black smoke. Thus, the combustion bowl should have an optimally large diameter.

In accordance with these considerations, it was determined that the MIQCS combustion bowl should have a diameter of at least 90 mm. The large-diameter toroidal combustion bowl adopted was of the type shown in **Fig. 3**.

2.5 Selection of fuel-injection system

Since the QCS depends primarily upon the fuel-injection energy to mix the fuel with the air, a high injection pressure is necessary. With marine engines and with the diesel engines of non-Japanese heavy-duty vehicles, manufacturers have frequently achieved the required injection pressure by combining the QCS with jerk-type electronic unit injectors (EUIs) or with unit pumps (PLDs)[6].

Bearing these points in mind, the designing staff considered the most suitable fuel-injection system for the QCS of the engine in a heavy-duty truck for domestic use.

(1) Results of tests on QCS with in-line pump

Fig. 4 shows the results achieved when a conventional in-line fuel-injection pump was used with the QCS.

Reductions in fuel consumption and black smoke were observed with high engine speeds. Since the injection pressure was linked to the engine speed, however, low-speed operation made the injection pressure insufficient, resulting in increased emissions of black smoke.

To minimize emissions of particulate matter (PM) at all engine speeds, it is clearly necessary to employ a fuel-injection system that can produce a high injection pressure even during low-speed operation.

(2) Comparison of characteristics of high-pressure fuel-injection systems

The characteristics of high-pressure fuel-injection systems are compared in **Table 2**.

In European countries and the United States, road and traffic conditions permit a significant proportion of driving to take place at high speeds. For compliance

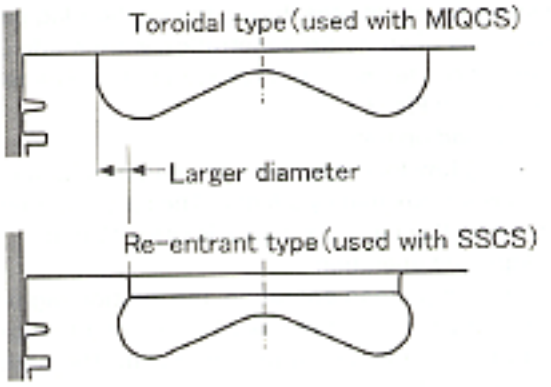

Fig. 3 Cross-section of combustion bowl

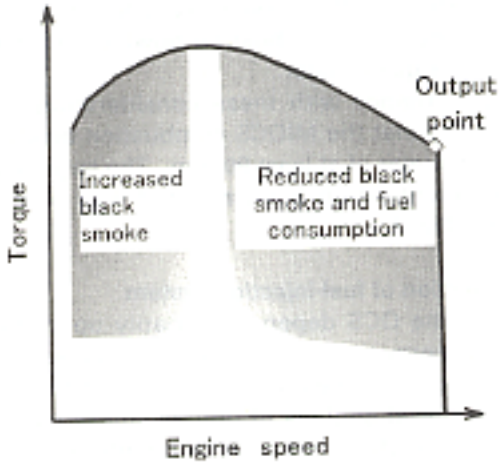

Fig. 4 Results of QCS test with in-line pump

Table 2 Characteristics of high-pressure fuel-injection systems

Characteristic	High-pressure fuel-injection system			
	Jerk-type EUIs	CRS	New TICS	High-pressure distributor-type
① Maximum injection pressure	○	○	△	△
② High-pressure injection with low operating speed	△	○	△	△
③ Independent control of injection timing and pressure	△	○	△	△
④ Control of injection-rate shape	○	△	○	△
⑤ Quietness	△	○	○	○
⑥ Lightness	×	△	△	○
⑦ Affordability	×	△	△	○

○ = Good △ = Acceptable × = Bad
TICS: Timing and Injection rate Control System

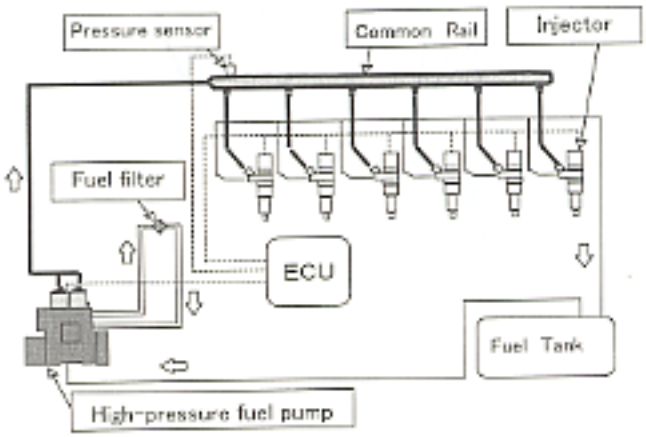

Fig. 5 Common-rail system

with these countries' exhaust-emissions standards, therefore, it is advantageous to optimize the injection pressure for high-speed, high-load conditions. In Japan, by contrast, compliance with exhaust-emissions standards necessitates optimization of the fuel-injection pressure for low, moderate, and high levels of speed and loading.

EUIs and PLDs offer high maximum injection pressures, but the highest possible injection pressure at any given time is linked to the current levels of engine speed and loading. Consequently, the injection pressure is insufficient during low-speed operation. Clearly, neither EUIs nor PLDs readily permit optimization of the injection pressure for the whole range of operating conditions.

Another important factor is controllability: For a fuel-injection system to minimize exhaust emissions over the whole range of operating conditions, it must, in addition to being capable of producing a high injection pressure, permit optimized control of the injection pressure and injection timing.

In light of these considerations, a CRS[7] for fuel supply with the MIQCS was selected. The CRS is slightly inferior to EUIs and other systems in terms of maximum possible injection pressure, but it offers a sufficiently high injection pressure over the whole range of operating conditions and permits independent control of the injection pressure and injection timing.

The CRS is shown in Fig. 5.

MMC has used this type of system in certain heavy-duty trucks since 1996[8].

Through this process of selection, the MIQCS was configured such that it combined a high-flow-coefficient, low-swirl-ratio intake port and a large-diameter toroidal combustion bowl and was supplied with fuel by a CRS, which gave the above mentioned benefits in terms of optimum injection pressure and injection timing over the whole range of operating conditions. Then investigated was the MIQCS's ability to simultaneously minimize exhaust emissions and fuel consumption over the whole range of operating conditions.

3. Results of tests on MIQCS

3.1 Test points

For evaluation purposes, two test points (one each for low-load conditions and high-load conditions; see Fig. 6) were selected from Japan's 13-mode test procedure. These test points were as follows:

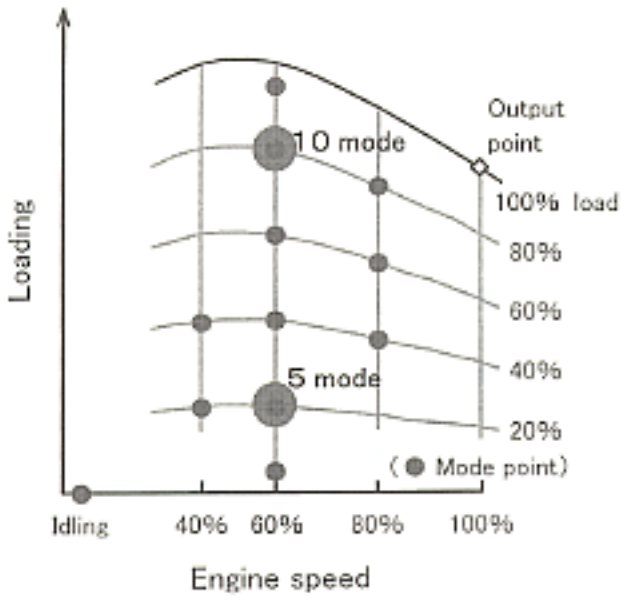

Fig. 6 Test points

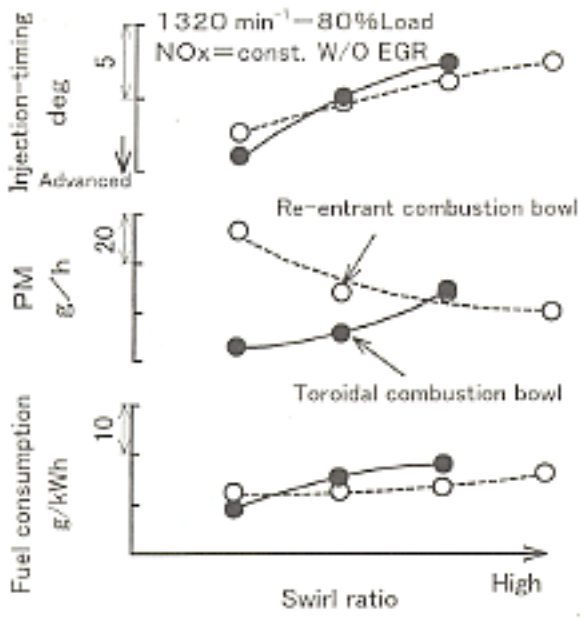

Fig. 7 Influence of swirl ratio and combustion-bowl shape on exhaust emissions and fuel consumption

(1) Low-load test point
5-mode point (1320 min^{-1}; 20 % loading)
(2) High-load test point
10-mode point (1320 min^{-1}; 80 % loading)

3.2 Optimization of in-cylinder swirl ratio and combustion-bowl shape

With a view to selecting an appropriate in-cylinder swirl ratio for the MIQCS, comparison was made of the influence of various swirl ratios with the two aforementioned combustion-chamber types, i.e., re-entrant (used with the SSCS) and toroidal (used with the MIQCS). The results are shown in **Fig. 7**.

Decreases in the swirl ratio caused fuel consumption to decrease with both combustion-chamber types. The same decreases in the swirl ratio caused PM emissions to increase with the re-entrant type and to decrease with the toroidal type.

The toroidal type combining a low-swirl-ratio intake port and a large combustion-bowl diameter was clearly the better choice for simultaneous minimization of fuel consumption and PM emissions.

3.3 Optimization of number of injection-nozzle holes

Since the MIQCS uses the energy of the fuel spray to mix the fuel and air, appropriate fuel-spray dispersion, which depends largely on an appropriate number of nozzle holes, is vital. Consequently, various numbers of nozzle holes were compared in terms of NOx emissions, black-smoke emissions, and fuel consumption. Constant injection timing was a precondition for the tests, so the nozzle holes' total area was the same with every number of nozzle holes. The results are shown in **Fig. 8**.

(1) Low-load operation

Increases in the number of nozzle holes were accompanied by decreases in fuel consumption, black-smoke emissions, and NOx emissions. These decreases were attributable to improved mixing of the fuel and air: Since the nozzle holes' total area was kept the same with every number of nozzle holes, each increase in the number of nozzle holes caused a decrease in the size of each nozzle hole. Smaller nozzle holes yielded better spray atomization, thereby increasing the rate at which air was introduced into the spray.

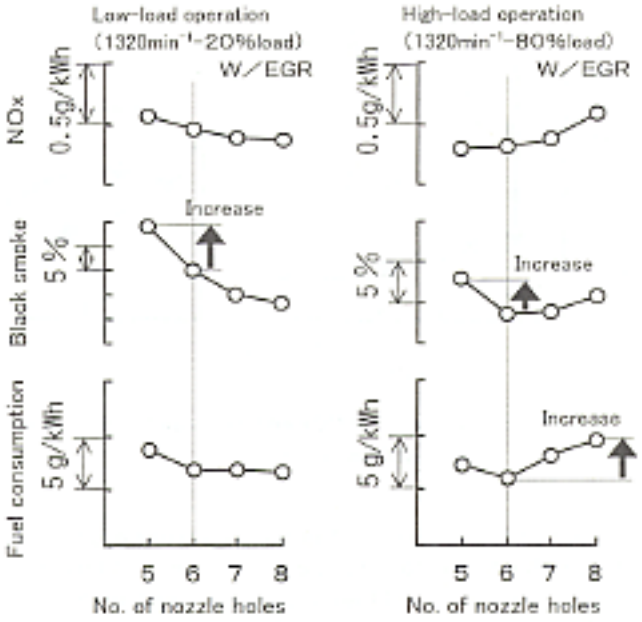

Fig. 8 Influence of number of nozzle holes on exhaust emissions and fuel consumption

(2) High-load operation

Fuel consumption and black-smoke emissions were lowest with six nozzle holes. Fuel consumption and NOx emissions increased when the number of nozzle holes was increased beyond six. The increases in fuel

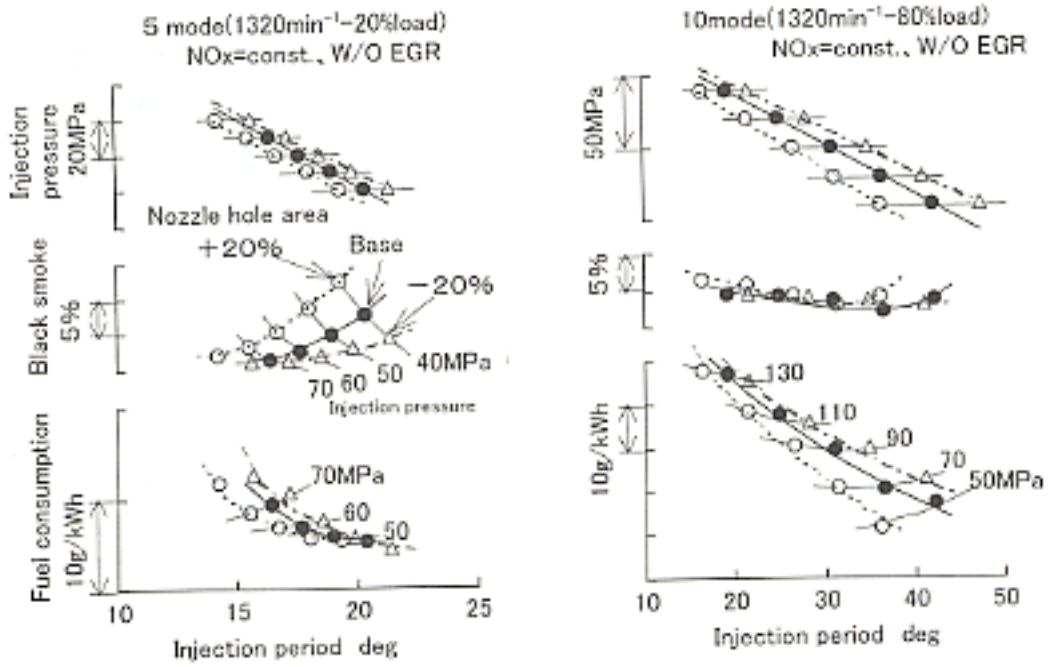

Fig. 9 Influence of nozzle-hole area on black-smoke emissions and fuel consumption

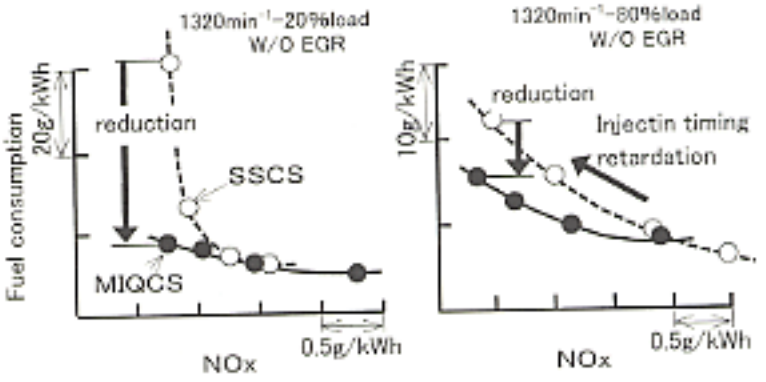

Fig. 10 Trade-off of NOx emissions and fuel consumption with MIQCS and SSCS

consumption and exhaust emissions were apparently attributable to increased initial combustion and to interference when sprayed fuel underwent combustion.

Determined from these findings was that six nozzle holes gave the best balance of fuel consumption, black-smoke emissions, and NOx emissions with the selected swirl ratio and combustion-bowl shape.

3.4 Optimization of total nozzle-hole area and injection pressure

The total nozzle-hole area has a significant influence on spray atomization and is an important factor determining the injection timing. Therefore, the influence of the total nozzle-hole area on black-smoke emissions and fuel consumption with the MIQCS was investigated. With each nozzle, NOx emissions were kept constant and the common-rail pressure was varied. The results are shown in **Fig. 9.**

(1) Low-load operation

Black-smoke emissions increased as the common-rail pressure was reduced and the injection period became longer, but the rate of increase in black-smoke emissions was lower with a smaller total nozzle-hole area than with a larger one. Fuel consumption was lower with a larger total nozzle-hole area than with a smaller one.

(2) High-load operation

As with low-load operation, a smaller nozzle-hole area yielded a slower increase in black-smoke emissions than a larger one as the injection period was lengthened. Also as with low-load operation, fuel consumption was lower with a larger total nozzle-hole area than with a smaller one.

These findings indicated that it was possible to optimize the MIQCS's nozzle-hole area for the best balance of fuel consumption, black-smoke emissions, and NOx emissions.

3.5 Summary of MIQCS tests

The MIQCS and SSCS were compared in terms of NOx emissions and fuel consumption after the number of nozzle holes, the nozzle-hole area, and other injection-related parameters had been carefully selected. The results are shown in **Fig. 10.**

At the low end of the NOx-emissions range, the MIQCS's fuel consumption was lower than the SSCS's during both low-load operation and high-load operation; with any given injection timing, the MIQCS's NOx emissions were lower than the SSCS's and the degree of injection-timing retardation was smaller.

These results indicated that the MIQCS was superior to the SSCS in terms of the trade-off between NOx emissions and fuel consumption at the low end of the NOx-emissions range and that it had the potential to

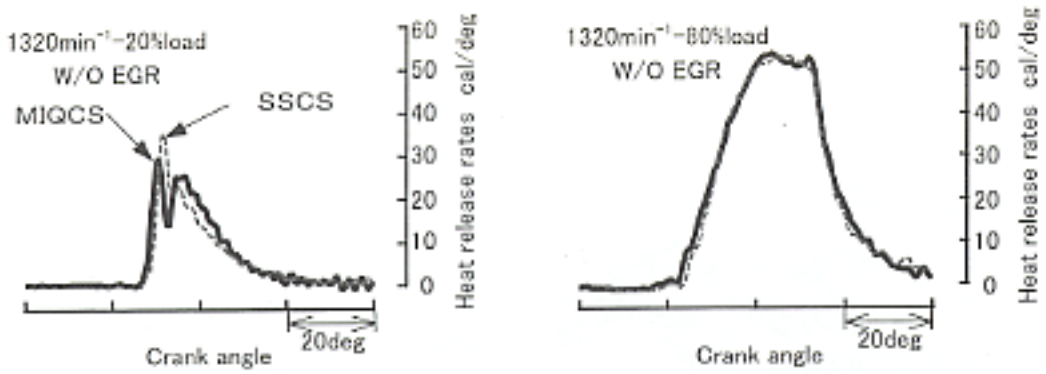

Fig. 11 Heat-release rates of MIQCS and SSCS

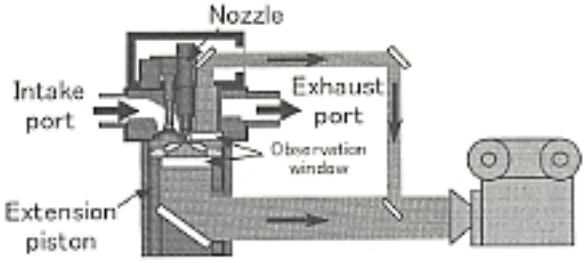

Fig. 12 Visualization engine

enable further NOx-emission reductions that will be necessary in the future.

4. Clarification of MIQCS combustion phenomena

4.1 Comparison of combustion analyses

As stated, the MIQCS showed itself superior to the SSCS in terms of the trade-off between NOx emissions and fuel consumption at the low end of the NOx-emissions range. With a view to clarifying the reasons, the two combustion systems' respective heat-release rates were compared. The results are shown in **Fig. 11**.

During low-load operation, the MIQCS had a relatively short ignition-lag period, a relatively low premixed-combustion peak, and a relatively short combustion period. Thus, its heat-release-rate peak was relatively low and relatively advanced in terms of ignition timing. The MIQCS's superior ability to minimize NOx emissions and fuel consumption simultaneously was apparently attributable to these factors.

Differences in heat-release rate between the two combustion systems were smaller during high-load operation than during low-load operation, but the MIQCS's slightly shorter ignition-lag period, slightly shorter combustion period, and earlier start of combustion were apparently to thank for the MIQCS's lower fuel consumption. Reasons for the MIQCS's superior NOx-reduction performance were not possible to infer from changes in the heat-release rate.

4.2 Comparison based on combustion analyses

Since the reasons for the MIQCS's superior NOx-reduction performance could not be inferred from changes in the heat-release rate, an attempt was made to do so by comparing the MIQCS's and SSCS's combustion characteristics using a single-cylinder combustion-observation engine of the type shown in **Fig. 12**.

The initial combustion peak apparently contributes greatly to NOx formation. Images of the flame at this time (taken simultaneously from above the piston and from below the piston) are shown in **Fig. 13** together with the results of flame-temperature analyses performed using the two-color method[9].

(Owing to the effects of unburned fuel that adhered to the bottom of the combustion chamber, the flame-temperature analyses reflect only the results of observations made from above.)

It can be seen from the results of the flame-temperature analyses that high-temperature combustion occurred in the combustion bowl with the SSCS and that relatively low-temperature combustion occurred throughout the cylinder with the MIQCS.

By means of observations made from above, the respective flame areas of the SSCS and MIQCS were further determined and compared. The results are plotted against the crank angle in **Fig. 14**.

The MIQCS's total flame area was relatively small at the beginning of combustion, suggesting that relatively little initial combustion took place.

Also, the MIQCS's flame area during high-temperature combustion (with temperatures in excess of 2800 K) was approximately half that of the SSCS. High-temperature combustion apparently contributes greatly to NOx formation, so the relatively small flame area can be interpreted as one reason for the MIQCS's relatively low NOx emissions.

4.3 Comparison based on numerical analyses

To further clarify the reasons for the MIQCS's superior ability to reduce emissions of NOx and black smoke, numerical analyses were performed using the KIVA-II computer program[10]. For the combustion model, the KIVA software's original Arrhenius type was used, and for the NO formation model the extended Zeldovich model was used. The results are shown in **Fig. 15**.

The results of the calculations showed that the region of combustion at or near the peak cylinder tem-

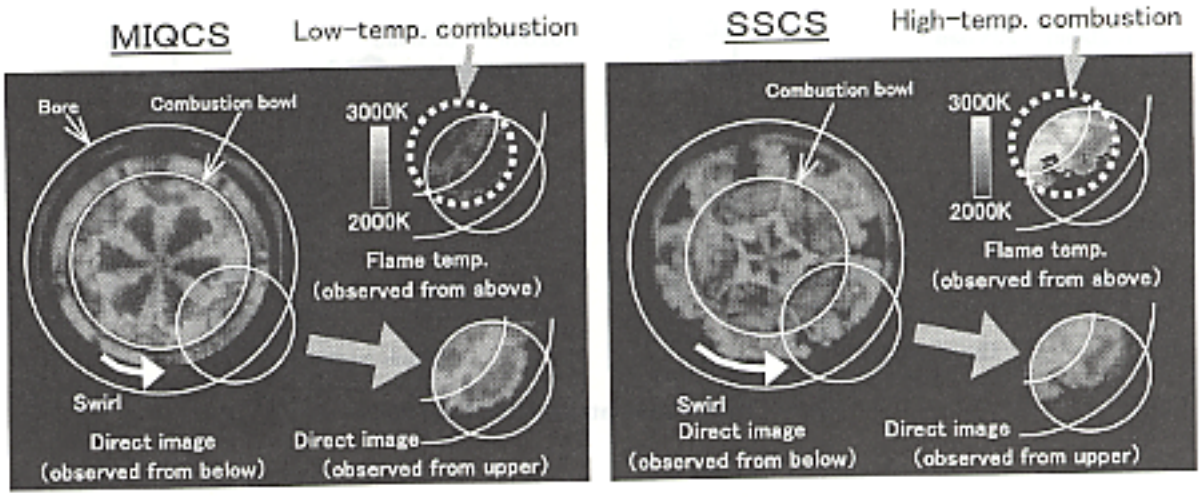

Fig. 13 Combustion images and flame temperatures for MIQCS and SSCS

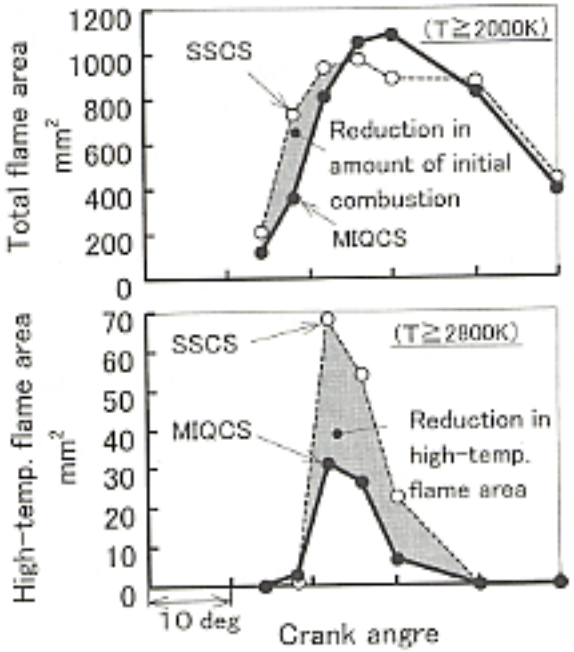

Fig. 14 Flame areas of MIQCS and SSCS

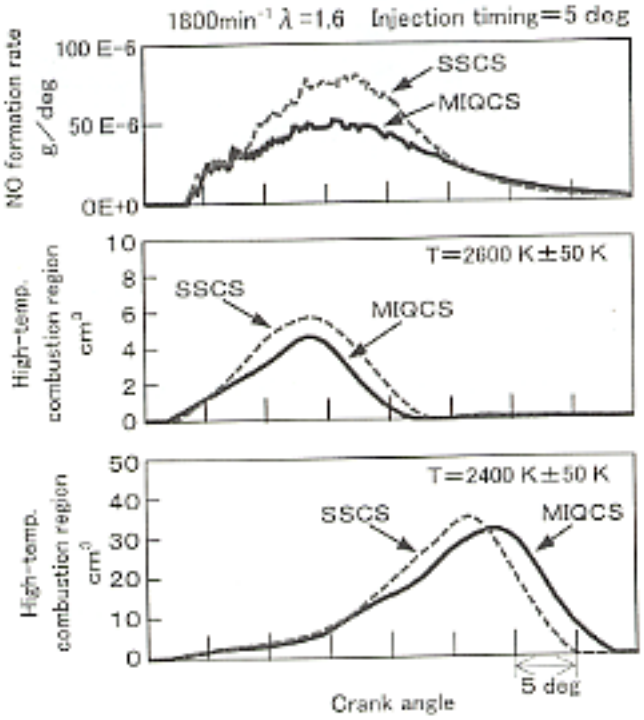

Fig. 15 Results of numerical analyses of combustion

perature (2600 ± 50 K) occurring in the first half of the combustion cycle was smaller with the MIQCS than with the SSCS and that the NOx formation rate during this period was lower with the MIQCS than with the SSCS. These results were consistent with those of the combustion observations.

Further, the results of the calculations showed that combustion in the second half of the combustion cycle was more vigorous with the MIQCS than with the SSCS. Superior recombustion of soot owing to more vigorous combustion late in the cycle can be interpreted as one reason for the MIQCS's relatively low emissions of black smoke.

5. Application of EGR to MIQCS

It was believed that EGR[11] would be effective as a means of further reducing NOx emissions and fuel consumption with the MIQCS. Therefore, investigation was made into the influence of an EGR system.

5.1 EGR system

The EGR system of the test engine is shown in Fig. 16.

The engine was equipped with a variable-geometry (VG) turbocharger. Control of the EGR rate was effected by coordinated control of the VG turbocharger and EGR valve.

Exhaust gases were recirculated using a high-pressure-loop arrangement that drew the gases from the upstream side of the turbocharger and returned them to the downstream side of the intercooler.

5.2 Effects of increases in EGR rate

The results of tests performed with EGR to establish the possibility of further reductions in NOx emissions are shown in **Fig. 17**. During both low-load operation and high-load operation, increases in the EGR rate caused NOx emissions to decrease but caused fuel consumption and black-smoke emissions to increase. Nevertheless, the fuel consumption and black-smoke emissions of the MIQCS were better than those of the SSCS with all EGR rates. It was thus clear that the MIQCS and an EGR system could be used together to realize not only superior NOx emissions but also minimal fuel consumption and black-smoke emissions.

5.3 Optimization of fuel-injection pressure during EGR application

Although EGR is an effective means of reducing NOx emissions, it typically exacerbates the production of black smoke and is thus unfavorable with regard to PM emissions. With a view to finding a means of simultaneously reducing NOx and PM emissions during application of EGR to the MIQCS, investigation was made into the influence of changes in the fuel-injection pressure. The results are shown in **Fig. 18**.

During both low-load operation and high-load operation, the application of EGR was accompanied by significant increases in fuel consumption and black-smoke emissions. Since the application of EGR was also accompanied by significant reductions in NOx emissions, however, it was possible to retain a NOx-reducing effect while using increases in the fuel-injection pressure to achieve lower fuel consumption and black-smoke emissions than those observed without EGR.

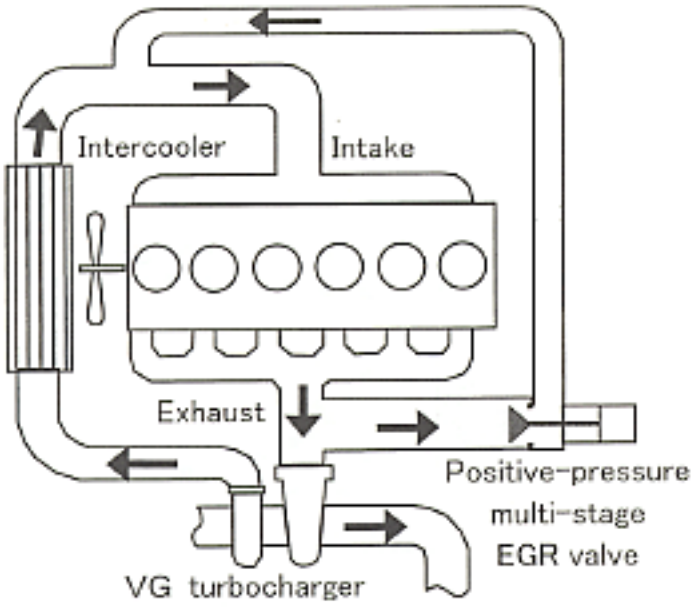

Fig. 16 EGR system

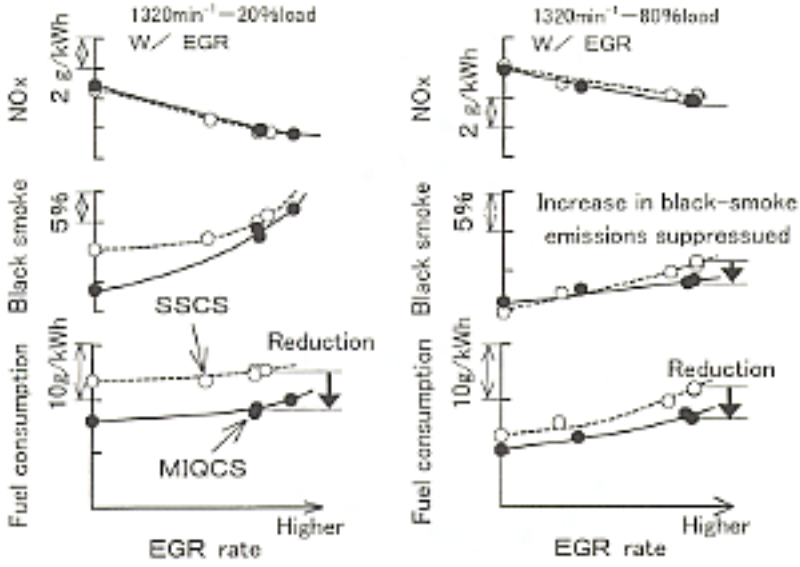

Fig. 17 Influence of EGR rate with MIQCS and SSCS

These findings indicated that an effective way to simultaneously reduce exhaust emissions and fuel consumption was to combine EGR with an injection system that allowed the injection pressure and injection timing to be controlled freely over the entire operating range. The common-rail high-pressure injection system used with the MIQCS allows a high degree of control over the injection timing and injection pressure, and it permits pilot injection and other forms of multi-stage injection. This system thus proved particularly valuable during the application of EGR.

6. Real-world potential of MIQCS

Since it was established that application of EGR to the MIQCS enabled simultaneous reduction of exhaust emissions and fuel consumption, full-load and 13-mode exhaust-emissions tests were conducted to ascertain the real-world potential of this technology.

6.1 Full-load performance

Comparison was made of the full-load characteristics of the MIQCS and SSCS with each combustion system's fuel-injection pressure, fuel-injection timing, turbocharger-vane opening, and EGR-valve opening set for compliance with Japan's long-term exhaust emission standards. The results are shown in **Fig. 19**.

(1) Fuel consumption

The MIQCS achieved lower fuel consumption than the SSCS at all engine speeds. Its minimum fuel consumption was 2 % lower than that of the SSCS, and its concurrent thermal efficiency was relatively high at 45

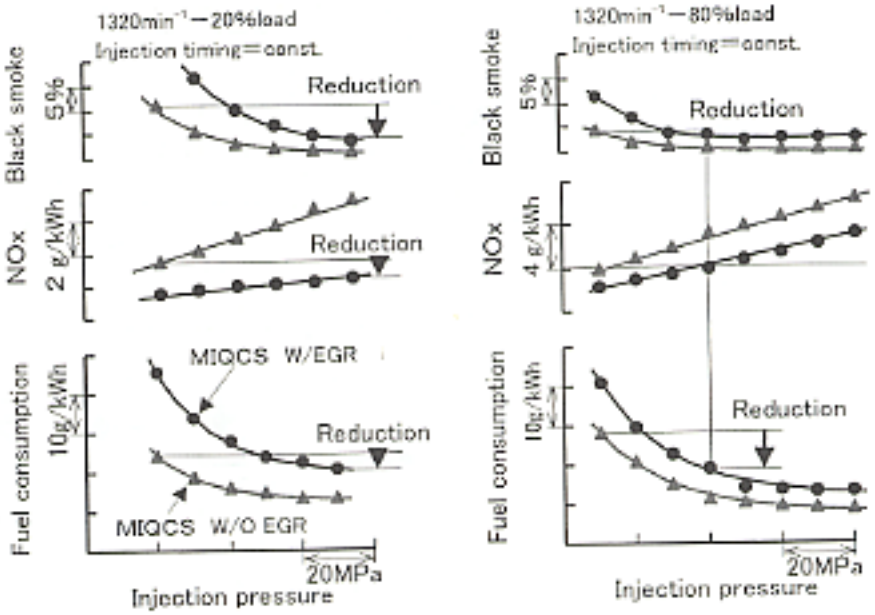

Fig. 18 Influence of rail pressure with and without EGR

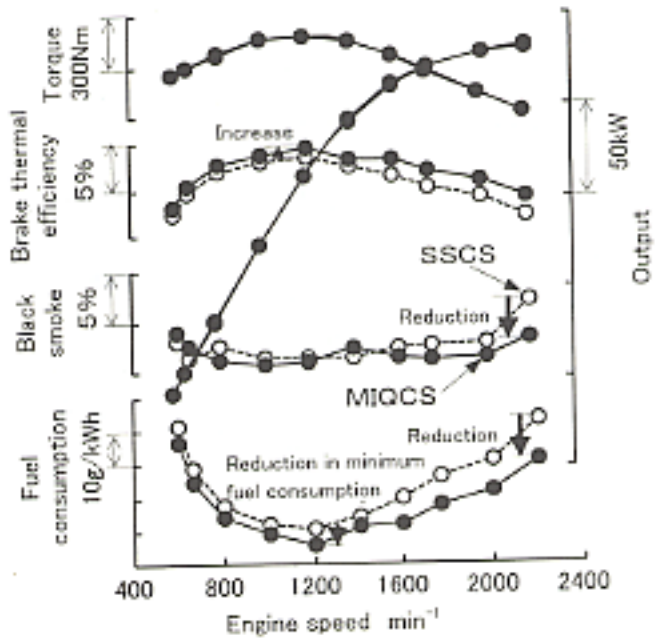

Fig. 19 Full-load performance

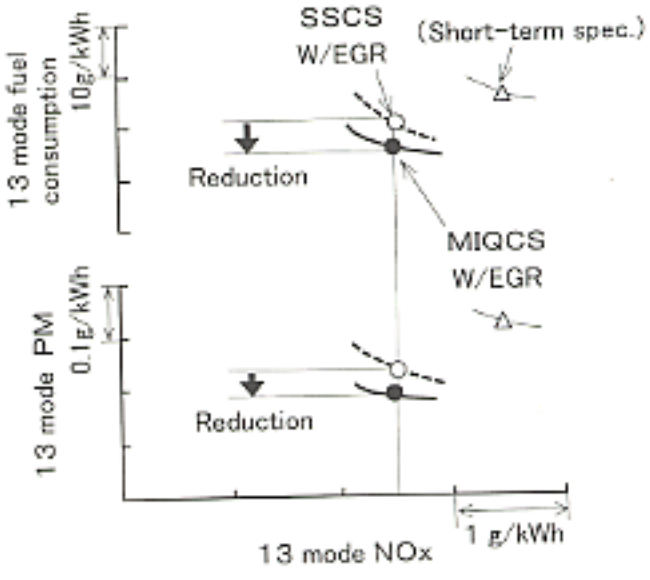

Fig. 20 Exhaust emissions and fuel consumption in Japan's 13-mode test cycle

%. The MIQCS also achieved a significant reduction in fuel consumption at the output point. Clearly, the MIQCS proved an extremely effective means of minimizing fuel consumption.

(2) Black-smoke emissions

The MIQCS achieved lower black-smoke emissions than the SSCS at all engine speeds and performed particularly well toward the high end of the speed range. Indeed, it achieved virtually smokeless engine operation at most engine speeds. Since black smoke is the main contributor to PM, the MIQCS is clearly an effective means of minimizing PM emissions.

6.2 Performance in 13-mode test cycle

To more fully ascertain the MIQCS's potential for minimized exhaust emissions, comparison was made of the exhaust emissions of the MIQCS and SSCS in Japan's 13-mode test cycle. The results are shown in Fig. 20.

The MIQCS realized lower PM emissions and fuel consumption than the SSCS with any given level of NOx emissions. Its emissions levels were low enough to satisfy Japan's long-term exhaust emission standards, and its fuel consumption was lower than that of an engine complying with Japan's short-term regulations.

Toward the low end of the NOx-emission range, the MIQCS's merits with respect to reduction of fuel consumption and PM emissions will become increasingly

significant. The MIQCS clearly has greater potential than the SSCS for further improvements in the NOx/PM/fuel-consumption trade-off that will be necessary for future reductions in fuel consumption and exhaust emissions.

7. Summary

(1) The MIQCS (a QCS combined with a CRS) is superior to the widely used SSCS with regard to simultaneous reduction of exhaust emissions and fuel consumption.
(2) Compared with the SSCS, the MIQCS effects less initial premixed combustion and has a lower combustion temperature. These factors are apparently responsible for the MIQCS's lower NOx emissions.
(3) The application of EGR yields greater reductions in NOx emissions with the MIQCS than with the SSCS. And concomitant increases in black-smoke emissions can be suppressed more effectively with the MIQCS than with the SSCS.
(4) The CRS, which offers a high degree of freedom in control over injection characteristics, is particularly effective as a means of reducing NOx emissions and suppressing concomitant increases in black-smoke emissions when combined with EGR.
(5) The MIQCS has sufficient potential for future reductions in NOx emissions, and it is capable of reducing fuel consumption sufficiently for compliance with Japan's long-term exhaust emission standards.

References

(1) K. Mori, et al.: "Worldwide Trends in Heavy-Duty Diesel Engine Exhaust Emission Legislation and Compliance Technologies", SAE Paper 970753
(2) P. Zelenka, et al.: "Cooled EGR a Key Technology for Future Efficient HD Diesels", SAE Paper 980190
(3) W. P. Cartellieri, et al.: "Swirl Supported or Quiescent Combustion for 1990's Heavy-Duty DI Diesel Engines – An Analysis", SAE Paper 860342
(4) K. Kunberger,: "New Medium-Speed Diesel Designed to Combine Economy with Ecology Features", Diesel & Gas Turbine Worldwide, July – August, 1993
(5) H. Hiroyasu, et al.: "Structures of Fuel Spray in Diesel Engines", SAE Paper 900475
(6) M. Schitter, et al.: "Leistungsmerkmale der neuen Nutzfahrzeugmotoren OM 501 LA und OM 502 LA von Mercedes-Benz", MTZ, Vol. 57, No. 11
(7) Y. Yamaki, et al.: "Heavy duty diesel engine with common rail type fuel injection system", IPC-8, No. 9530139
(8) Y. Fujino, et al.: "New Mitsubishi V8 19 L turbocharged and intercooled diesel engine", SAE Paper 971673
(9) H. Nakajima, et al.: "The Analysis of Flame in DI Diesel Engine – Part 3: Measurement and Analysis of Flame Temperature", JSAE Vol. No. 945
(10) R. J. Donahue, et al.: "Cylinder-Averaged Histories of Nitrogen Oxide in a DI Diesel with Simulated Turbocharging", SAE Paper 942046
(11) S. Kohketsu, et al.: "EGR Technologies for a Turbocharged and Intercooled Heavy-Duty Diesel Engine", SAE Paper 970340


Hiroshi JYOUTAKI


Kenji SAKAI


Masayuki TAKAHASHI


Kenji KAWAI


Kazutoshi MORI

TECHNICAL PAPERS

Effects on Reduction of Exhaust Emissions of Flexibly Controlled Fuel Injection Rate Shape with Next Generation Common Rail Fuel Injection System (NCRS)

Keiki TANABE* Susumu KOHKETSU*
Koji MORI* Kenji KAWAI*

Abstract

A next generation common rail fuel injection system (NCRS) has been designed and the effects on exhaust emissions and fuel consumption of a controlled fuel injection rate shape were examined using the prototype system. The system comprises two common rails – one for high fuel pressure; the other for low fuel pressure – and this allows the shape of fuel injection rate to be optimally controlled by switching the pressure of the fuel delivered to fuel injectors from low to high while said fuel is being injected. It was confirmed that favorable results could be accomplished with regard to both exhaust emissions and fuel consumption through the use of this system since control of the shape would make it possible to control the condition of combustion, and consequently, to improve the trade-off between NOx and fuel consumption, as well as between NOx and particulate matter.

Key words: *Diesel Engine, Fuel Injection, Combustion, Emissions*

1. Introduction

Standards on the exhaust emissions of diesel engines are becoming increasingly stringent around the world, necessitating ever-greater reductions in exhaust emissions, fuel consumption, and noise. To enable the necessary reductions, it is necessary to employ fuel injection systems with a wide range of capabilities including high-pressure injection, independent control of the injection pressure and injection timing, and control of the injection rate shape.

The common rail system (CRS), which allows independent control of the injection pressure and injection timing and is not restricted by the engine speed and loading[1][2], is an increasingly popular choice of fuel injection system for mass-produced automotive diesel engines[3][4]. However, it is important to note that the CRS gives an almost square fuel injection rate shape and that its initial injection quantity is greater than that of systems employing jerk type fuel injection system; it is not necessarily ideal for reduction of NOx emissions and combustion noise.

Optimized control of the fuel injection rate shape is well known as a highly effective means of reducing exhaust emissions, fuel consumption, and combustion noise[5] - [7]. Thus, adding some means of controlling the fuel injection rate shape to the CRS, which already permits a high degree of freedom in control of the injection pressure and injection timing, would in theory yield greater flexibility than that offered by other fuel injection systems with regard to further reductions in permitted exhaust emissions and fuel consumption.

In light of the above mentioned potential benefits, the authors conceived a next generation common rail fuel injection system (NCRS) capable of controlling the fuel injection rate shape. In the development of the NCRS, a prototype suitable for a single-cylinder engine was first constructed and its influence on exhaust-emissions characteristics and combustion characteristics was investigated. The findings from the investigation showed that appropriate control of the injection rate shape had a significant reducing effect on exhaust emissions and fuel consumption. It was thus confirmed that the NCRS had significant potential as a means of reducing the exhaust emissions and fuel consumption of diesel engines and that it was a viable fuel injection system for future use.

2. NCRS concept

2.1 Methods for control of injection rate shape with CRS

With the CRS, the injection rate can be controlled by changing the common rail pressure but the basic injection rate shape cannot be changed from square. One conceivable way to change the injection rate shape as desired is to effect control over the injection pressure during the injection period. One conceivable way to realize such control with the CRS is to vary the pressure of fuel supplied to the injectors during the injection peri-

* Engine Research Dept., Truck & Bus Dev. Office

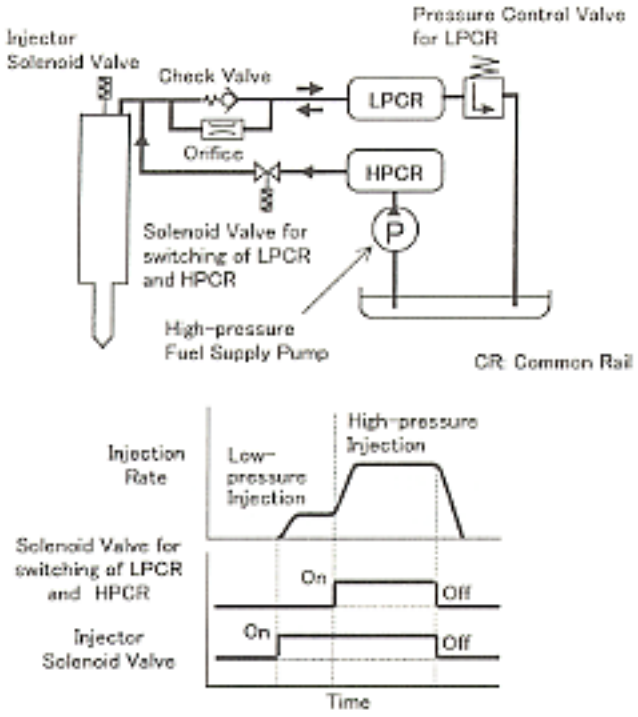

Fig. 1 Schematic diagram of NCRS

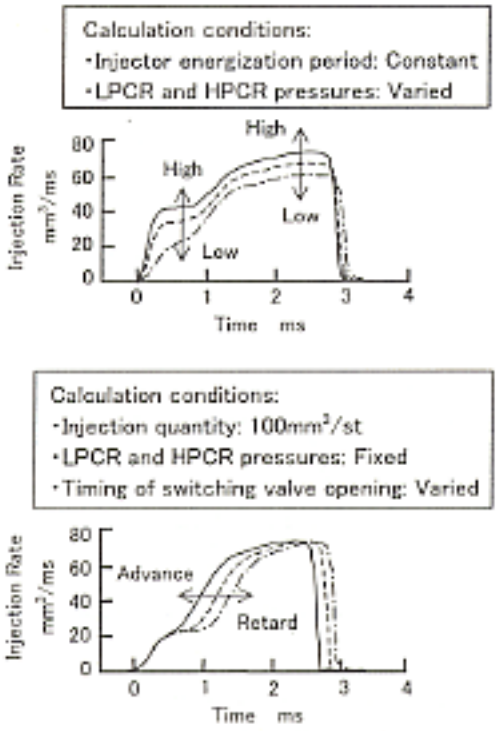

Fig. 2 NCRS injection rate shapes (calculated)

od. Another is to spill off high-pressure fuel for a fixed portion of the injection period such that injection takes place at a pressure lower than the common rail pressure. Compared with injection rate control methods that depend on control of the needle lift, these pressure control methods are superior because they make it possible to prevent inconsistent needle-to-seat clearances and differences in injection quantity between nozzle holes and because they make it possible to prevent deterioration in fuel spray .

2.2 Overview of NCRS

The configuration and operating method of the NCRS are shown in **Fig. 1**. The NCRS has two common rails: one each for high-pressure and low-pressure fuel. It controls the injection rate shape by switching the source of fuel supplied to the injectors from the low-pressure common rail (LPCR) to the high-pressure common rail (HPCR) during the injection period. In addition to the LPCR and HPCR, the NCRS's main elements are injectors; a high-pressure fuel supply pump; a pressure control valve used to control the pressure in the LPCR; and a switching valve used to change the source of fuel supplied to the injectors from the LPCR to the HPCR. The LPCR, the LPCR's pressure control valve, and the switching valve are not included in the conventional CRS configuration.

As shown in **Fig. 1**, the NCRS controls the injection rate shape by switching the fuel supplied to the injectors from low-pressure to high-pressure. The injectors are supplied with fuel from the LPCR from the start of injection, so initial injection takes place at the lower pressure. When a predetermined period of time has elapsed from the start of injection, the switching valve opens such that injection takes place using fuel from the HPCR. The NCRS is capable of controlling the pressure in the LPCR, the pressure in the HPCR, and the switchover timing independently. By selecting appropriate values for these variables, it is possible to achieve a range of injection rate shapes.

2.3 NCRS simulation

The NCRS is relatively complex in hydraulic-system terms. Before construction of a system for test purposes, therefore, it was necessary to establish the specifications of components (for example, the injection-pipe diameter and length, the CR volumes, and the orifice diameter) as accurately as possible. To establish these specifications, computer simulations[5] were used to ascertain the influence of each parameter on the injection rate shape.

Figs. 2 and **3** show the results of the computer simulations. Specifically, **Fig. 2** shows the results of a simulation performed to verify the NCRS's ability to control the injection rate shape and **Fig. 3** shows the results of a simulation performed as a parameter study to ascertain the influence of the injection-pipe length.

3. Results of rig tests

In accordance with the component specifications established through the simulations, an NCRS test rig was constructed such that it was capable of handling the injection quantities of a heavy-duty diesel engine. Then this test rig was used to examine the NCRS's injection rate shape.

Fig. 4 shows the typical injection rate shape and injector inlet pressure (during operation) of the NCRS and those of the conventional CRS. The injector inlet

Calculation conditions:
- Injector energization period: Constant
- HPCR pressure: 120MPa
- Length of pipe between HPCR and switching valve: Varied

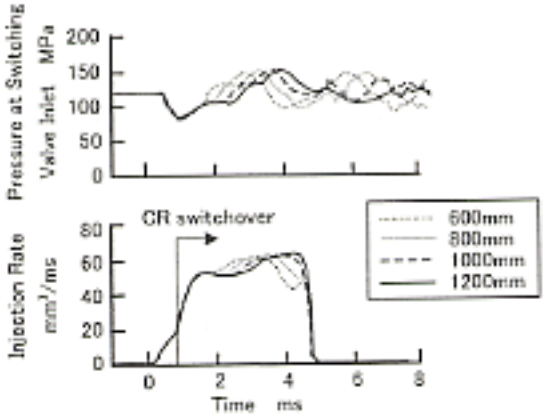

Fig. 3 Effect of injection-pipe length (calculated)

pressure with the conventional CRS was more-or-less constant in line with the CR pressure in the area near the start of injection, and the conventional CRS produced a quasi-square injection rate shape. By contrast, the injector inlet pressure with the NCRS changed from low to high during the injection period, yielding a boot type injection rate shape.

The NCRS was designed to cause high-pressure fuel remaining between the switching valve and injectors after injection to be introduced via an orifice into the LPCR such that the injector inlet pressure is reduced to the LPCR's set-pressure level ready for the next injection cycle and such that the same residual high-pressure fuel is reused as a supply source for the LPCR. This arrangement allows the NCRS to function with only one fuel pump (for the HPCR), so the NCRS can be fitted to an engine in place of the conventional CRS with a minimum of engine modifications.

Fig. 5 shows differences in the NCRS's injection rate shape resulting from changes in the LPCR pressure and in the timing of switching valve opening. Since the NCRS permits the LPCR pressure, the HPCR pressure, and the timing of switching valve opening to be controlled independently, it was possible to achieve boot type, delta type, and other types of injection rate shape without inconsistency. Although the results are not shown in Fig. 5, it was also possible (by causing the switching valve to open before the injector valve) to achieve a quasi-square injection rate shape like that of the conventional CRS.

4. Results of engine tests and study thereof

The NCRS was applied to a research-use single-cylinder diesel engine (displacement: two liters) and verification was conducted to clarify the effects on exhaust emissions and fuel consumption of control over the injection rate shape. The specifications of the engine and injection system are shown in Table 1.

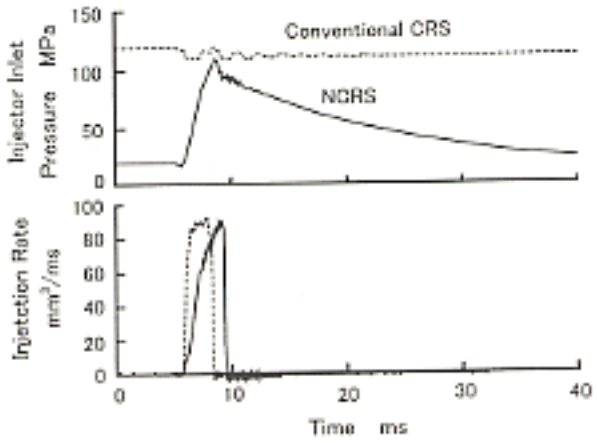

Fig. 4 Typical NCRS injection rate shape and injector inlet pressure (results of rig test)

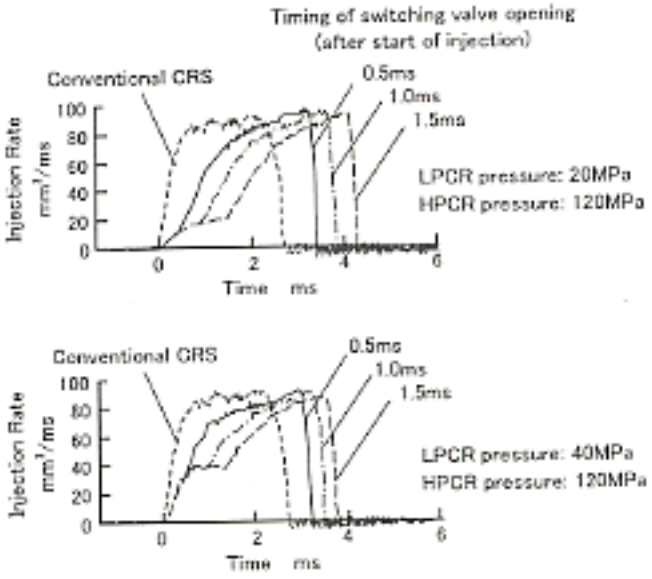

Fig. 5 NCRS injection rate shapes (results of rig tests)

Since the NCRS offers a high degree of control freedom and has a large number of injection rate shape control parameters, it was necessary before any engine tests to logically establish relevant parameters as narrowly as possible in accordance with engine operating conditions with a view to realizing the optimum injection rate shape. For research purposes, a medium speed and a high degree of loading were selected as representative engine operating conditions. With these conditions established and the timing of switching valve opening fixed at 0.5 ms after the start of injection, the LPCR pressure and HPCR pressure were varied and the effects on exhaust emissions and fuel consumption were examined. The 0.5 ms timing selected for switching valve opening corresponds to the average ignition delay period in a diesel engine running at a medium speed under high loading. Thus, varying the LPCR pressure had the effect of varying the quantity of fuel injected during the ignition delay period, i.e., the initial injec-

Table 1 Engine specifications

Engine type	Direct injection, single cylinder, four cycle, naturally aspirated
Bore x stroke	φ135 mm x 140 mm
Displacement	2004 cc
Cylinder head	2 inlet, 2 exhaust valves
Compression ratio	17.5
Swirl ratio	2.2
Fuel-injection system	NCRS prototype
Fuel-injection nozzle	φ0.235 mm x 5
Switching valve seat diameter and lift	φ2 mm – 0.35 mm

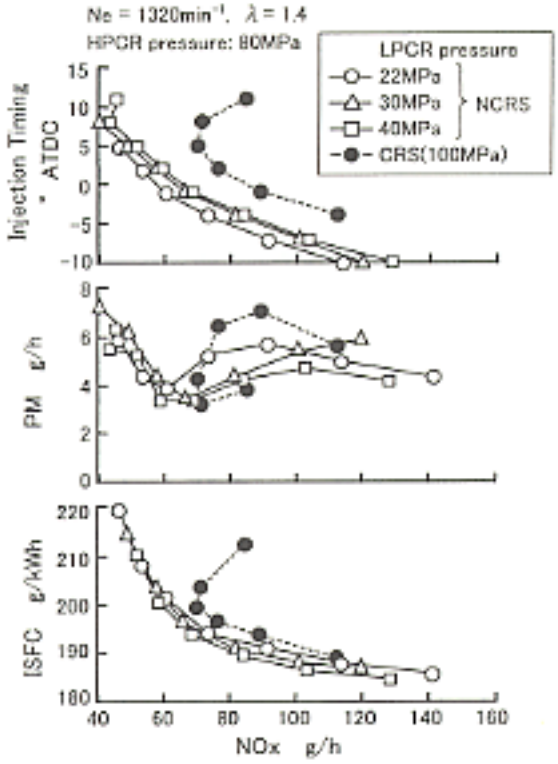

Fig. 6 Effect of LPCR pressure on trade-offs

tion quantity. All conventional CRS test results shown hereafter for reference were obtained with a CR pressure of 100 MPa.

4.1 Influence of LPCR pressure

Examined first were the exhaust emissions characteristics and fuel consumption achieved with different levels of LPCR pressure. **Fig. 6** shows the NOx/fuel-consumption and NOx/PM trade-offs achieved with the injection timing varied under each the following sets of conditions: LPCR pressure of 22 MPa and HPCR pressure of 80 MPa; LPCR pressure of 30 MPa and HPCR pressure of 80 MPa; and LPCR pressure of 40 MPa and HPCR pressure of 80 MPa. The benefits of the NCRS's injection rate shape control were, as shown, evident in NOx/fuel-consumption and NOx/PM trade-offs that were superior to those of the conventional CRS with

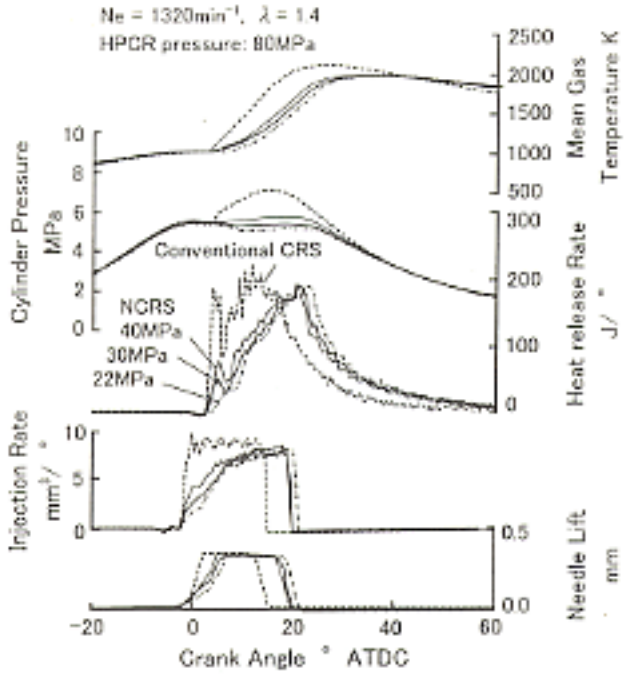

Fig. 7 Effect of LPCR pressure on heat release rate

every level of LPCR pressure.

Fig. 7 shows the heat release rates and injection rate shapes achieved with the injection timing fixed at −1°after top dead center (ATDC) and with the LPCR and other parameters established as in **Fig. 6**. Comparison of the NCRS's and conventional CRS's respective heat release rates reveals that the amount of premixed combustion was significantly smaller with the NCRS than with the conventional CRS. The amount of premixed combustion was significantly smaller with the NCRS because control of the LPCR pressure kept the initial injection quantity relatively small (as can be seen from the injection rate shapes). The NCRS's superior trade-offs shown in **Fig. 6** can thus be attributed to the NCRS's injection rate shape control.

The LPCR pressure with which the NCRS yielded the greatest improvements in the trade-offs was 40 MPa. Comparison of the heat release rates reveals that increases in the LPCR pressure caused slight increases in the amount of premixed combustion but also caused the heat release rate during diffusion combustion to rise earlier, yielding significant improvements in the diffusion combustion area. These phenomena were apparently responsible for simultaneous reductions in fuel consumption and PM emissions.

These findings indicated that merely reducing the initial injection quantity and pressure was not sufficient and that, rather, it was necessary to establish the optimum conditions taking activation at the beginning of diffusion combustion (following premixed combustion) into account.

4.2 Influence of HPCR pressure

Examined next were the effects of different levels of HPCR pressure. **Fig. 8** shows the trade-offs achieved with HPCR pressures of 80 MPa, 100 MPa, and 120 MPa.

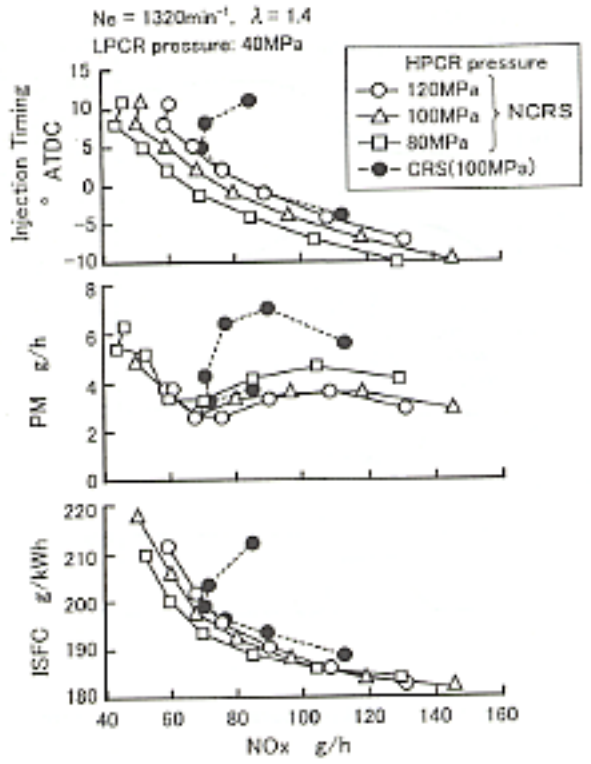

Fig. 8 Effect of HPCR pressure on trade-offs

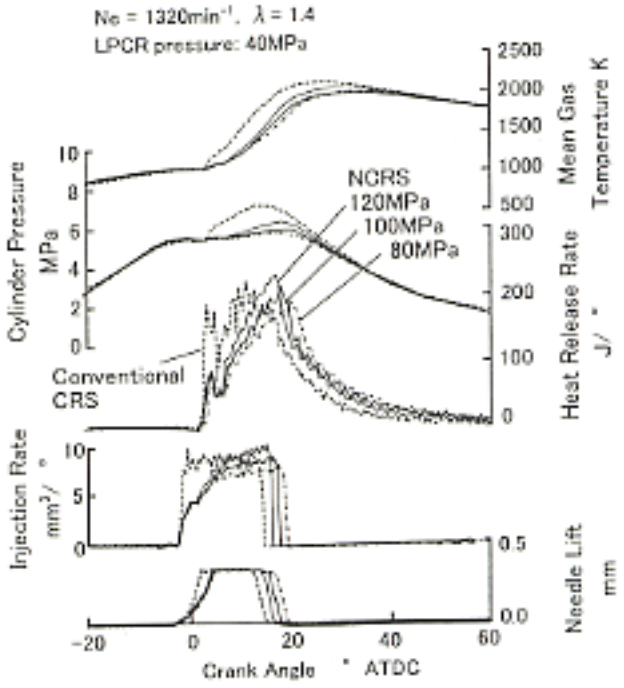

Fig. 9 Effect of HPCR pressure on heat release rate

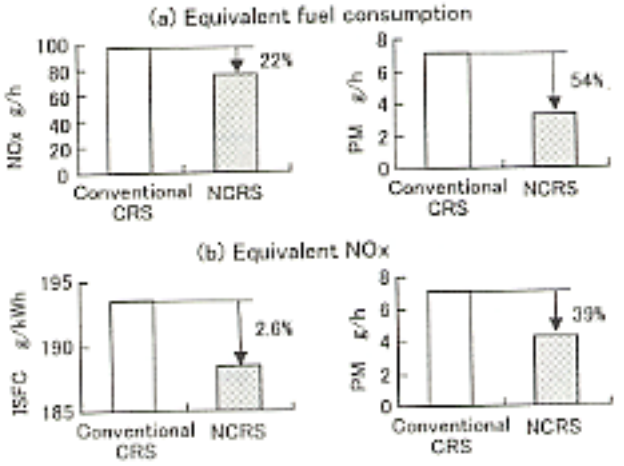

Fig. 10 Reductions in exhaust emissions and fuel consumption realized by control of injection rate shape with NCRS

With each test, the LPCR pressure was fixed at 40 MPa (the level that yielded the lowest exhaust emissions and fuel consumption in the tests described earlier). The results reflected those of the earlier tests, with the NCRS's injection rate shape control yielding NOx/fuel-consumption and NOx/PM trade-offs that were superior to those of the conventional CRS with every level of HPCR pressure.

With the NCRS, the NOx/fuel-consumption trade-off was better with lower HPCR pressures than with higher ones but the NOx/PM trade-off was, conversely, better with higher HPCR pressures than with lower ones. The reasons for these phenomena can be ascertained from **Fig. 9**, which shows the heat release rates and injection rate shapes achieved with the injection timing fixed at −1°ATDC and with the HPCR and other parameters established as in **Fig. 8**. Irrespective of changes in the HPCR pressure, the LPCR pressure and initial injection quantity were fixed, meaning that the amount of premixed combustion did not change. Thus, the HPCR pressure's effects on exhaust emissions and fuel consumption can be attributed to diffusion combustion. Since diffusion combustion became more active and the heat release rate peak concomitantly became higher as the HPCR pressure was increased, it can be inferred that diffusion combustion improvements yielded by high-pressure injection in the latter half of the injection cycle corresponded to the NOx/PM-trade-off improvements shown in **Fig. 8**. However, NOx formation is apparently promoted by activation of diffusion combustion; with any given level of NOx emissions shown in **Fig. 8**, it was necessary to retard the injection timing, leading to increased fuel consumption.

4.3 Benefits of injection rate shape control during operation at medium-speed with high loading

From the results of the aforementioned tests performed with the LPCR and HPCR pressures as parameters, it was established that the greatest improvements in the NOx/fuel-consumption trade-off and NOx/PM trade-off could be achieved with an LPCR pressure of 40 MPa and an HPCR pressure of 80 MPa. **Fig. 10** indicates the superiority of the NCRS over the conventional CRS with equivalent levels of fuel consumption and NOx emissions. The fuel consumption and PM emissions of the NCRS were respectively 2.6 % lower and 39 % lower than those of the conventional CRS with equivalent

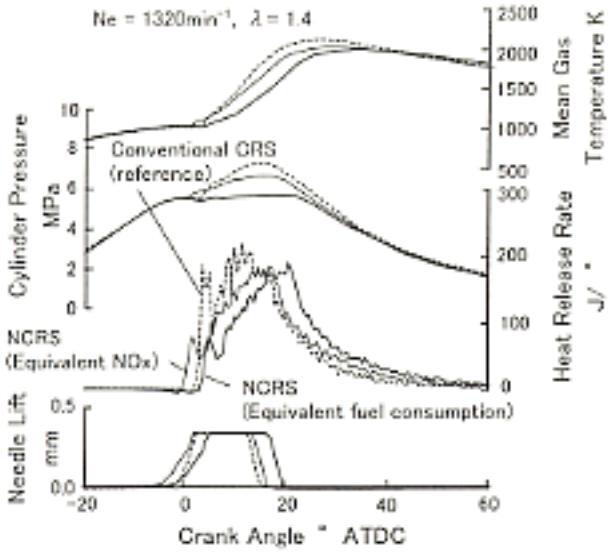

Fig. 11 Comparison of heat release rates

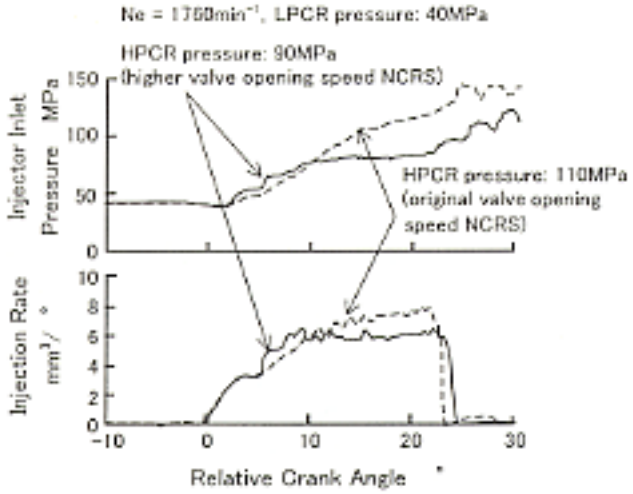

Fig. 12 Effect of injection rate slope during main injection

NOx emissions. And the NOx emissions and PM emissions of the NCRS were respectively 22 % lower and 54 % lower than those of the conventional CRS with equivalent fuel consumption. The heat release rates are shown in **Fig. 11**. The NCRS's lower NOx emission with equivalent fuel consumption are attributable to the NCRS's relatively small amount of premixed combustion, and the NCRS's lower fuel consumption with equivalent NOx emission is attributable to the NCRS's ability to operate with relatively advanced injection timing. The NCRS is capable of reducing NOx emissions without increasing fuel consumption apparently because it realizes combustion in a near-ideal diesel cycle combustion, in which the absence of rapid increases in cylinder pressure can be seen in the graphs in this paper.

4.4 Effect of injection rate slope during main injection

One possible method for control of diffusion combustion with the NCRS is variation of the HPCR pressure. Another is variation of the injection rate slope during main injection. The NCRS's switching valve employs a two-way, high-pressure valve mechanism similar to that of an injector[9]. In this mechanism, two control orifices are used to determine the fuel pressure acting on a control piston, which in turn controls the timing of valve opening and closing. Thus, it is possible to change the switching valve's opening speed by changing the control orifices. By the use of this technique to change the switching valve's opening speed, the injection rate slope was increased during main injection and the effects on exhaust emissions and fuel consumption were examined.

Fig. 12 shows the respective injection rate shapes with different speeds of switching valve opening NCRSs. The LPCR pressure of both NCRSs was fixed at 40 MPa. The HPCR pressure of the NCRS with the higher-valve-opening speed was 90 MPa, and that of the NCRS with the lower, original valve-opening speed was 110 MPa. Since the higher-valve-opening-speed NCRS had a relatively low HPCR pressure, its injection rate was, as shown in **Fig. 12**, lower than that of the original-valve-opening-speed NCRS in the latter half of main injection. However, the higher-valve-opening-speed NCRS yielded a relatively steep injection rate slope immediately after the start of main injection and its injection rate was higher than that of the original-valve-opening-speed NCRS in the period until 10°. Also, lengthening of the injection period with the higher-valve-opening-speed NCRS was negligible.

Fig. 13 shows the respective NOx/fuel-consumption and NOx/PM trade-offs of the two aforementioned NCRSs with high-speed, high-load engine operation. Despite its relatively low HPCR pressure, the higher-valve-opening-speed NCRS realized a NOx/PM trade-off comparable with that of the original-valve-opening-speed NCRS. It can be seen, for example, that for any given level of NOx emissions the higher-valve-opening-speed NCRS (which had an HPCR pressure of 90 MPa) kept PM emissions down to approximately the level realized by the original-valve-opening-speed NCRS (which had an HPCR pressure of 110 MPa). In other words, the increase in the injection rate slope realized the same benefit as 20 MPa of injection pressure. At the same time, the NOx/fuel-consumption trade-off of the higher-valve-opening-speed NCRS was better than that of the original-valve-opening-speed NCRS owing, as explained in part 4.2 of this paper, to the lower HPCR pressure.

Fig. 14 shows the respective heat release rates of two NCRSs with the same injection timing of –4°ATDC. The higher-valve-opening-speed NCRS realized a higher heat release rate than the original-valve-opening-speed NCRS during the first half of diffusion combustion, and its combustion period was relatively short. The ability of the higher-valve-opening-speed NCRS to reduce PM emission to approximately the level realized by the original-valve-opening-speed NCRS while realizing superior fuel efficiency was apparently attributable to these factors.

From the aforementioned results, it was verified that

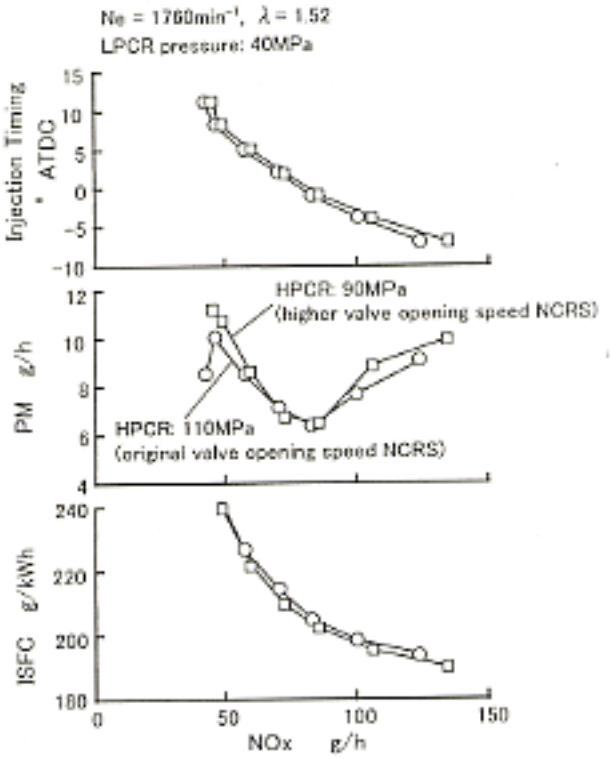

Fig. 13 Effect on trade-offs of injection rate slope during main injection

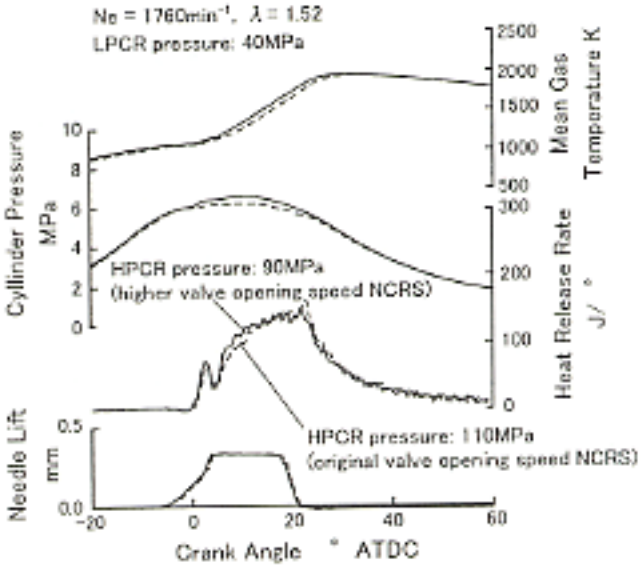

Fig. 14 Effect on heat release rate of injection rate slope during main injection

increasing the injection rate slope during main injection activated the first half of diffusion combustion, enabling a shorter combustion period even with a relatively low main injection pressure and realizing approximately the same PM-reducing effect as a higher main injection pressure.

5. Summary

The authors made a prototype of the NCRS, an injection system that enables control of the injection rate shape by changing the pressure of the fuel supplied to the injectors during the injection period. This system was applied to a single-cylinder engine and investigation was conducted to clarify the influence of injection rate shape control on exhaust emissions and on the heat release rate. The results were as follows:

(1) It was possible to control the heat release rate by controlling the injection rate shape with the NCRS. Varying the LPCR pressure yielded control primarily over premixed combustion, and varying the HPCR pressure yielded control primarily over diffusion combustion.

(2) Injection rate shape control had a reducing effect on both exhaust emissions and fuel consumption. Under medium-speed, high-load conditions, the NOx/fuel-consumption and NOx/PM trade-offs were both better with the NCRS than with the conventional CRS. With equivalent fuel consumption, NOx emissions were 22 % lower with the NCRS. And with equivalent NOx emissions, fuel consumption was 2.6 % lower with the NCRS.

(3) An increase in the switching valve's opening speed and a concomitant increase in the injection rate slope during main combustion made it possible to increase the heat release rate in the first half of diffusion combustion, resulting in a PM reduction similar to that achievable with an increase in the injection pressure.

References

(1) Funai, K., Yamaguchi, T., Itoh, S.: "Injection Rate Shaping Technology With Common Rail Fuel System (ECD-U2)", SAE Paper 960107

(2) Kato, T., Koyama, T., Sakai, K., Mori, K. J., Mori, K. Z.: "Common Rail Fuel Injection System for Improvement of Engine Performance on Heavy-Duty Diesel Engine", SAE Paper 980806

(3) Yamaki, Y., Mori, K. Z., Kamikubo, H., Kohketsu, S., Mori, K. J., Kato, T.: "Application of Common Rail Fuel Injection System to a Heavy-Duty Diesel Engine", SAE Paper 942294

(4) Fujino, Y., Itabashi, K., Kamikubo, H., Takami, K.: "New Mitsubishi V8 19-Liter Turbocharged and Intercooled Diesel Engine", SAE Paper 971673

(5) Erlach, H., Chmela, F., Cartellieri., W., Herzog, P.: "Pressure Modulated Injection and its Effects on Combustion and Emissions of a HD Diesel Engine", SAE Paper 952059

(6) Wakisaka, Y., Azetsu, A., Oikawa, C.: "Effect of Fuel Injection Rate Shaping on Spray Combustion – Effect of Slope of Injection Rate Rise on Spray Combustion", The 14th Internal Combustion System Symposium paper collection, No. 9737563

(7) Takahashi, Sato, Itoh, Nishimura, Yokota: "Effect of Fuel Injection Rate on Combustion and Emissions in a DI Diesel Engine", The 14th Internal Combustion System Symposium paper collection, No. 9737635

(8) Tanabe, K., Kohketsu, S., Mori, K., Koyama, T.: "Computer Simulation of Fuel Injetion Characteristics in a Common Rail System", JSAE symposium proceedings, No. 9838066

(9) Kato, T., Koyama, T., Sasaki, K., Kawai, K.: "Improvement in Engine Performance and Exhaust Emission of Heavy-Duty Diesel Engines by Using a Common Rail Fuel Injection System", Mitsubishi Motors Technical Review, NO. 11, 1999


Keiki TANABE


Susumu KOHKETSU


Koji MORI


Kenji KAWAI

TECHNICAL PAPERS

Development of Prediction Method for Performance of Cooling Air Flow in Engine Compartment Using Computational Fluid Dynamics

Tatsuya OHSHIMA* Tetsuji UKITA* Minoru YAMAMOTO*

Abstract

A prediction method for the performance of the cooling air flow in an engine compartment has been developed using computational fluid dynamics (CFD) for implementation at the design model stage. To reduce the number of grid of computational models and the amount of CPU time required for analysis, we adopted a mathematical model for the cooling fan based on axial-flow fan theory, and we improved the model to be able to predict the flow field with accuracy; furthermore, this was done as a means of achieving maximum efficiency from the cooling fan. The computational model mentioned above was created by combining an external flow analytic grid with an engine compartment model, and as a result of this, the time required for model creation was reduced, thus ensuring that this prediction method may be easily applied at the early stage of vehicle development.

Key words: *Cooling, Engine Compartment, Computational Fluid Dynamics*

1. Introduction

The performance of the cooling air flow in a vehicle's engine compartment is a major factor determining the efficiency with which the radiator and cooler condenser are cooled and thus has a significant influence on engine-cooling and air-conditioning performance. The manner in which air flows through the engine compartment also influences the vehicle's aerodynamic characteristics[1][2], so it is essential for engineers engaged in the development of any new vehicle to design an engine compartment that optimizes air-flow performance with respect to both cooling and aerodynamics. Engineers must also consider the vehicle's appearance: The vehicle's front end constitutes not only the engine compartment's air inlet but also an important styling element; a design reflecting an excessive emphasis on cooling and aerodynamic considerations can limit the vehicle's aesthetic potential. For both cooling performance and aesthetic quality to be optimized, it is essential for the performance of the cooling air flow in the engine compartment to be predicted with a high degree of accuracy at the design-model stage. The flow field in the engine compartment can be predicted by using computational fluid dynamics (CFD). This technique is extremely effective for simulation of the air flow in the engine compartment since it enables the influence of the vehicle's body shape and the influence of components in the engine compartment to be reflected in calculation results.

With a passenger car, engine cooling is generally most critical when the vehicle speed is low and the engine is heavily loaded, i.e., when the contribution to engine cooling of air drawn by the fan is greater than that of air pushed into the engine compartment by ram pressure. To ensure sufficient cooling efficiency under such conditions, engineers must be able to accurately predict the performance of the relevant cooling air flow. For this reason, some researches into flows of cooling air influenced by fans have recently been established[3][4].

With methods used thus far to predict air flow in an engine compartment, the effect of the fan has been defined only in terms of the fan's pressure-drop/flow (P-Q) characteristics. Such methods do not permit swirls in the fan's wake to be taken into account, so they do not make it possible to simulate the effects of the swirls on the flow field in the engine compartment. Since a flow field with swirls may differ from one without swirls in terms of air-flow resistance, the establishment of a method that allows the flow field around the cooling fan to contain swirls is a prerequisite for higher accuracy in predictions.

There are two conceivable methods for detailed analysis of the flow field around the fan. One method involves calculating in detail the flow field around the airfoils using a numerical analysis that simulates the shape of the fan. The other method involves mathematically determining the directional components of the kinetic momentum that results from rotation of the fan and introducing them into the momentum source term of fundamental equation.

The former method has been applied by Mitsubishi Motors Corporation (MMC) to truck-engine-compartment analysis using multiple rotating reference frames[5]. However, this method is time-consuming

* Performance Proving Dept., Car Research & Dev. Office

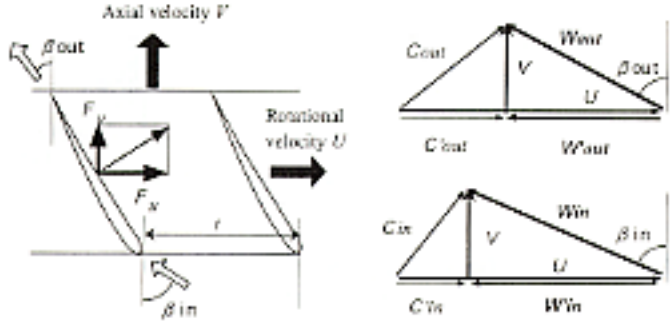

C : Absolute velocity
C' : Rotational component of absolute velocity
F : Force exerted by airfoil
U : Rotating velocity
V : Axial velocity
W : Relative velocity
W' : Rotational component of relative velocity
suffixes
in : Inlet
out : Outlet
u : Rotational direction
v : Axial direction

Fig. 1 Relationship between flow and force around airfoil

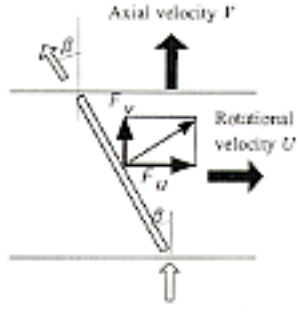

Fig. 2 Simplified model

since it necessitates calculation of the flow field around the blades with a high degree of accuracy and is thus accompanied by a significant increase in the number of grids and processing time. It is thus not suitable for use with passenger cars, which must be developed rapidly. The latter method is inferior to the former one in terms of accuracy in flow-field prediction, but it creates a smaller processing burden and is thus more suitable for vehicle development.

This paper discusses the use of the latter method in the development of a computational fan model that simulates experimentally obtained fan characteristics, and it describes the effectiveness of the model as applied to an actual car-design model.

The solver used for calculations was STAR-CD, a general purpose CFD code.

2. Modeling the cooling fan

2.1 Modeling an axial-flow fan

A vehicle's cooling fan usually operates under low loading, so is generally reasonable to regard the fan as an axial blower and to take only the kinetic-momentum components in the rotational and axial directions into account when modeling it. In accordance with this reasoning, the authors decided to model the cooling fan with respect to only the rotational and axial components of kinetic momentum. The modeling concept they adopted is described hereafter[6]. **Fig. 1** shows schematically the relationship between the flow and forces of fluid passing through a row of airfoils. The triangles in the figure are velocity diagrams. From these velocity diagrams, an equation (shown below) that defines the rotational force F_u acting on each airfoil is formulated taking the change in kinetic momentum of the fluid into account.

$$F_u = \rho V t (W'_{out} - W'_{in})$$
$$W'_{in} = U - V \tan \beta_{in}$$
$$W'_{out} = U - V \tan \beta_{out}$$

Here, U is the velocity in the rotational direction; V is the velocity in the axial direction; and W'_{in} and W'_{out} are the rotational-direction components of the airfoil's velocities relative to the air inlet and air outlet, respectively.

The axial-direction force F_v is generated by the difference in pressure between the inlet and outlet irrespective of any change in kinetic momentum, so it can be expressed using the following equation:

$$F_v = t(P_{in} - P_{out})$$

The force can also be expressed in terms of the velocity using the Bernoulli equation as follows:

$$F_v = \frac{\rho}{2} t \left(W'^2_{out} - W'^2_{in}\right)$$

The rotational-direction and axial-direction component forces thus defined are given to the basic momentum formula as an momentum source term.

When the air flow in an actual design model is calculated, the characteristics of the fan under study must be simulated and reflected in the calculation results. To enable simulation of the fan characteristics using the equations shown above, it is necessary to vary β_{in} and β_{out} in accordance with the fan's operating condition. However, it is not easy to determine β_{in} and β_{out} for different points on the fan's characteristic curve either by theoretical inference or by experimental approaches. To overcome this problem, a simplification technique is adopted in accordance with the assumption described hereafter.

It is postulated that a flat plate is placed in a flow field at an angle of β to the axis of flow as shown in **Fig. 2**. The incoming air is assumed to flow along the plate

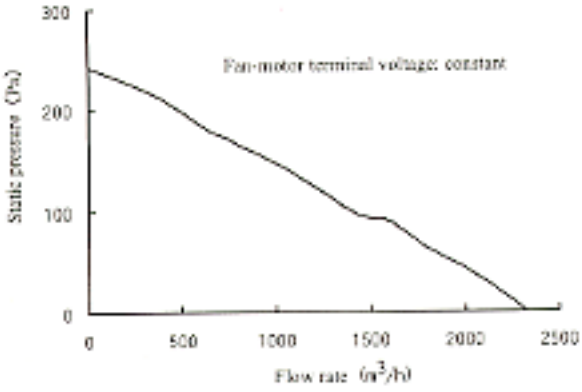

Fig. 3 Characteristic curve of axial-flow fan

at an angle of β to the axis of flow and not to involve any swirl component at any point on the fan's characteristic curve. It is also postulated that the fan's characteristics are simulated not by variation of the value of β but by variation of a separately introduced coefficient α in accordance with points on the characteristic curve[7]. Since W'_{in} is zero with this assumption, the rotational-direction component force F_u can be redefined as follows:

$$F_u = \alpha \{\rho Vt (U - V \tan \beta_{out})\}$$

Likewise, a simple geometric relationship consequential to this assumption allows the axial-direction component force F_v to be redefined by the following equation:

$$F_v = F_u \tan \beta$$

Handling of the experimentally obtained fan characteristics is described hereafter. When the air flow is calculated using the model, coefficient α is adjusted such that the calculated fan draft flow rate and the calculated pressure difference between the front and rear of the fan agree with those derived from the experimentally obtained fan characteristics. The pressures at the front and rear of the fan are represented by the average pressures at the inlet and outlet, respectively, of the fan shroud. The shroud's inlet and outlet typically have different opening areas. If the pressure difference was expressed in static-pressure terms, therefore, it would have to include factors that are affected by the fan and by the difference in opening area. Thus, the pressure difference between the front and rear of the fan is expressed in total pressure terms. For consistency, the experimental fan-characteristics data used for the abovementioned adjustment are blower total pressures rather than blower static pressures.

Fig. 3 shows the characteristic curve of an axial-flow fan typically used in vehicles. The data for this characteristic curve were collected using the apparatus shown in **Fig. 4**. Pressure *P* in **Fig. 4** is the blower static pressure, which is defined as the pressure difference between the chamber static pressure *Pc* and the atmospheric pressure *Patm*. Since the blower pressure used

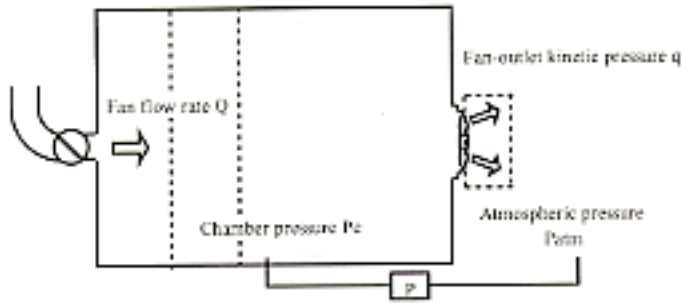

Fig. 4 Experimental apparatus for measurement of cooling-fan performance

with the calculation model needs to be a total pressure, the fan-characteristics data expressing the blower pressure in static-pressure terms are corrected in accordance with the following reasoning: The total pressure of the draft immediately after the fan is the sum of the chamber total pressure (equal to the static pressure) *Pc* and blower total pressure *Pt*. It is equal to the sum of the atmospheric pressure *Patm* and fan-wake kinetic pressure *q*. This relationship can be expressed as follows:

$$Pc + Pt = Patm + q$$

The blower total pressure *Pt* can therefore be expressed as follows:

$$Pt = (Patm - Pc) + q$$
$$= P + q$$

Thus, the blower total pressure is defined as the sum of the blower static pressure and chamber-outlet kinetic pressure. The chamber-outlet kinetic pressure is represented by the average air velocity obtained by dividing the fan-draft flow rate by the outlet opening area.

2.2 Result of fan-characteristics calculation

For evaluation of the validity of the fan model, the experimentally-obtained fan characteristics were simulated by calculation using the computational model shown in **Fig. 5**. The model's fluid domain (the doughnut-shaped portion around the fan motor) corresponded to the fan blades, and to this domain was applied the abovementioned concept, i.e., the axial velocity *V* was defined using the *X*-direction velocity u_1, which was obtained in each cell element, and the rotational-direction velocity *U* was defined using both the fan rotation speed, which varies between points on the fan's characteristic curve, and the radial distance *r* from the center of rotation of each cell.

To enable expression of points on the fan's characteristic curve in a manner appropriate for calculation, both the fan characteristics with fan-outlet kinetic-pressure component corrected and the fan rotation speed at each characteristic-curve point were defined as functions of the fan-draft flow rate *Q*. These functions are shown in **Fig. 6**.

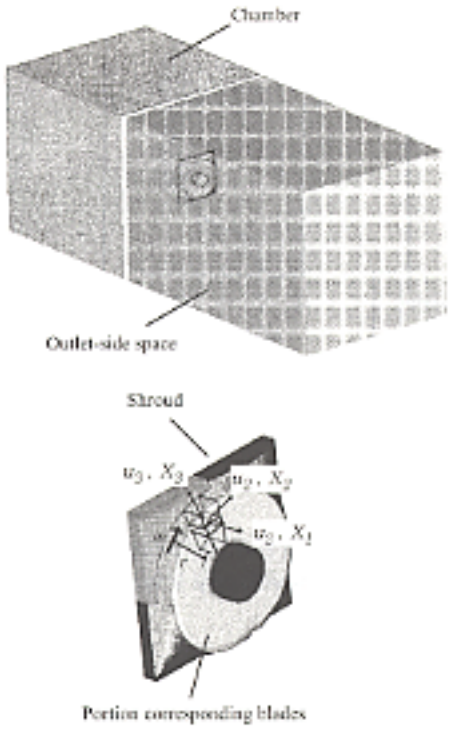

Fig. 5 Computational model of cooling fan

The mathematical methods actually used to incorporate this model into the air flow calculation scheme are described hereafter. The following momentum equation was used to express the rotational domain corresponding to the fan blade.

$$\frac{Du_i}{Dt} = -\frac{1}{\rho}\frac{\partial p}{\partial x_j} + \nu\nabla^2 u_i - \frac{\partial \overline{u_i' u_j'}}{\partial x_j} + \frac{1}{\rho}X_i$$

Here, i corresponds to the axial direction when it takes the value of 1, the rotational direction when it takes the value of 2, and the centrifugal direction when it takes the value of 3. With the fan's angular velocity represented by ω and the blade thickness in the flow direction represented by L, the component velocities were expressed as follows:

$$U = r \cdot \omega$$
$$V = \sqrt{u_1 \cdot u_1}$$
$$X_2 = \left\{\alpha \cdot \rho \cdot V \cdot t \cdot (U - V \cdot \tan\beta)\right\} / (t \cdot L)$$
$$X_1 = X_2 \cdot \tan\beta$$
$$X_3 = 0 \text{(i.e., centrifugal component not considered)}$$

The fan's angular velocity ω was given by the functions shown in **Fig. 6**. Coefficient α was defaulted to 1 and increased or decreased appropriately to match the fan characteristics, which were expressed as a function of variables.

Fig. 7 shows the fan characteristics calculated using this model. The predicted characteristic curve closely matches the experimentally obtained curve.

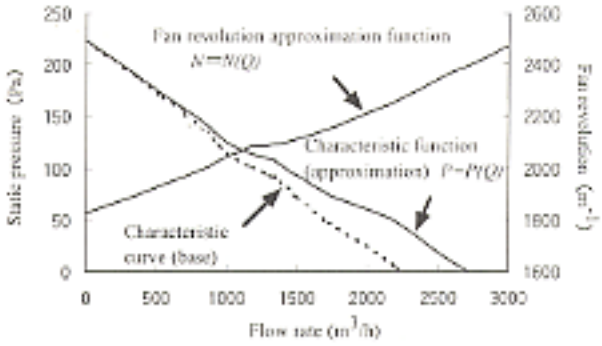

Fig. 6 Fitting function

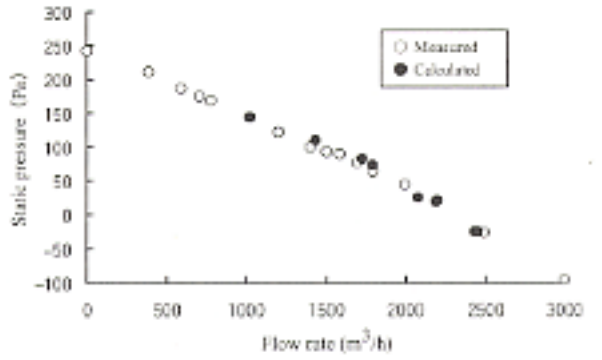

Fig. 7 Calculated characteristic curve of cooling fan

Next, the calculated and experimentally obtained results were compared in terms of the distribution of flow velocities in the fan wake. It is known that the airflow pattern around the fan varies significantly with fan operating conditions[8]. Under high-load operating conditions, a reverse-flow zone develops around the root of each blade, making the overall flow pattern diagonal. Under low-load conditions, on the other hand, the flow pattern becomes axial as the reverse-flow zone decreases. For examination of the validity of the model for prediction of high-load operation and low-load operation, calculated and experimentally obtained results corresponding to fan-draft flow rates of 1800 m^3/h and 2400 m^3/h were compared. The measurements were made using a laser Doppler velocimeter (LDV). Data were taken three-dimensionally for points positioned radially 5 mm apart on a plane 20 mm from the rear end of the fan.

Fig. 8 compares the calculated and experimentally obtained flow-velocity distributions in the fan wake. For the high-load condition, the measurements indicate a reverse-flow zone (or negative-velocity zone) around the root of the blade and an axial-flow zone (or positive-velocity zone) in the portion between the halfway point and tip of the blade. They also show a distinct centrifugal component at the tip of the blade. The calculation results show that the model worked well in simulation of the reverse-flow zone around the root of the blade, but they also show that the model did not simulate at all the centrifugal velocity components at the tip of the blade. For the low-load condition, the measured and calculated velocity distributions closely matched each

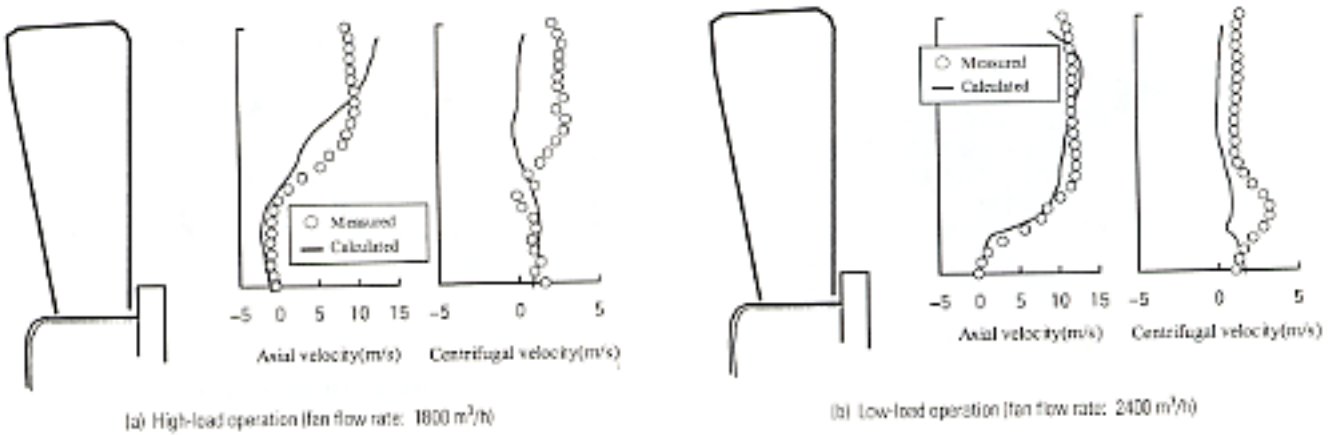

Fig. 8 Calculated velocity distribution of fan wake

other and the model simulated the centrifugal velocity component relatively well albeit with small discrepancies between the measured and calculated results for the portion around the blade root.

The difference in calculation accuracy with different levels of fan loading is attributable to the centrifugal components of moments not being taken into account when the fan characteristics were modeled. For fan operation with low loading, i.e., with hardly any centrifugal velocity component, the flow-velocity distribution can be simulated satisfactorily using the model. For operation with high loading, however, the flow velocity includes a significant centrifugal component, which has a particularly marked effect on the flow velocity around the tip of the blade. The effects are reflected in the accuracy of the calculated flow-velocity distribution in both the centrifugal and axial directions.

Nevertheless, the fan actually operates under a high load only when the engine is idling. Even during low-speed driving, when cooling demands are severe, the fan's operating point is in the low-load zone thanks to air flow caused by ram pressure. Thus, the model was considered capable of making predictions of sufficient accuracy for use in development of new vehicle models.

2.3 Simplified modeling

Although the model yielded low prediction accuracy when simulating flow fields that exist during high-load operation of the fan, it offered sufficient accuracy when applied to flow fields that exist during low-load operation. Since the model was also capable of predicting fan characteristics with sufficient accuracy, it offered sufficiently accurate prediction of air flow corresponding to the conditions most frequently encountered by the fan during vehicle operation.

However, the model was unable to provide consistent solution during the initial stage of calculation, which handles an unstable flow field, because it directly integrated into itself as axial velocity V the velocity u_i of each cell element obtained through calculation.

To overcome this problem, a method was devised to enable the axial velocity V to be defined using the fan-draft flow rate Q and a function that is given the velocity distribution in the fan's radial direction. With this method, the axial velocity V was expressed as follows:

$$V = V(Q, r)$$
$$Q = \int u_i \cdot ds$$

Although the initial-stage calculation still involved fluctuation in the flow rate with this method applied to the model, the influence of the fluctuation was smaller than when the calculated velocity u_i was directly used since the fluctuation was shared among all portions of the fan.

There were two candidate methods for giving velocity distribution to the function: ① using the mean flow velocity obtained by dividing the fan-draft flow rates by the sectional area of the draft passage; and ② using the approximated velocity distribution in radial directions represented by a straight line. **Fig. 9** shows conceptual diagrams of the models using these two methods: the model with velocity distribution given by simple mean flow velocity (C-Model) and the model with velocity distribution represented by a straight line (B-Model). This figure also shows the aforementioned model using calculated velocity directly (A-Model).

The velocity distributions in the fan-wake flow field calculated using these methods are shown in **Fig. 10.**

With regard to the velocity distribution in the axial direction with high-load operation, the B-Model yielded almost the same prediction results as the A-Model albeit with slight differences from the experimentally obtained results. The simulation by the C-Model, however, included significant exaggeration in prediction of the reverse-flow velocities around the blade root and in prediction of the forward-flow velocity at the blade tip. Also with prediction of the velocity distribution in the axial direction with low-load operation, the B-Model yielded almost the same prediction results as the A-Model and the C-Model yielded inferior prediction accuracy.

The above mentioned results can be presumed easily from the definition equations of fan-induced kinetic momentum shown earlier. With the C-Model, $V \tan \beta$ is defined by a constant value irrespective of radial posi-

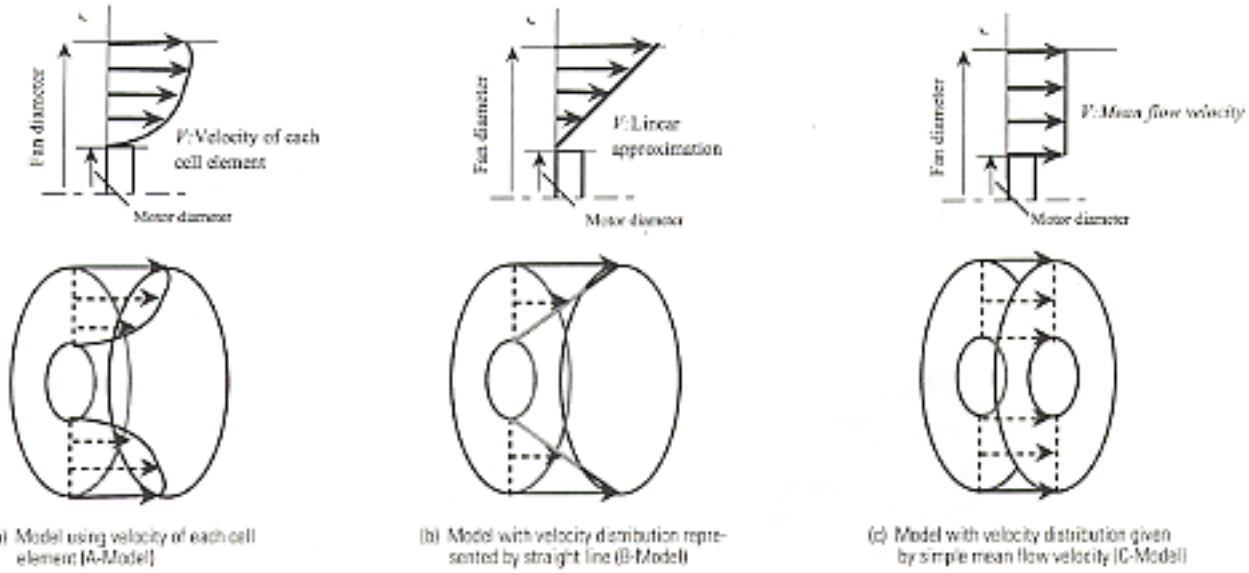

(a) Model using velocity of each cell element (A-Model)

(b) Model with velocity distribution represented by straight line (B-Model)

(c) Model with velocity distribution given by simple mean flow velocity (C-Model)

Fig. 9 Axial velocity distribution with simplified fan model

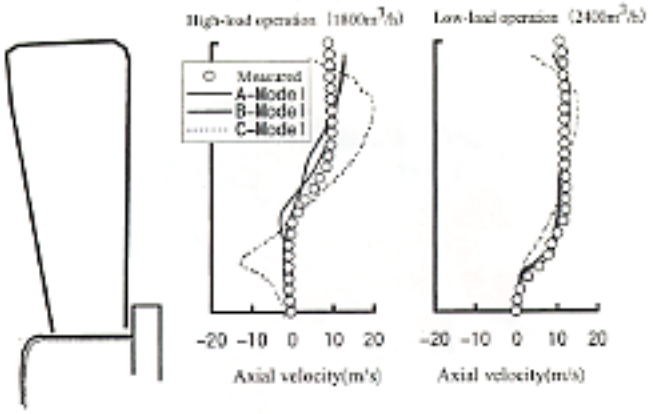

Fig. 10 Comparison of velocity distributions with different fan models

tion. The rotational speed U, however, is defined by the product of the fan's rotational speed and the distance r from the fan's center, meaning that there must exist a zone in which speed U is smaller than $V \tan \beta$ near the root of the blade. Since the result of subtraction ($U < V \tan \beta$) is negative in that zone, negative momentum is given around the blade root in the simulation. The fan is thus seen as producing a reverse-direction force.

From the studies described above, it was determined that the simplified B-model (which was given the velocity distribution by an approximative line) was, like the A-Model (which directly used calculated velocities), capable of yielding sufficient prediction accuracy for application to simulation of air flow with low-load fan operation even though its prediction accuracy with high-load fan operation was poor.

3. Verification using vehicle model

3.1 Creation of engine-compartment design model

Making the time from presentation of design data to output of simulation results as short as possible is vital for rapid development of any new vehicle. Computational-model creation is a particularly time-consuming task, so a technique enabling it to be performed in the shortest possible time is essential.

MMC has long used numerical simulation of aerodynamics[9] in product development, and it has constructed an in-house grid-generating system for this purpose. The system allows an external-flow analytic grid to be generated relatively easily. However, it is a hexahedron-structure-based grid-generating system and thus cannot easily be used to create the grid of a complexly shaped engine compartment; even a skilled designer requires a period as long as two months to make a detailed computational model of an engine compartment.

The method employed by the authors to shorten the model-making period is to combine a separately created engine-compartment model and external-flow analytic model. This method is outlined in **Fig. 11**. The external-flow analytic model of the vehicle under development is created in the same way as a conventional aerodynamics-analysis model, and the engine-compartment model is created in parallel using hexahedron grids. The two models are then combined using discontinuous grid junctions. Finally, the cooling openings are formed in the model. This method enables an engine-compartment computational model to be created in a period as short as one week.

3.2 Calculation results

This section of the paper describes the results of the simulation carried out using the computational model created by the abovementioned method. The created computational model was, as shown in **Fig. 11**, of an entire two-box car with a single cooling fan located in a position offset from the center of the radiator. The RNG-type k-ε model was used as turbulence model for calculation, and QUICK was used as the differential scheme for the convection term.

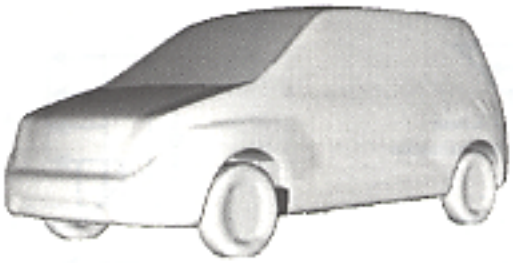

Model for aerodynamics analysis

Model for engine compartment analysis

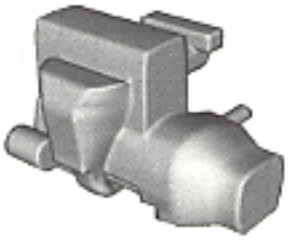

Engine model

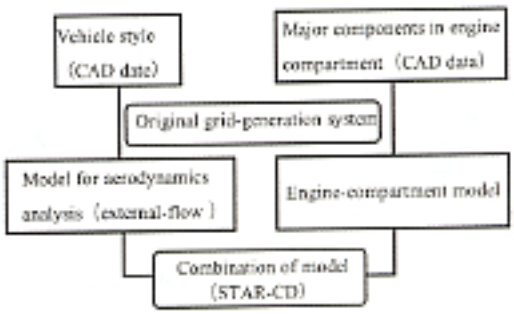

Fig. 11 Creation of computational model for engine-compartment analysis

The B-Model was used for the fan model. The following description also includes for comparison purposes the simulation results obtained using the conventional model that takes only the fan characteristics into account.

Fig. 12 shows calculated air flows in the engine compartment for engine idling. The streak lines calculated using the conventional model with only the fan characteristics taken into account do not include any swirl in the fan wake; they extend almost straight toward the rear along the top of the transmission then bend down toward the underfloor area. The simulation result using the B-Model, however, reproduces swirls in the fan wake and complicated flows along the rear and top surfaces of the engine.

Figs. 13 and **14** show the calculated streak lines of air flowing along external surfaces of the vehicle and in the engine compartment under the influence of vehicle-movement-induced oncoming air with low and high vehicle speeds.

With a low vehicle speed, the oncoming air contributes to the air flow in the engine compartment but the fan's influence is dominant, hence the distinct difference between the simulation by the conventional model and that by the B-Model. The B-Model, which takes swirls into account, is able to predict complicated air flows around the engine (such as those occurring with the engine idling), whereas the streak lines predicted by the conventional model go toward the underfloor area without involving any irregularity around the engine.

There is almost no difference between the models' respective simulation results for high-speed driving since the fan has a relatively small influence on the air flow in the engine compartment under such conditions.

Fig. 15 shows the calculated and measured velocities of air flowing through the radiator for various operating conditions ranging from operation with the engine idling to operation with a high vehicle speed. The air velocity during engine idling predicted by the conventional model differs from the measured velocity by a

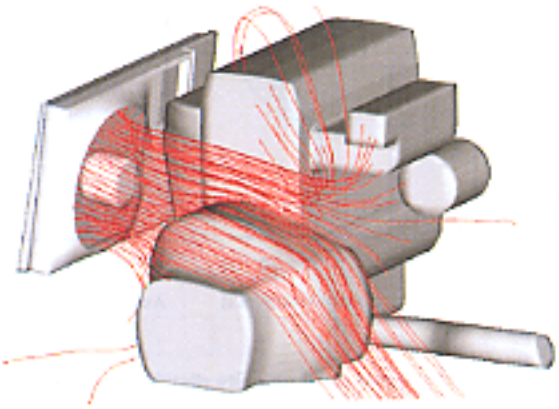

(a) Conventional model

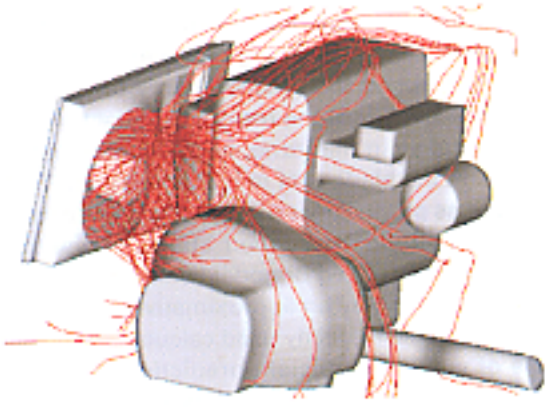

(b) B-Model

Fig. 12 Streak lines in engine compartment

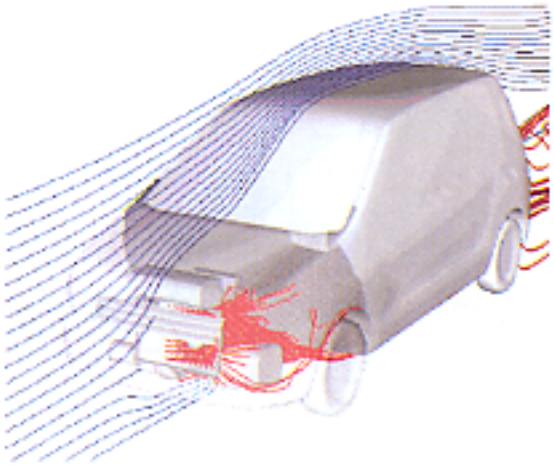

(a) Conventional model

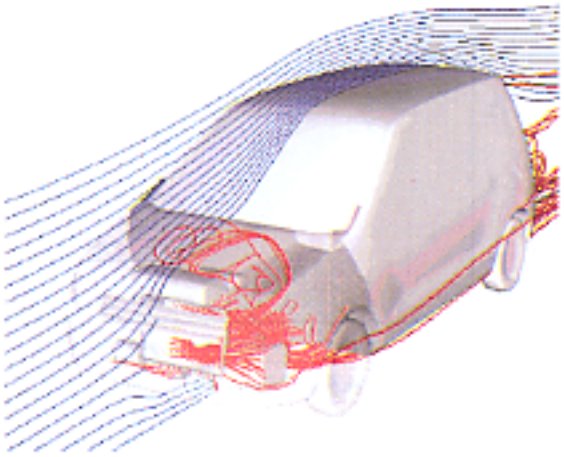

(b) B-Model

Fig. 13 Streak lines of air flowing outside vehicle and inside engine compartment with low vehicle speed

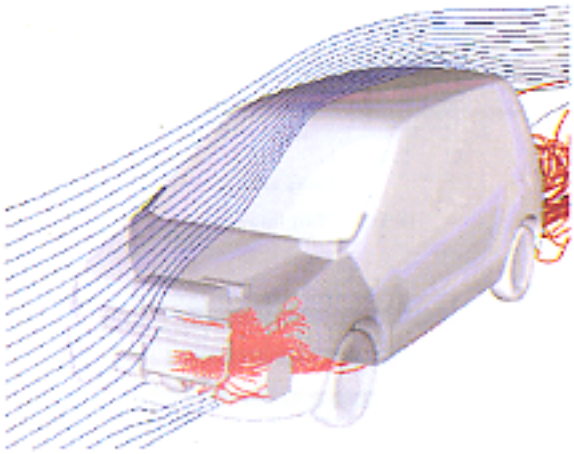

(a) Conventional model

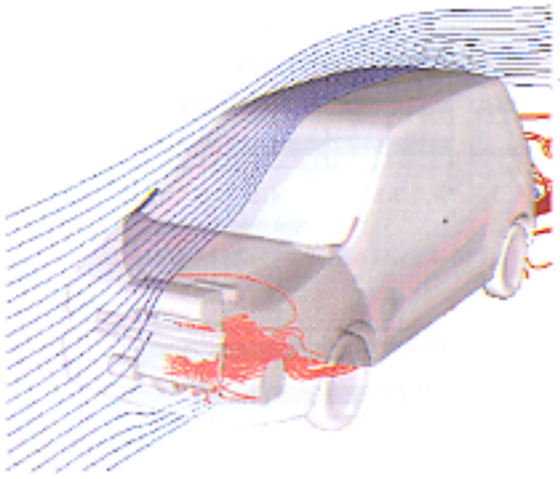

(b) B-Model

Fig. 14 Streak lines of air flowing outside vehicle and inside engine compartment with high vehicle speed

margin of 20 %, but that predicted by the B-Model differs from the measured velocity by a margin of only 10 %, indicating significantly higher prediction accuracy. As stated earlier, the conventional model is poor in terms of accuracy in prediction of the flow field around the fan because of its inability to reproduce complicated air flows in the engine compartment; the B-Model's ability to simulate swirls around the fan contributes to the B-Model's higher accuracy in prediction of the flow field around the fan. These factors explain why predictions of cooling-air velocity yielded by the B-Model are more accurate than those yielded by the conventional model.

With regard to the air-velocity prediction for low-speed driving, the low level of fan loading gives a favorable effect to the prediction yielded by both models. Notably, the prediction error of the B-Model is only 8 %, which is more or less acceptable.

With simulation of the air velocity during high-speed driving, where the cooling fan has only a small effect on air flow, the prediction results of the two models are similar to each other with a margin of error as small as 5 %. The result of prediction for vehicle operation with the fan turned off (also shown in the figure for reference) includes a margin of error of only 3 % and thus indicates extremely high accuracy.

From the verification results described above, it can be seen that the model that takes both fan characteristics and fan-induced swirl components into account is capable of predicting cooling-air velocity with significantly higher accuracy than the model that takes only fan characteristics into account. Although the accuracy of air-velocity predictions made by the newly developed model is lower for high-load fan operation (e.g., during engine idling) than for low-load fan operation, it is sufficient for application to vehicle development. These results show that the newly developed model is a highly effective tool for predicting the characteristics of air flow in the engine compartment.

4. Example of application

4.1 Simulation of dual-fan system

The discussion in the preceding sections of this paper pertains to an engine compartment with a single fan system. However, the fan system employed most

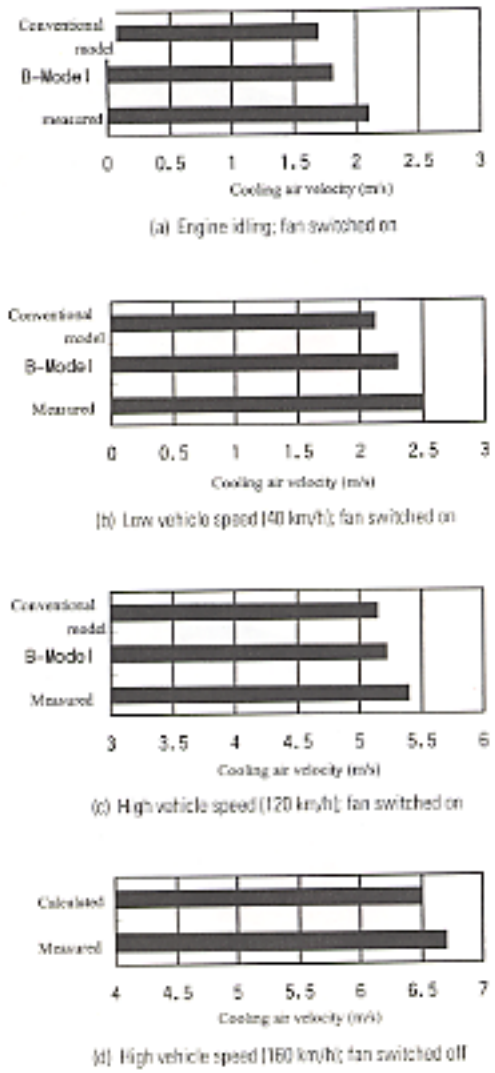

Fig. 15 Predicted velocity of cooling air flowing through radiator

often in passenger cars is a dual type in which two fans are arranged in parallel behind the radiator. The fan model can be applied to a dual-fan system just as it can be applied to a single-fan system. **Fig. 16** shows airflow streak lines in the engine compartment calculated for a dual-fan system with the engine idling.

For convenience, the left and right fans (as seen from the rear) are here called the radiator fan and condenser fan, respectively. The streak lines shown in red are of the air blown by the radiator fan, and those shown in blue are of the air blown by the condenser fan. This calculation result obtained using the B-Model successfully reproduces swirls. It also shows complex intermixing of flows from the two fans in the engine compartment.

4.2 Study of fan specifications

This simulation model is also applicable to studies of fan specifications in the initial stage of vehicle development. **Fig. 17** shows estimated and experimentally obtained velocities of air passing through the radiator with various fan-motor capacities (wattages). The fan system under study was a dual type with the fans

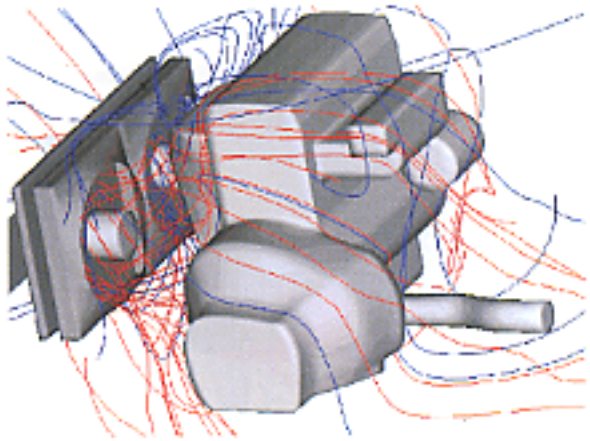

Fig. 16 Streak lines in engine compartment with parallel fans

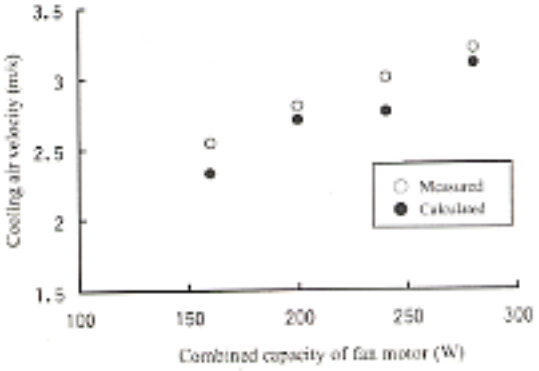

Fig. 17 Predicted velocities of cooling air flowing through radiator for fans with different motor capacities

arranged in parallel. The total motor capacity of each fan pair is plotted against the horizontal axis of the graph, and air velocities are plotted against the vertical axis. The calculated velocities differ from the experimentally obtained velocities by margins of only 5 – 10 %.

5. Summary

Study of the CFD-based simulation model developed for prediction of the performance of the cooling air flow in an engine compartment yielded the following conclusions:

(1) A mathematical model of the cooling fan that takes swirl components into account enables prediction of the fan characteristics and of the distribution of air velocities in the fan wake.

(2) In prediction of the performance of the cooling air flow in an engine compartment, the new model, which takes swirl components into account, yields significantly higher accuracy than the conventional model, which does not.

(3) The new model's prediction accuracy is low with respect to fan operation with the engine idling, but the level of accuracy is adequate for vehicle-development purposes. The model can simulate air flow

during low-speed driving (when cooling demands are particularly critical) with a margin of error as small as a few percent.

(4) It is possible to shorten the time required for creation of an analytic model of an engine compartment by combining a separately created engine-compartment model and external-flow analytic model.

(5) The model created using the above mentioned method yields accurate predictions of the performance of cooling air flow and is used by MMC for prediction of cooling performance at an early stage in the development of new vehicles.

References

(1) Kataoka, Ukita, and China: Numerically Simulating Aerodynamic Characteristics of Vehicle Body Including Underfloor and Engine Compartment, Journal of JSAE, Vol. 25, No. 2, 1994

(2) Ohshima, Hamatani, Ninoyu, and Nakagawa: Influence of Cooling Air Venting Method on Aerodynamics Characteristics, Journal of JSAE, Vol. 29, No. 3, 1998

(3) Abe and Suzuki: Simulation of Airflow in Engine Compartment, Proceedings of JSAE Convention 952, May 1995, No. 9535314

(4) Matsushima, Takeuchi, and Kohri: A study for Improvement in CFD Prediction Accuracy of Engine Cooling Air, Proceedings of JSAE Convention No. 34-99, No. 993402

(5) Matsushima, Takeuchi, and Kohri: Prediction Method of Engine Compartment Airflow Using CFD Analysis, JSAE Review 21, p.197 - 203, 2000

(6) Murakami and Buya: Fluid Machine, Morikita Shuppan

(7) STAR-CD News Letter, Vol. 14, 1998

(8) Shimada, Kuriwada, Sakai, and Ohyama: Design of Aerodynamic Diagonal Flow Fan for Engine Cooling, SAE Paper 980059, 1998

(9) Kataoka, China, Nakagawa, and Yanagimoto: Numerical Simulation of Road Vehicle Aerodynamics and Effect of Aerodynamic Devices, SAE Paper 910597, 1991

Tatsuya OHSHIMA

Tetsuji UKITA

Minoru YAMAMOTO

NEW TECHNOLOGIES

Development of Mitsubishi Advanced Safety Vehicle (ASV-2)

Yoshiki MIICHI* Sumio MOTOYAMA* Masayoshi ITO*
Keiichi YAMAMOTO** Shigeki FUKUSHIMA‡*

Abstract

Mitsubishi Motors Corporation has been participating actively in the second stage of the ASV project as started in 1996 under the auspices of the Japanese Ministry of Transport (current Ministry of Land, Infrastructure and Transport). In this regard, the company produced three different types of passenger vehicle – namely, the ITS-ASV, the Hi-mobility ASV, and the Smart Cruise 21 ASV – in addition to an ASV-2 truck. The wide-ranging technical expertise relating to vehicle safety as gained by this company has been fully employed in these vehicles together with the advancement of practical application technologies for the 21st century. In addition to the concepts of active safety technology and passive safety technology, these vehicles also fully embody the concept of ITS technology which may be easily put to use by older drivers. The principal technologies employed in the three types of Mitsubishi ASV-2 passenger vehicle and ASV-2 truck will be discussed in this paper. The new vehicle-safety technologies incorporated in these Mitsubishi vehicles were developed with an intent of practical application in future vehicles.

Key words: Intelligent Transport Systems, Advanced Safety Vehicle, Automated Highway System, Safety

1. Introduction

The annual number of traffic fatalities in Japan has remained below 10000 since 1996. Nevertheless, the annual number of injury accidents continues to increase. Traffic safety therefore remains a major social issue.

Against this background, Mitsubishi Motors Corporation (MMC) has actively participated in the Advanced Safety Vehicle (ASV) project, which was inaugurated by Japan's former Ministry of Transport. (The Ministry of Transport, Ministry of Construction, and National Land Agency were incorporated into the new Ministry of Land, Infrastructure and Transport in January 2001.) After participating in the ASV project's first stage, which ran from 1991 to 1996[1], MMC renewed its commitment by participating in the ASV project's second five year stage, in which it developed a wide range of industry-leading safety technologies and applied them to production vehicles[2][3].

The primary goal of the ASV project's first stage was to improve traffic safety by employing electronics and other new technologies to realize ASVs with a high level of intelligence. Work in the project's second stage was additionally focused on the role of such vehicles as platforms for Intelligent Transport Systems (ITS) technologies. In this stage of the project, domestic passenger-car manufacturers were joined by domestic truck, bus and motorcycle manufacturers. Studies conducted by these manufacturers included those into ways to put ASV technologies to practical use[4] and those into ways to ensure compatibility with the road infrastructure[5].

This paper describes three Mitsubishi ASV-2 passenger cars[6] and a Mitsubishi ASV-2 truck[7] that MMC finished developing in 2000, the final year of the ASV project's second stage.

2. The three Mitsubishi ASV-2 passenger cars (Fig. 1)

The three Mitsubishi ASV-2 passenger cars – namely the ITS-ASV, the Hi-mobility ASV, and the Smart Cruise 21 ASV – incorporate technologies that MMC aims to apply to production vehicles in the near future. These technologies include not only active-safety technologies (these are intended to prevent accidents) and passive-safety technologies (these are intended to maximize protection in the event of a collision) but also ITS technologies that are intended to ensure ease of use for all drivers (even elderly ones).

2.1 The ITS-ASV: Acts in harmony with the information-oriented-society and surrounding vehicles

The ITS-ASV uses various onboard sensors and communication systems to monitor the road environment (a key system is the Multi-Eye System shown in Fig. 2), and it provides the driver with information in audible and visible forms. It also incorporates systems

* Electronics Engineering Dept., Car Research & Dev. Office
** Vehicle Research Dept., Truck & Bus Dev. Office
‡* Electronics Engineering Dept., Truck & Bus Dev. Office

Fig. 1 The three Mitsubishi ASV-2 passenger cars

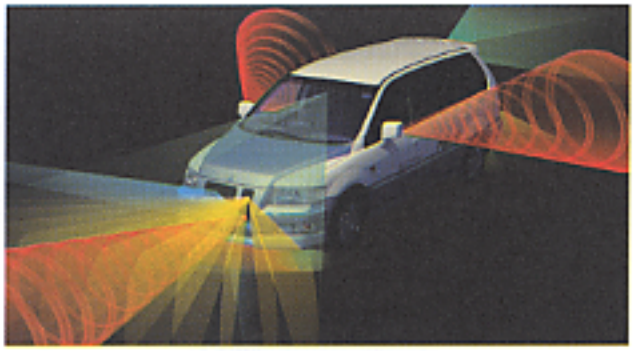

Fig. 2 Multi-Eye System

Table 1 Main technologies of ITS-ASV

Driver alertness monitor	Uses compact camera on instrument panel to monitor blinking of driver's eyes. Issues audible and visible alerts if driver falls asleep or otherwise displays reduced alertness.
Light distribution control headlight	Maximizes nighttime visibility by controlling distribution of illuminant in accordance with operating conditions (indicated by steering wheel angle, etc), and road shape (indicated by navigation data).
Night pedestrian monitor	Uses infrared camera in center of grille to monitor road conditions ahead of vehicle. Issues audible and visible alerts to driver when pedestrians are present.
Road surface monitor	Uses road surface sensors under front bumper to estimate slipperiness of road surface. Issues audible and visible alerts to driver when tires are in danger of losing grip.
Side-rear warning	Uses radar and camera to sense automobiles and motorcycles in adjacent lanes. Helps to prevent any dangerous lane change maneuver by issuing audible and visible alerts and by conferring weak information torque on steering wheel in direction opposite to that of lane change maneuver.
Advanced high-mount stop lamp	Informs following drivers of vehicle's rate of deceleration (and thus enables them to avoid rear end collision) by altering width of illuminated section of high-mount stop lamp in accordance with rate of deceleration.
Advanced brake assist	Optimizes brake assistance force in accordance with conditions in forward direction (for example, distance to preceding vehicle and rate at which vehicle is closing on preceding one).
Advanced preview distance control	Prevents excessive proximity to preceding vehicle during on-road operation and automatically applies brake to stop vehicle when preceding one stops. Alerts driver audibly and visibly when preceding vehicle subsequently starts moving and permits standing start upon switch input from driver.
Lane trace assist	Senses white lines on road using compact camera in rear-view mirror. Helps to keep vehicle in lane by applying weak assistance torque to steering wheel, thus minimizing driver's steering effort and enhancing safety.
Corner entry deceleration system	Uses navigation data on curves on road ahead to determine whether speed of entry to curve is too high. Alerts driver audibly and visibly when speed is too high. Applies brakes automatically when deceleration effected by driver is insufficient.
Collision damage mitigating braking system	Applies brakes automatically to prevent collision (or minimize damage caused by unavoidable collision) when driver fails to take corrective action in response to warning of impending frontal collision.
Advanced airbag	Minimizes shock inflicted on occupants by employing sensors to sense occupants and their positions and by effecting coordinated control of multiple airbags accordingly.
Pedestrian injury mitigating body	Employs shock absorbing front end to minimize pedestrian injuries in event that active safety technologies are not able to prevent collision with pedestrian.
Mayday call	Transmits information on vehicle's position and on severity of accident to traffic control center in event that collision sensors detect collision, enabling operator to rapidly confirm accident and call ambulance.
Drive recorder	Facilitates analysis of accidents and prevention of recurrence by recording vehicle's speed and driver's actions (operation of brake pedal, accelerator pedal, steering wheel, and other controls) before, during and after any accident.
Driver's card	Card locks/unlocks doors when placed near antenna on door window. Related system requires insertion of card into slot in instrument panel and successful comparison of driver's fingerprint with identification data in card before engine can be started. Card can hold personal information for use with non-automotive services. Card incorporates integrated circuit that permits convenience and security.

that help the driver take action to avoid hazards (**Table 1** and **Fig. 3**).

2.2 High-mobility ASV: High driving performance regardless of individual ability

The Hi-mobility ASV incorporates a new system of driver's controls based on MMC's universal design concept (see the universal-design cockpit in **Fig. 4**) plus intelligent, integrated systems for control of vehicle dynamics. It uses these systems to provide outstanding mobility irrespective of the driver's physical characteristics (**Table 2**).

The universal-design cockpit uses drive-by-wire technologies to realize a pedal-less system of driver's controls.

2.3 The Smart Cruise 21 ASV: increasing safety by utilizing information from the infrastructure (Fig. 5)

The Smart Cruise 21 ASV is an experimental vehicle created specifically for use in the Smart Cruise 21 proving program inaugurated by Japan's former Ministry of Transport and former Ministry of Construction. It supports the driver by employing information from the road infrastructure to help prevent the following types

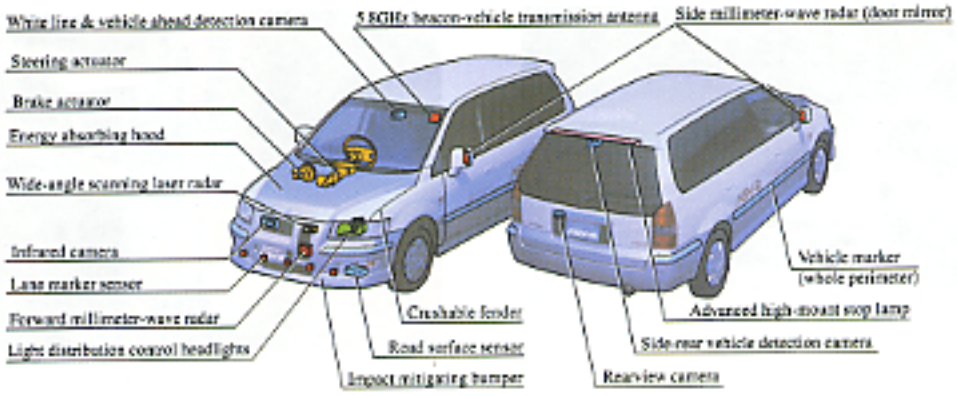

Fig.3 Main components of ITS-ASV

Table 2 Main technologies of Hi-mobility ASV

(1) Universal design cockpit

High ratio steering	Uses active-front wheel steering actuator to adjust steering gear ratio in accordance with vehicle speed. Allows driver to perform all steering actions without moving hands from initial positions on steering wheel.
Hand-operated accelerator and brake levers	Provided instead of conventional pedals. Allow driver to control throttle and brakes more quickly and precisely than with pedals.
Drive mode switch	Allow driver to fine-tune vehicle's responses to control inputs.
Multi-mode LCD instrumentation	Large liquid-crystal meters are positioned directly in front of driver for optimum visibility. Driver can select information displayed by each meter.
Swivel seats	Permit easy ingress and egress. Provided for driver and front passenger.

(2) Integrated vehicle dynamics management

Active four-wheel steering	Controls front and rear wheel steering angles in accordance with driver's steering wheel inputs and state of vehicle motion. Optimizes vehicle's response to rapid steering wheel inputs by steering front wheels through larger angle than that of steering wheel and by steering rear wheels in same phase.
Integrated yaw moment control	Maximizes controllability and stability near vehicle's cornering limits by creating yaw moment using differences in traction and braking force between left and right wheels. Uses throttle-by-wire and brake-by-wire technologies for smooth, precise control.

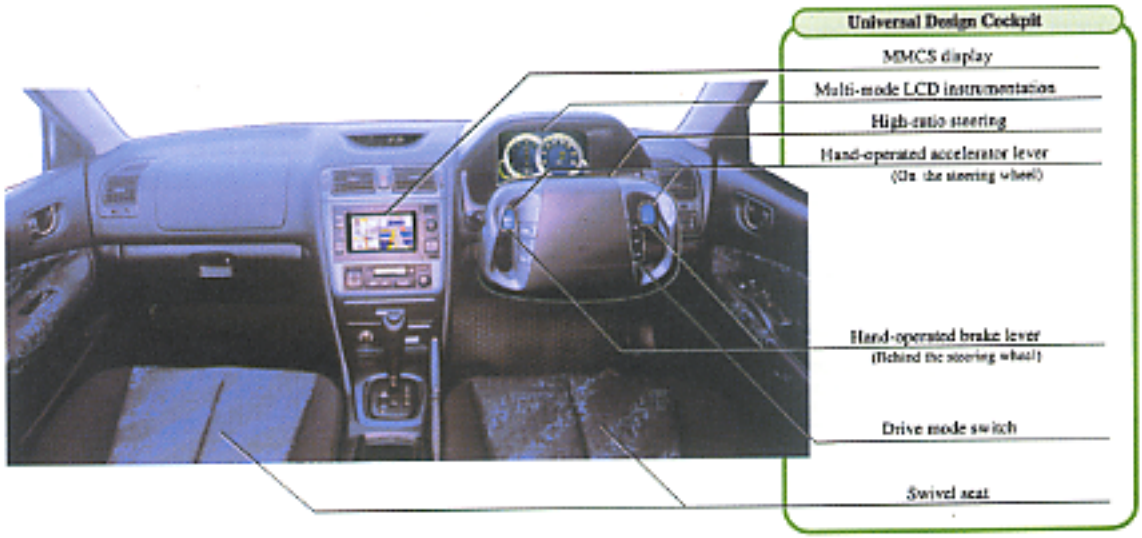

Fig.4 Universal design cockpit

of incident:

- Support for prevention of collisions with forward obstacles
- Support for prevention of overshooting on curve
- Support for prevention of lane departure
- Support for prevention of crossing collisions
- Support for prevention of right turn collisions

Systems in the Smart Cruise 21 ASV are a consolidation of those systems in the ITS-ASV that use information from the road infrastructure.

3. The Mitsubishi ASV-2 truck (Fig. 6)

The Mitsubishi ASV-2 truck, which MMC developed

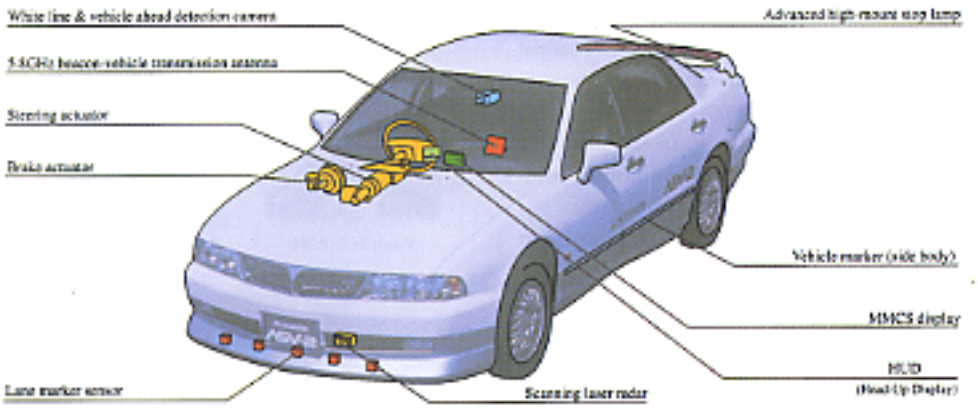

Fig. 5 Main components of Smart Cruise 21 ASV

Fig. 6 Mitsubishi ASV-2 truck

and refined in the second stage of the ASV project, incorporates numerous state-of-the-art technologies. Given the serious consequences of any accidents involving a heavy-duty vehicle, these technologies relate mainly to active safety and are designed to enable compatibility and interaction with Smart Cruise 21 systems.

Some of the technologies (such as the MDAS-II) have already proven their effectiveness in production vehicles. Others (such as an automatic following system) are for future use (**Table 3**).

Table 3 Main technologies of Mitsubishi ASV-2 truck

MDAS-II[*1] (already used in production vehicle)	Infers driver's alertness level from meandering of vehicle and from operations of driver, and issues warnings when necessary. Has function that maintains driver's alertness using scent and function that issues headway distance warnings taking driver's alertness level into account.
Adaptive front-lighting system	Maximizes nighttime visibility by controlling distribution of illuminant in accordance with vehicle's operating and loading conditions and with driver's operations.
Adaptive cruise control system with brake control	Controls service brakes to adjust vehicle's speed in accordance with headway distance.
Automatic following system	Cruise vehicle to follow preceding vehicle in accordance with information received from preceding vehicle by means of vehicle-to-vehicle communication.
Vehicle stability control	Controls each wheel's braking force independently to help prevent vehicle from spinning and drifting out.
Front underrun protector device	Prevents underrun in event of head-on collision with passenger car, thereby minimizing harm inflicted.
FTSS[*2] (already used in production vehicle)	Collects and analyses information on vehicle's loading condition, location, and maintenance using Internet.
Smart Cruise 21 related technologies	Support two services: forward obstacle collision prevention support system and curve overshooting prevention support system.

*1: MDAS (Mitsubishi Driver's Attention Monitoring System)
*2: FTSS (FUSO Total Support System)

4. Summary

The Mitsubishi ASV-2 models described in this paper incorporate ITS technologies and other technologies that ensure user-friendliness for all drivers – even elderly ones. As computer and telecommunication functions are increasingly combined with vehicles and society continues to age, these technologies will support elderly drivers and other drivers with different levels of driving ability.

Numerous driver-support systems potentially offer increased safety and convenience. However, a wide range of technological obstacles (notably with regard to environment-recognition capability, systems reliability[8], and human interfaces) and social obstacles (notably with regard to cost, driver familiarization, and system standardization) must be overcome before such systems can be put to practical use.

In the second stage of the ASV project, corporate, academic, and government-related bodies cooperated not only in the development of automotive technologies that function autonomously but also in the development of driver-support systems that employ the road infrastructure. They also considered and discussed obstacles to practical application of driver-support systems that offer increased safety and convenience[9].

MMC intends to remain actively involved in ITS-related projects and to continue promoting the commercial application of driver-support systems that offer increased safety and convenience.

References

(1) T. Mimuro et al: "Mitsubishi Advanced Safety Vehicle", 4th World Congress on ITS, October 1997
(2) Y. Miichi et al: "Development of Mitsubishi Driver Support System", 6th World Congress on ITS, November 1999
(3) K. Yamamoto et al: "Development of Driver's Alertness Monitoring System", 3rd World Congress on ITS, October 1996

(4) Hiramatsu and Sato: "Study on Linkage with Road Infrastructure and Consolidation of Conditions for Practical Application", meeting for presentation of mid-term reports on outcome of ASV research, April 1999
(5) Yoshimoto and Sato: "Important points for Practical Application of ASVs", meeting for presentation of mid-term reports on outcome of ASV research, April 1999
(6) Promotional literature on Mitsubishi ASV-2 passenger cars, MMC Public Relations Dept., June 2000
(7) Promotional literature on Mitsubishi ASV-2 truck, MMC Public Relations Dept., June 2000
(8) T. Ohta et al: "System Safety Study on Steering Assist Control", 5th World Congress on ITS, October 1998
(9) M. Kume et al: "Design Principle of the Advanced Safety Vehicle", 7th World Congress on ITS, October 2000


Yoshiki MIICHI


Sumio MOTOYAMA


Masayoshi ITO


Kaiichi YAMAMOTO


Shigeki FUKUSHIMA

NEW TECHNOLOGIES

Development of a Large-HEV-Type, Step-Free Public-Transport Bus

Takashi YANASE* Yuta SUSUKI* Nobuaki TAKEDA**

Abstract

As part of MMC's efforts to realize a step-free transit bus which can repeat frequent stopping and starting in daily operation, a highly-efficient electricity generation system has been accomplished through the optimization of generator engine operation; furthermore, this technology has been combined with newly-developed, powerful lithium ion batteries and reduced pollution through the implementation of braking-energy regeneration, thus enabling the development of a practical large-HEV-type, step-free, public-transport bus which is both highly fuel efficient and is characterized by both comfort and ease-of-use. In accordance with this development, levels of NOx and particulate matter contained in exhaust emissions from public-transport operation have been reduced by 49 % and 82 % respectively, and fuel consumption has been reduced by 42 %.

Key words: *Bus, Hybrid Vehicle, Diesel Engine, Energy Regeneration Electric Motor, Electric Generator, Battery, Environment*

1. Introduction

Social demand for reductions in the environmental burden created by large vehicles is growing year by year. The need for a response to this demand is particularly great with public-transport buses that operate primarily in urban areas. At the same time, an increasingly aged population is driving demand for barrier-free methods of transport.

With a view to meeting these requirements, MMC developed a people- and environment-friendly, hybrid-electric-vehicle (HEV) type, step-free bus employing a compact hybrid drive system that minimizes emissions and fuel consumption and allows significantly improved comfort (Fig. 1).

Fig. 1 Exterior view of HEV-type step-free public-transport bus

2. Development targets

The new bus employs a series hybrid system that generates electricity using a diesel engine. (This system requires no special infrastructure and is suitable for public-transport use in urban areas.) The bus was developed to have the following key characteristics:

(1) Minimal exhaust emissions and fuel consumption

Minimal exhaust emissions and fuel consumption were sought by setting the generator engine to operate at its point of highest efficiency and by implementing braking-energy regeneration.

(2) Good running performance

Compact, high-performance motors were employed with a view to realizing running performance equivalent or superior to that of current vehicles.

(3) Increased cabin space

Maximizing the stepless floor area was sought by employing compact drive-train components and making the drive-train layout as efficient as possible. Sought in particular was greatly expanding the aisle width over the rear axle.

(4) Optimum driveability

Fully automatic operation with no need for a transmission was sought by taking advantage of the motors' high torque at low speeds. Also sought was to achieve optimal coordination with regenerative braking and a good brake feeling by implementing electronic control of the service brakes.

3. Overview of HEV-type step-free bus

3.1 Series hybrid system

The series hybrid system allows high braking-ener-

* Vehicle Research Dept., Truck & Bus Dev. Office

** Electronics Engineering Dept., Truck & Bus Dev. Office

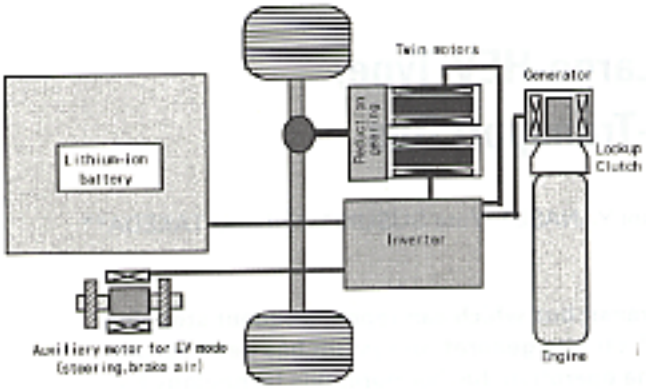

Fig. 2 Hybrid system

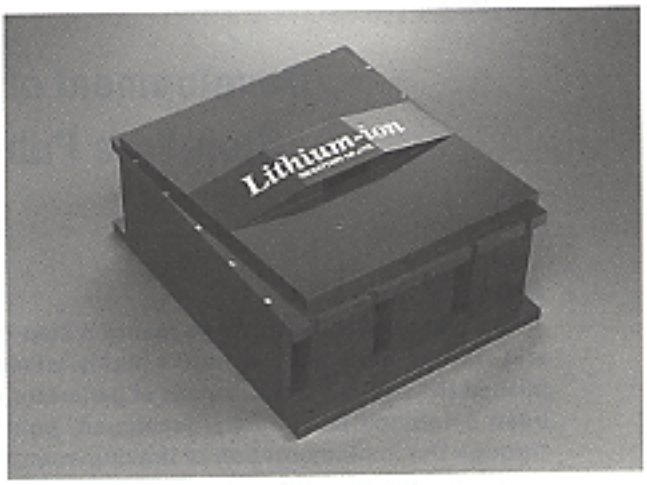

Fig. 3 Lithium-ion battery

Table 1 System specifications

Drive motors	Induction type
Max. output	150 kW x 2
Continuous rating	67 kW x 2
Max. speed	10000 rpm
Drive train	Single-stage reduction
Generator engine	L6 diesel, naturally aspirated (with continuously regenerating DPF)
Displacement	8.201 L
Max. output	165 kW
Emissions regulations satisfied	Current Japanese exhaust emission regulations
Generator	Permanent-magnet synchronous type
Max. output	100 kW
Battery	Manganese lithium-ion type
Total voltage	640 V
Capacity	33 Ah

Table 2 Comparison of energy storage device

		Lithium-ion battery	Sealed lead-acid battery	Capacitor
Energy density	(Wh/kg)	100 – 130	35 – 40	0.8 – 2.4
Output density	(kW/kg)	400 – 800	200 – 400	500 – 5000

gy-regeneration efficiency during public-transport use in urban areas. It also makes possible the use of a compact engine and allows a high degree of freedom in selection of the vehicle layout.

The motors are used for propulsion and for braking-energy regeneration, and the engine is used to drive the generator. Generator operation is controlled in accordance with the battery's state of charge; the engine and generator are stopped when their operation is not necessary.

During normal generation, the engine is run at a constant, low speed to minimize noise inside and outside the cabin. During deceleration, the recovered power is used to charge the battery.

The alternator, air compressor, power steering pump, air compressor, and other accessories are attached to the generator engine. Since the power steering pump and the air compressor (this supplies compressed air to the braking and suspension systems) must continue operating after the generator engine is stopped, the system permits them to be driven by a separate auxiliary motor when necessary. The hybrid system is shown in **Fig. 2**, and its specifications are shown in **Table 1**.

3.2 Lithium-ion battery

A newly developed lithium-ion type battery was selected. The battery offers sufficient energy density and output density for public-transport use in urban areas (**Table 2** and **Fig. 3**).

3.3 Vehicle layout

The vehicle's specifications are shown in **Table 3**, and a perspective view of the vehicle is shown in **Fig. 4**. The diesel engine drives the generator, which in turn powers the motors and charges the battery. The engine and generator are transverse-mounted at the rear of the body, and the battery is mounted on the roof. A combination of compact, high-performance motors and wide single rear tires maximizes the stepless floor area and realizes a rear aisle width approximately 1.4 times that of a conventional vehicle.

3.4 Wide single rear tires

With the wide single rear tires, the vehicle's overall rolling resistance is approximately 13 % lower than that of a conventional vehicle (**Fig. 5**).

4. Performance

4.1 Running performance

Running performance is equivalent or superior to that of conventional vehicles (**Fig. 6**).

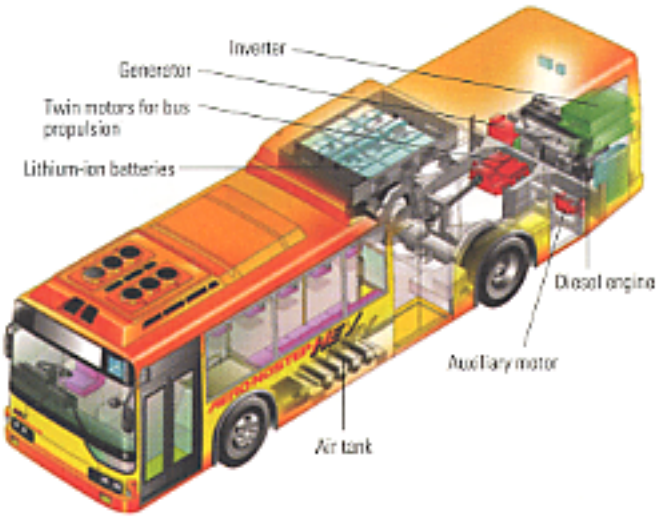

Fig. 4 Perspective view

Table 3 Vehicle specifications

Overall length		10.955 m
Overall width		2.490 m
Overall height		3.085 m
Wheelbase		5.300 m
Gross vehicle weight		14085 kg
Body structure		Stepless
Braking system	Type	Air over hydraulic (electronically controlled)
	Control	Coordinated with regenerative braking
Tires	Front	275/70R22.5
	Rear	435/45R22.5 (single)

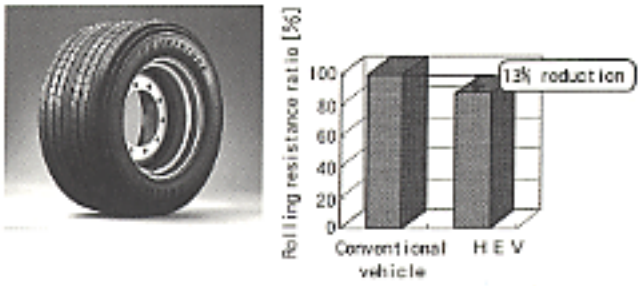

Fig. 5 Wide single rear tire

4.2 Fuel consumption and exhaust emissions

A chassis dynamometer at the Japan Automobile Research Institute (JARI) was used to measure the vehicle's exhaust emissions and fuel consumption during operation in the JARI city-bus mode. The findings were as follows:

(1) Exhaust emissions

The rate of emission of nitrogen oxides (NOx) and the rate of emission of particulate matter (PM) were 49 % lower and 82 % lower, respectively, than those of a conventional automatic-transmission vehicle (**Fig. 7**).

(2) Fuel consumption

The rate of fuel consumption was 42 % lower than that of a conventional automatic-transmission vehicle (**Fig. 8**).

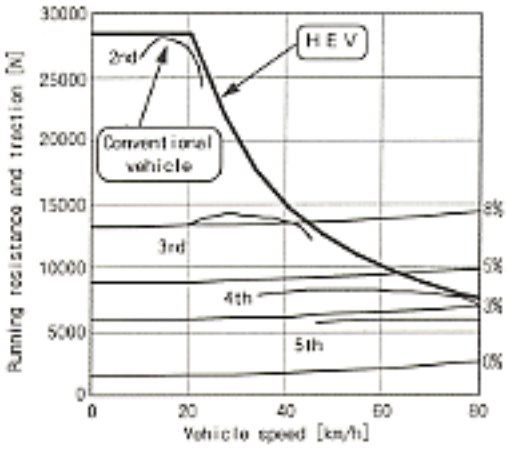

Fig. 6 Running performance

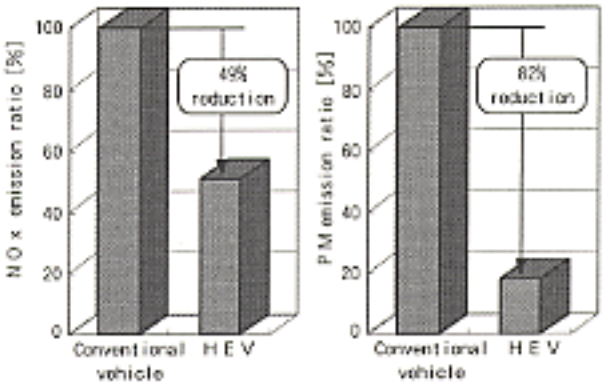

Fig. 7 Reductions in exhaust emissions

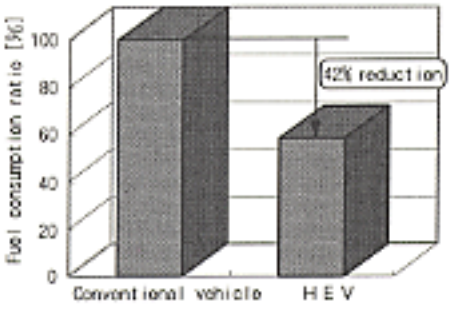

Fig. 8 Reduction in fuel consumption

5. Summary

With its series hybrid system and high-performance lithium-ion battery, the newly developed large, HEV-type, step-free bus realizes outstandingly low emissions and fuel consumption together with the practical benefits of good performance and increased cabin space. MMC believes it has the potential to become the main

type of public-transport bus in urban areas.

In view of the need to protect the global environment, we at MMC intend to pursue further reductions in emissions and to pave the way for widespread adoption by reducing costs and verifying reliability.


Takashi YANASE


Yuta SUSUKI


Nobuaki TAKEDA

NEW TECHNOLOGIES

Development of Center-Differential Control System for High-Performance Four-Wheel-Drive Vehicles

Kaoru SAWASE* Yuichi USHIRODA* Tadashi YOSHIOKA*
Keiji SUZUKI** Kunihiro MANABE** Takao MATSUI‡*

Abstract

Beginning with the introduction in 1987 of the Mitsubishi GALANT – a full-time four-wheel drive (4WD) vehicle equipped with a center differential for which a VCU (Viscous Coupling Unit) is used – Mitsubishi Motors Corporation has been advancing the constant evolution of the 4WD system. Furthermore, in consideration of 4WD vehicles that are often used in various types of motor-sports events, an ACD (Active Center Differential) system has been developed. Combined with the existing AYC (Active Yaw Control) system, the ACD system will allow remarkable advancements to be made with respect to the driveability and cornering characteristics of the vehicle.

Key words: *Torque Split, Limited Slip Differential, Four-Wheel Drive*

1. Introduction

Among active-safety technologies, which are intended to enable safe, enjoyable driving for all vehicle users by causing all four tires to perform to their maximum potential, a significant role is played by four-wheel drive (4WD) systems, which are capable of equally dividing the burden borne by the tires. Mitsubishi Motors Corporation (MMC) produced ahead of others the first high-performance 4WD vehicle in 1987, when it equipped the GALANT VR-4 with a full-time 4WD system that had a center differential employing a viscous coupling unit (VCU). Since then, MMC has steadily evolved its 4WD technologies through such developments as a full-time 4WD system with electronically controlled center differential (this maximizes controllability by varying the front/rear torque distribution between 30:70 and that of rigid 4WD)[1] and an Active Yaw Control (AYC) system (this improves cornering performance by directly controlling the vehicle's yaw moment using the difference in driving and braking forces between the rear-left and rear-right wheels)[2] (Fig. 1).

In motorsports – and particularly in the field of rally competition – 4WD vehicles are the main choice of competitors owing to the ability of 4WD systems to transfer the output of high-performance engines to the road surface efficiently at all times. However, most of the 4WD systems used in such competition vehicles employ VCUs or mechanical limited-slip differentials (LSDs) with narrowly defined operating characteristics that are not necessarily optimal at all times; conventional technologies have left room for further improvement in differential-limiting characteristics and for concomitant improvement in competitiveness.

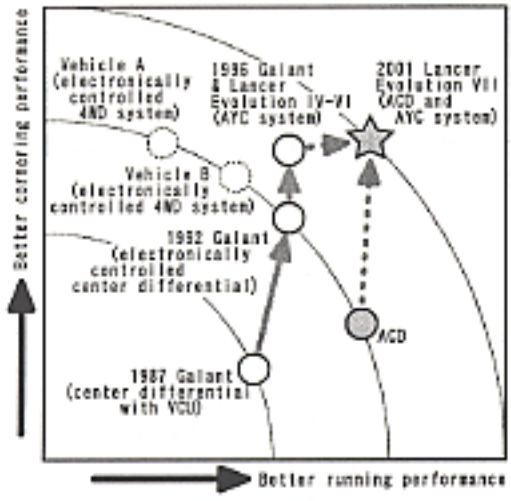

Fig. 1 Evolution of 4WD vehicles

Considering the demands placed on 4WD vehicles in various fields of motorsports, MMC recently developed an Active Center Differential (ACD) system that maximizes the vehicle's running, turning, and stopping capabilities through active control of the center differential's differential-limiting operation. MMC fitted this system in the Lancer Evolution VII. By combining the ACD system with the AYC system and effecting integrated control of the two systems, MMC achieved dramatic improvements in running and cornering performance.

This paper discusses the consideration and selection of the configuration of the LANCER EVOLUTION VII's 4WD system in light of the operating conditions encountered in motorsports. It also gives an overview of the ACD system that was developed in accordance with the selected configuration and describes the bene-

* Transmission and Final Drive Design Dept., Car Research & Dev. Office
** Transmission and Final Drive Proving Dept., Car Research & Dev. Office
‡* Vibration Proving Dept., Car Research & Dev. Office

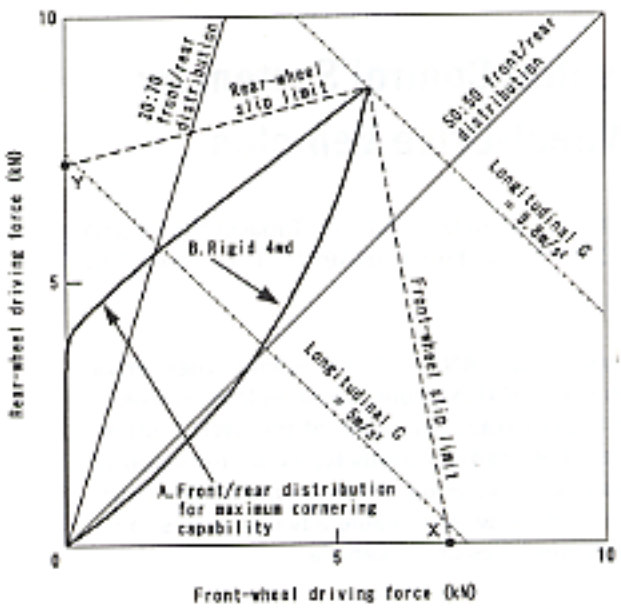

Fig. 2 Optimal front/rear distribution of driving force with respect to cornering properties

fits of integrated control of the ACD and AYC systems.

2. Consideration and selection of system configuration

For use in various motorsports activities, the ACD system was developed with particular importance attached to the following capabilities:

(1) Maximum directional response with no sacrifice in the superior vehicle stability offered by a full-time 4WD system with VCU-type center differential;

(2) Traction performance comparable with that realized by a rigid 4WD system (one that distributes torque to the front and rear wheels in front/rear weight ratio) under a wide range of driving conditions.

The optimum center-differential torque-distribution ratio and differential-limiting torque for these capabilities were considered and selected.

2.1 Center-differential torque-distribution ratio

Control of a vehicle's front/rear torque-distribution ratio is achieved using a mechanism that combines two devices: (1) a device that establishes a predetermined, base distribution ratio and (2) a differential-limiting device that allows the base ratio to be changed as desired. Operation of such a mechanism with a torque-distribution ratio different from the base ratio is accompanied by drive-train torque circulation, so it is difficult to realize stability in control of the ratio. Thus, the center differential's torque-distribution ratio fundamentally governs the vehicle's behavioral characteristics.

Fig. 2 shows the front/rear distribution of torque determined using the "dynamic-square" method with a two-wheel model that has one front wheel and one rear wheel. With the dynamic-square method, the maximum lateral force that the front and rear wheels can each produce is calculated taking into account the tire

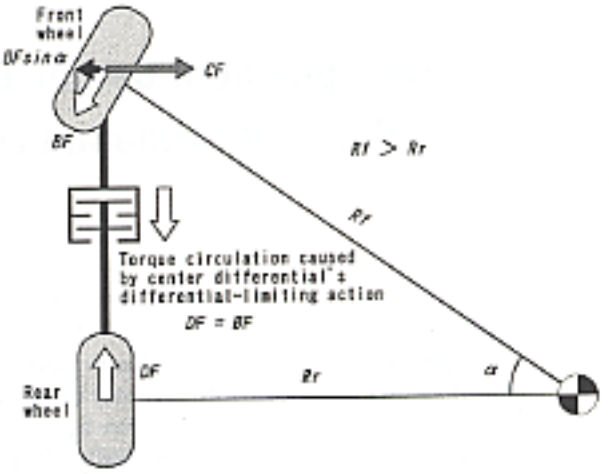

Fig. 3 Relationship between LSD torque and cornering force

friction circles, which change in accordance with acceleration/deceleration and cornering, and the vehicle's properties are evaluated using the calculated values[3]. A two-wheel model allows the influence of the suspension system properties to be ignored, so it is an effective tool for study of the front/rear torque distribution.

Understeer increases to the extent to which the rear wheel's maximum lateral force exceeds the front wheel's maximum lateral force. It is greatest at point X in **Fig. 2**. Conversely, oversteer increases to the extent to which the front wheel's maximum lateral force exceeds the rear wheel's maximum lateral force. It is greatest at point Y. Irrespective of the rate of longitudinal acceleration, cornering capability is, assuming a road-surface μ value of one, greatest when the front/rear torque distribution corresponds to line A, i.e., when the front and rear wheels' respective maximum lateral forces match, resulting in neutral steering. Oversteer and consequent instability occur with any torque distribution above and to the left of line A. If an emphasis on cornering performance is required, therefore, the center differential's front/rear torque-distribution should be established at about 30:70.

Line B corresponds to the front/rear torque distribution of a rigid 4WD system, which realizes stability even with sharp variations in the road surface and thus allows torque to be transmitted effectively at all times. If an emphasis on traction performance and stability is required, therefore, the center differential's front/rear torque-distribution should be established at 50:50.

Immediately after the application of a steering input to a vehicle that was previously moving in a straight line, the vehicle's instantaneous axis of rotation is, as shown in **Fig. 3**, located on the rear axle. At this time, the cornering radius followed by the front wheel is greater than that followed by the rear wheel, causing the front wheel to turn faster than the rear wheel. If the center differential limits the speed difference, torque circulation causes braking force BF to act on the front wheel and driving force DF to act on the rear wheel. The component force $BF \sin \alpha$ of the braking force acting on the front wheel acts in the direction opposite to

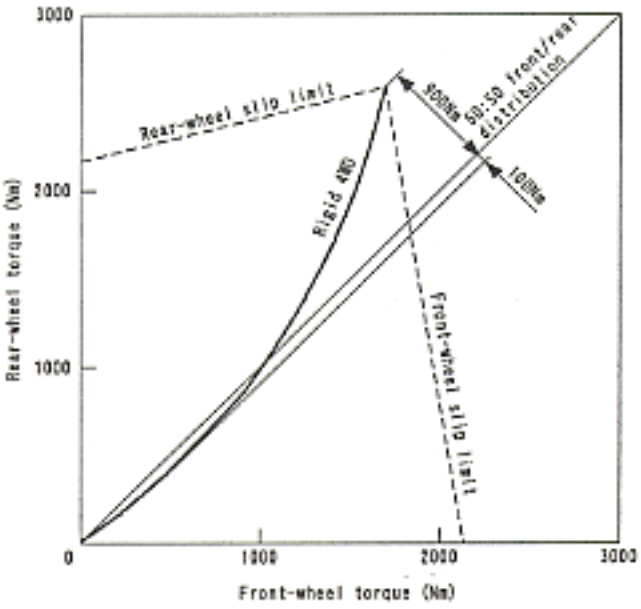

Fig. 4 Optimal capacity of LSD shown by static analysis

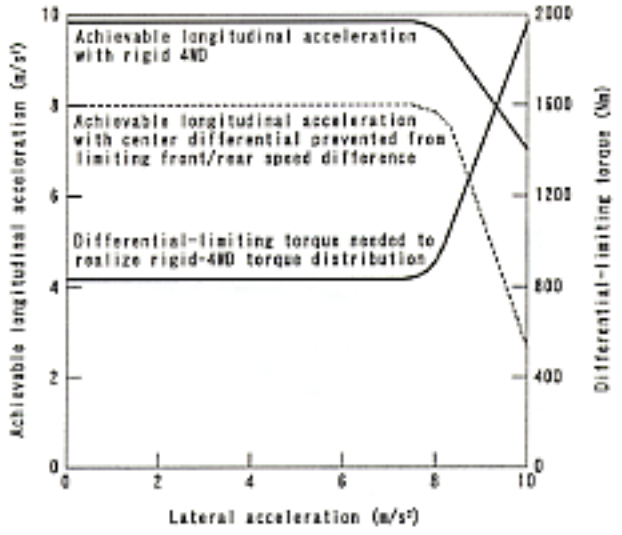

Fig. 5 Optimal capacity of LSD shown by dynamic analysis

that of the cornering force *CF* caused by the steering input, so directional response deteriorates if the center differential's differential-limiting action is strong. Irrespective of the center differential's torque-distribution ratio, then, better directional response can be realized by employing a differential-limiting device with controllable torque-transmission characteristics and preventing it from limiting the speed difference at the start of cornering maneuvers than by employing a VCU or other differential-limiting device whose torque-transmission characteristics are not variable.

In light of the factors described above, it was determined that the base front/rear torque-distribution ratio should be established at 50:50 (this ratio optimizes running performance and stability) and that directional response should be maximized by control of the center differential's differential-limiting action.

2.2 Differential-limiting torque

With a center differential that gives a 50:50 torque distribution, a differential-limiting torque of 900 Nm is, as shown in **Fig. 4**, sufficient to maintain a torque distribution equivalent to that of a rigid 4WD system under constant conditions. When the normal relationship between the total torque and the load borne by each of the four wheels is undone transiently (for example, when vehicle operation changes from full braking or hard cornering to acceleration with a wide-open throttle), however, the differential-limiting torque shown in **Fig. 4** is not sufficient to maintain a rigid-4WD torque distribution. To enable motorsports use, it is essential to ensure that a rigid-4WD torque distribution can be maintained (and running performance thus maximized) under such conditions.

One of the most severe transient conditions is brought about by a change in the vehicle's operation from hard cornering to rapid acceleration. The differential-limiting torque required to realize a rigid-4WD torque distribution is shown in **Fig. 5**. The calculations were performed using a four-wheel model to enable load shifts between the left and right wheels to be taken into account. Also, a model of a mechanical LSD with a transfer ratio of eight was used for each of the front and rear differentials to reflect the configuration of an actual vehicle. When an increase in lateral acceleration causes the left/right difference in wheel loading to exceed a certain value, the mechanical LSD at the rear becomes unable to limit the speed difference between the rear wheels and the inside rear wheel slips. If the center differential is prevented from limiting the front/rear speed difference at this time, the achievable rate of longitudinal acceleration drops significantly. With a rigid 4WD arrangement, by contrast, the proportion of torque applied to the front wheels is increased to compensate for the slipping inside rear wheel such that longitudinal acceleration does not decrease significantly. To realize a rigid-4WD torque distribution under these conditions, a differential-limiting torque of 2000 Nm was found to be necessary.

3. Structure and features

Fig. 6 shows the overall configuration of the system.

3.1 ACD transfer

In light of the factors described thus far, a highly reliable bevel-gear-type center differential with a front/rear torque-distribution ratio of 50:50 was adopted. Also, steel plates, which offer high dependability under conditions of high surface pressure, were specified for the hydraulic multi-plate clutch, which realizes a high differential-limiting-torque capacity of 2000 Nm (**Fig. 7**).

3.2 AYC differential

In terms of basic structure, the AYC differential is the same as that employed with earlier vehicles. However, various parts were reinforced to ensure reliable operation with higher levels of engine torque.

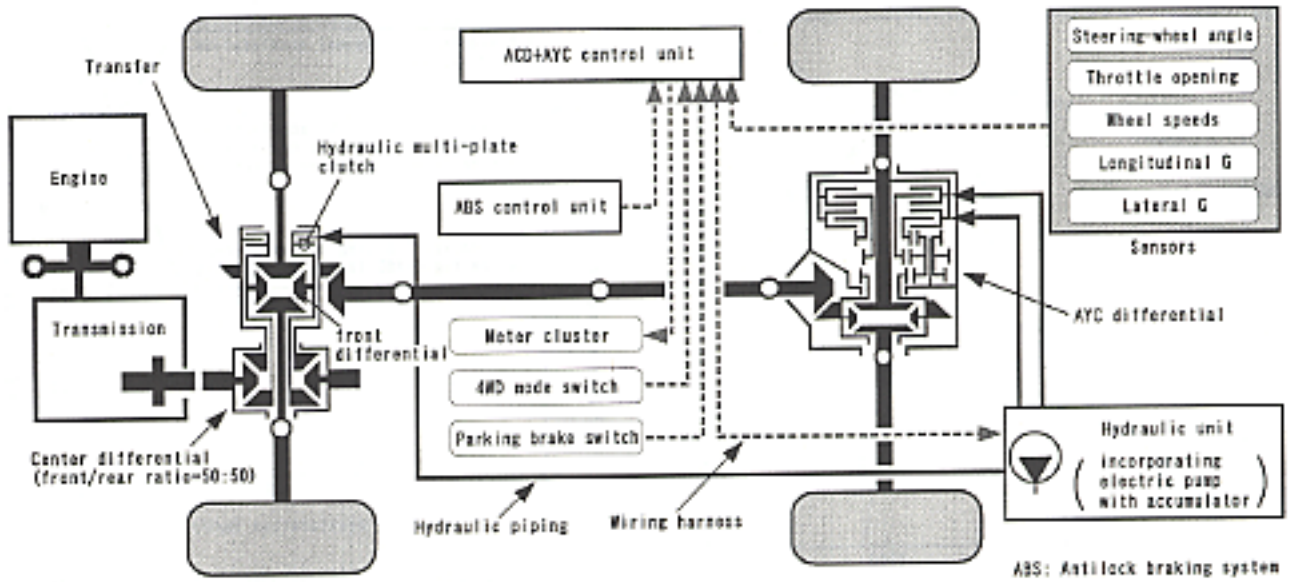

Fig. 6 Configuration of ACD + AYC system

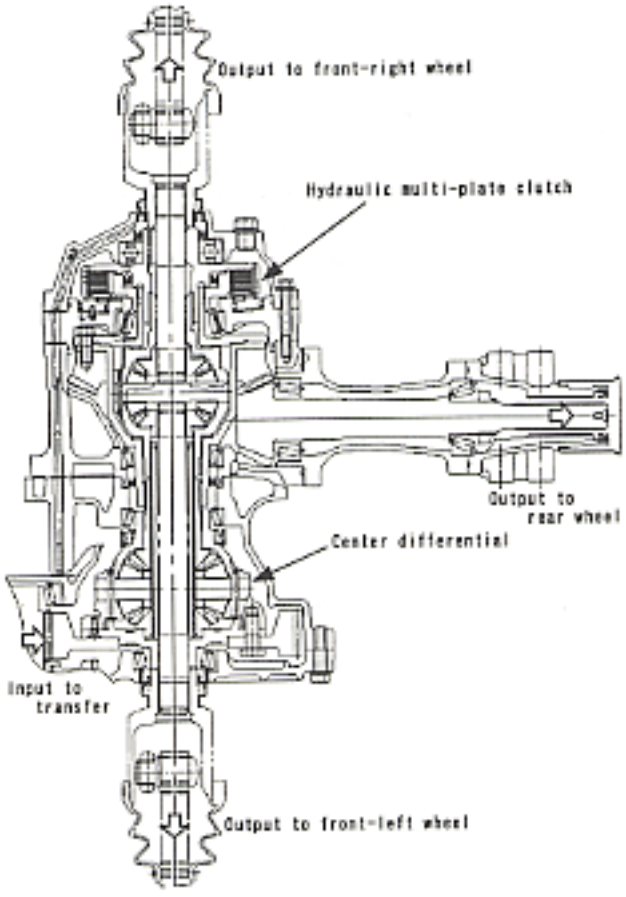

Fig. 7 ACD transfer

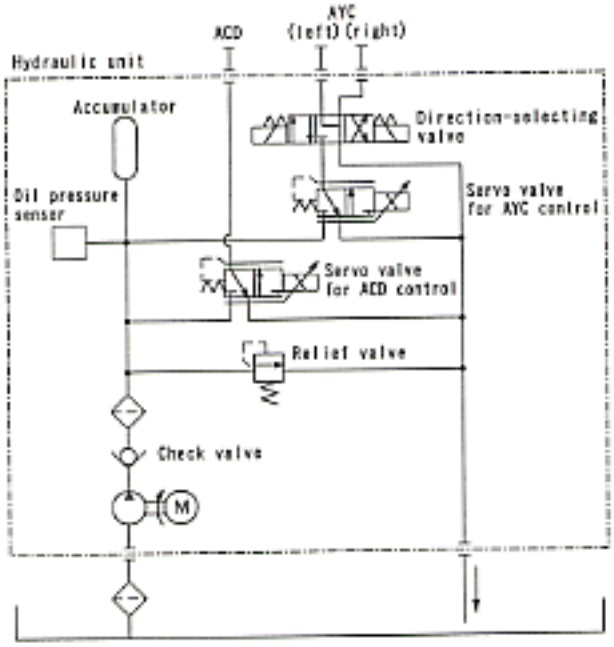

Fig. 8 Hydraulic unit

3.3 Hydraulic unit

A servo valve for ACD control was added to the previously employed AYC hydraulic unit, and the unit was made more compact. Also, an oil pressure sensor was adopted to increase reliability (Fig. 8).

3.4 4WD mode switch

For the system to operate with maximum effectiveness, its control must be tuned in accordance with current road-surface conditions. One possible means of enabling the necessary tuning was to cause the system to infer current road-surface conditions using data from sensors. However, such an arrangement was not adopted because its responsiveness was potentially unsatisfactory for motorsports use. Rather, the system was provided with a 4WD mode switch that gives the driver a choice of three control modes, each of which is tuned to suit a particular type of road surface (Table 1).

Table 1 ACD control modes

Mode	Type of road surface where beneficial
TARMAC	Dry paved surface
GRAVEL	Wet and/or unpaved surface
SNOW	Snow-covered surface

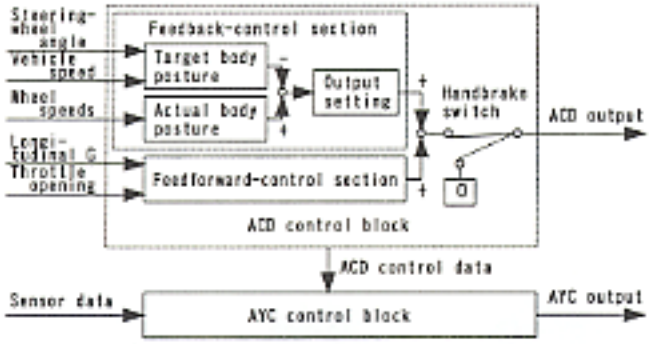

Fig. 9 Block diagram of ACD + AYC control

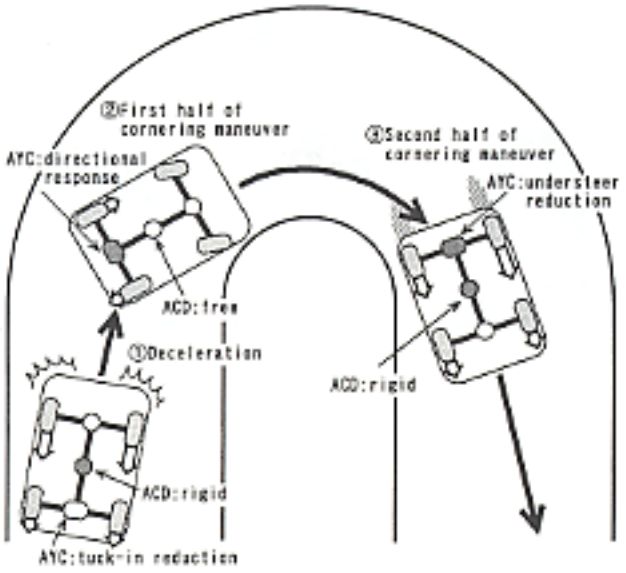

	ACD	AYC
(1) Deceleration (before curve)	Boosts center differential's differential-limiting action in line with rate of deceleration, thus improving stability.	In event of simultaneous cornering and deceleration: Transfers torque to inside wheel, thus reducing tuck-in.
(2) First half of cornering maneuver	Reduces center differential's restraint in accordance with steering-wheel angle and speed of rotation, thus improving directional response.	Transfers torque to outside wheel in accordance with steering-wheel angle and speed of rotation, thus improving direction response.
(3) Second half of cornering maneuver	Boosts center differential's differential-limiting action in accordance with extent of depression of accelerator pedal, thus improving driving performance.	Transfers torque to outside wheel in accordance with extent of depression of accelerator pedal, thus reducing acceleration understeer and improving directional response.

Fig. 10 Effects of ACD + AYC control

4. Overview of system control

Fig. 9 shows the ACD + AYC system's control process in the form of a block diagram. The newly developed ACD control block consists of two parts: (1) a feedback-control section that attempts to make the body's posture match a target posture that is determined from the steering-wheel angle and vehicle speed; and (2) a feedforward-control section that responds rapidly to the driver's acceleration and deceleration inputs. By altering the balance between the operations of these two sections, it is possible to tune the vehicle's behavior such that the vehicle responds more briskly or less briskly to steering inputs. Further, to facilitate handbrake turns the system weakens the center differential's differential-limiting action when the parking brake lever is pulled.

Differential-limiting data produced by the ACD control block for the center differential are modified by relevant parameters and passed to the AYC control block. The vehicle typically becomes prone to understeer in proportion to the strength of the center differential's differential-limiting action, so the AYC control block increases the oversteer moment accordingly.

The effects of this control arrangement are summarized in **Fig. 10**. Notably, at the exit of a curve ③ running performance is optimized primarily by the ACD and cornering performance is optimized primarily by the AYC, resulting in dramatically improved cornering performance during acceleration.

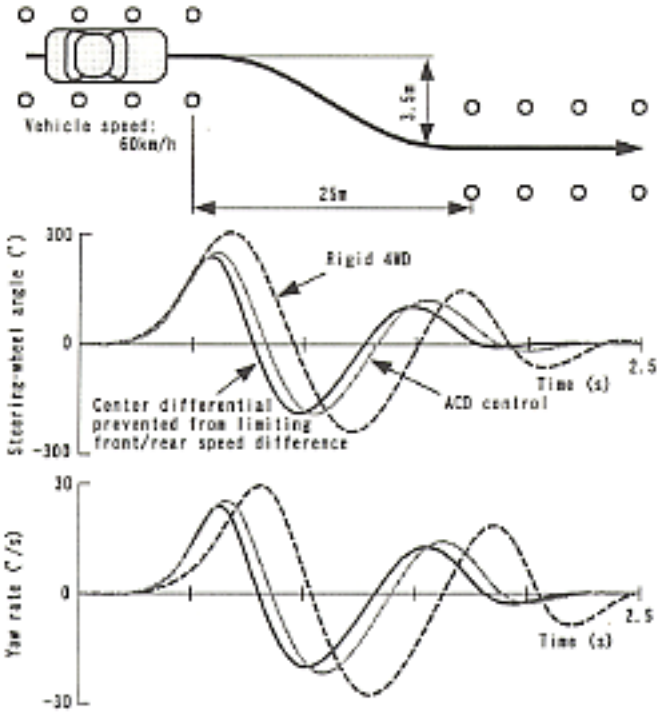

Fig. 11 Vehicle behavior observed during lane-change maneuver

5. Vehicle performance

The system was tested in an actual vehicle.

Fig. 11 shows the vehicle behavior observed during a lane-change maneuver on compressed snow. Yaw response at the beginning of the steering operation was

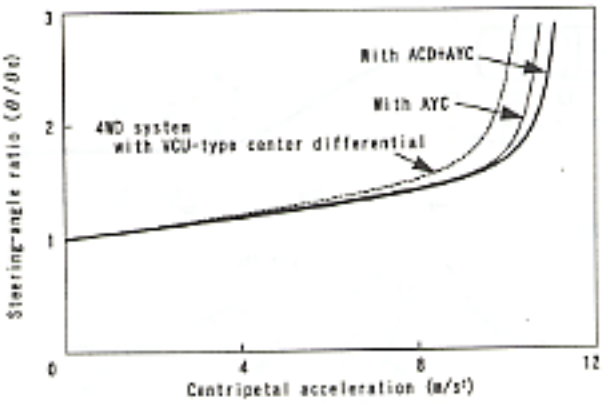

Fig. 12 Constant-radius cornering characteristics

superior with the center differential prevented from limiting the front/rear speed difference, and corrective steering inputs were concomitantly small. ACD control produced results similar to those observed with the center differential prevented from limiting the front/rear speed difference.

Fig. 12 shows the cornering characteristics observed with the vehicle gradually accelerating while being steered around a track with a constant radius of 30 m. As shown, the limits of the vehicle's cornering performance were expanded even further by the AYC and ACD together than by the AYC alone.

6. Summary

By setting the center differential's differential-limiting torque taking into account the relationship between the total torque and the load borne by each of the four wheels under transient conditions, the authors realized a 4WD-system ACD that can be used in motorsports. By combining the ACD with AYC, we expanded the limits of cornering performance even further.

We shall continue developing superior drive-train systems with a view to achieving further advances in high-performance 4WD vehicles.

References

(1) Sawase et al.: "Integrated Control of Driving Force", Journal of JSAE, Vol. 46, No. 10, 1992
(2) Sawase et al.: "Development of Active Yaw Control System", Journal of JSAE, Vol. 50, No. 11, 1996
(3) M. Kato et al.: "Study on Vehicle Dynamics in Marginal Condition Using Dynamic Square Method", IPC-8, 9531020, 1995


Kaoru SAWASE


Yuichi USHIRODA


Tadashi YOSHIOKA


Keiji SUZUKI


Kunihiro MANABE


Takao MATSUI

NEW TECHNOLOGIES

Development of Small-Bore Line-Boring Machine for Machining of Holes in Cylinder Head

Misao NAKAMURA* Hitoshi KAZUMI*

Abstract

The 4M5 diesel engine is a 5.2-liter, DOHC, 4-cylinder, direct fuel-injection unit developed for powering Mitsubishi Motors' small trucks and buses. This high-performance, highly-fuel-efficient engine complies with Japan's long-term exhaust emission standard and is used in the FUSO CANTER trucks and ROSA buses that were market launched in October 1997. Line production of this engine involves boring of two camshaft holes in the cylinder head – one of the engine's most important components. As the camshaft holes require an extremely high level of precision that is difficult to achieve with the conventional machine and process, a new boring machine and finishing process for the camshaft holes in the 4M5 engine's cylinder head have been developed. This paper describes details of the development.

Key words: *DOHC, Cylinder Head, Two Camshaft Holes, New Boring Machine*

1. Introduction

The camshaft holes in an engine's cylinder head must be machined not only with the correct diameter and roughness but also with a high degree of precision in terms of roundness, straightness, and cylindricity. To satisfy these requirements, they are typically finished by means of line-boring using line-boring bars.

Unfortunately, the accuracy achieved with line-boring is greatly influenced by the length-to-diameter (L/D) ratio of the workpiece; sufficient accuracy is more difficult to achieve with a higher L/D ratio than with a lower one since line-boring-bar rigidity is lower and the machined surfaces are more prone to irregularities caused by tool vibration.

With the cylinder head of a conventional truck diesel engine, the L/D ratio is no higher than 10. With the cylinder head of the 4M5 engine, however, the L/D ratio is significantly higher at 17.8. Further, the cylinder head of the 4M5 engine consists of materials that require different degrees of cutting force. (The main body of the cylinder head is made of FC250 cast iron, and the camshaft frame that retains the camshafts at the top is made of AC4AF aluminum alloy.) For these reasons, difficulty in achieving the required accuracy was expected.

Basic tests were conducted to establish production methods capable of yielding the required accuracy. The basic configuration of the necessary production machinery was established in accordance with the test results, and the machinery was designed and fabricated at Mitsubishi Motors Corporation's Tokyo Plant. This paper describes the work and the resulting machinery.

2. Overview of 4M5 engine's cylinder head

An external view of the 4M5 engine's cylinder head is shown in **Fig. 1**.

Since the main body is made of FC250 cast iron and the camshaft frame, which retains the camshafts at the top, is made of AC4AF aluminum alloy, the top and bottom halves of each camshaft hole are made of different materials.

As shown in **Fig. 1**, the cylinder head has an overall length (L) of 623.5 mm and the camshaft holes, which hold the intake and exhaust camshafts, each have a diameter (D) of 35 mm. Also as shown, there are five journals for each camshaft.

3. Basic tests for establishment of production methods

With line-boring, the required cutting conditions vary greatly in accordance with the relationship between the hole diameter (D) and workpiece length (L); the higher the L/D ratio becomes, the greater is the extent of line-boring-bar deflection and the higher is the risk that the machined surfaces will contain irregularities caused by tool vibration[1]–[3]. High-rigidity cemented-carbide line-boring bars, which are extremely costly, are thus widely used for line-boring in situations where accuracy is difficult to achieve because of a high L/D ratio.

Steel line-boring bars are less rigid than cemented-carbide line-boring bars, but they are only a third of the price and can be obtained more quickly. To minimize production costs with the 4M5 engine, therefore, basic tests were conducted with the goal of establishing production methods that would yield the required accuracy using steel line-boring bars.

* Car Production Headquarters, Tokyo Plant

3.1 Basic tests

Test workpieces with the same dimensions and materials as a production cylinder head were machined using a general-purpose horizontal machining center equipped with steel line-boring bars. The tests were conducted to clarify

(1) the influence on manufacturing quality of intermediate supports used to minimize line-boring-bar deflection; and

(2) the influence on form deviation of the combination of parts made of different materials (cast iron and aluminum alloy).

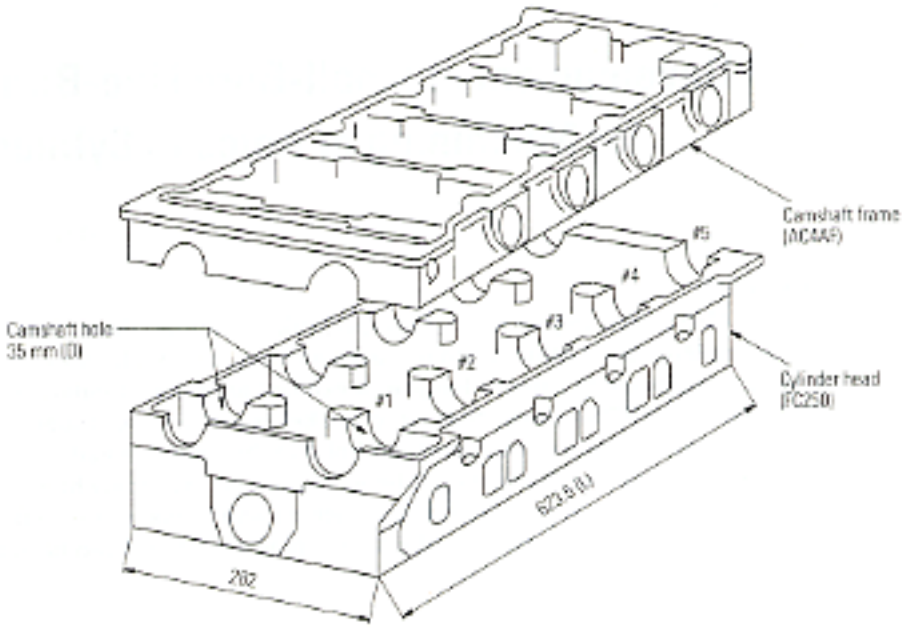

Fig. 1 Cylinder head of 4M5 engine

3.1.1 Influence of intermediate supports

Fig. 2 indicates the influence of an intermediate support on the extent of deflection of a line-boring-bar that was fixed support at one end and free support at the other. Measurements of deflection were taken separately with no intermediate support, with an intermediate support between journals #2 and #3 (position B in **Fig. 2**), with an intermediate support between journals #3 and #4 (position C in **Fig. 2**), and with an intermediate support between journals #4 and #5 (position D in **Fig. 2**). As shown, the inclusion of an intermediate support had a significant influence on line-boring-bar deflection.

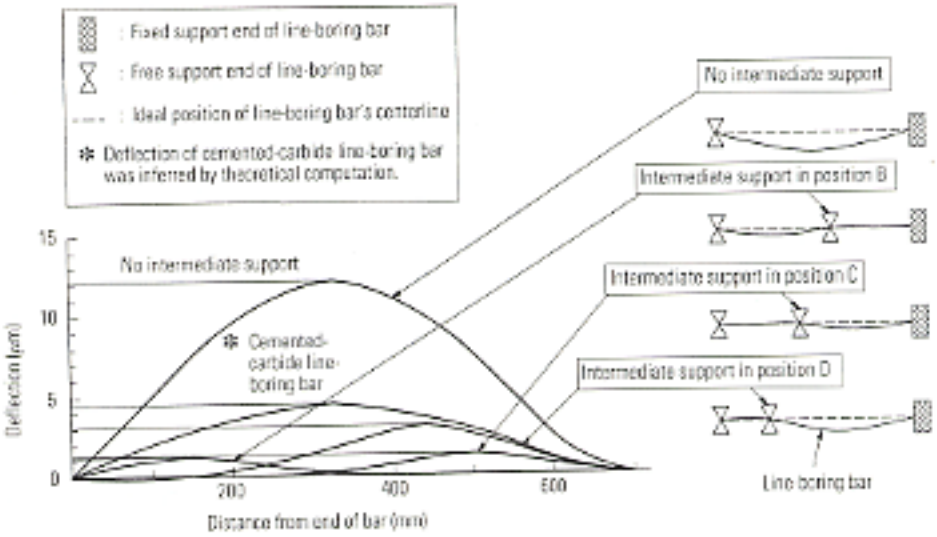

Fig. 2 Relationship between line-boring bar's deflection and support location

In the next stage of the investigation, test workpieces were machined with no intermediate support, with an intermediate support in position B, with an intermediate support in position C, and with an intermediate support in position D. The cutting speed at which the tool started vibrating and causing surface irregularities was noted each time. From the findings (shown in **Fig. 3**), correlation between the line-boring bar's maximum deflection and the cutting speed was confirmed and the existence of a distinct cutting-speed threshold between tool stability and tool vibration was inferred.

It was further determined from the findings shown in **Fig. 3** that the inclusion of intermediate supports in production machinery would be necessary to enable machining to be completed within the limited time available on the production line.

3.1.2 Machining of composite material

The influence on machining form deviation of the combination of different materials used for the cylinder head's main body and camshaft frame was next investigated.

Fig. 4 shows the roundness achieved by test machining under conditions identical to those described in part 3.1.1 of this paper. The stagger at the joint between the main body and camshaft frame was significantly greater without an intermediate support (see the left-hand results in **Fig. 4**) than with one (see the right-hand results in **Fig. 4**, which correspond to an intermediate support in position C). In other words, the roundness achieved without an intermediate support was significantly inferior to that achieved with one. Comparison of the holes bored in the respective journals without an intermediate support revealed that out-

of-roundness was greatest in journal #3 (near the middle of the cylinder head), i.e., in the journal nearest the line-boring bar's point of greatest deflection. In test machining, out-of-roundness reached a maximum of 27 μm in this journal.

In test machining performed with an intermediate support in position C, the maximum out-of-roundness at the joint was only 7 μm, i.e., approximately a quarter of the maximum out-of-roundness that resulted from boring without an intermediate support. Further, the degrees of roundness achieved in all of the respective journals were more or less consistent. The benefits of the presence of an intermediate support along the line-boring bar during machining of the composite material were thus verified.

From the findings described above, it was determined that intermediate supports for the line-boring bars would be beneficial parts of the production machinery's structure and that the undesirable effects on accuracy of the composite material could be minimized thereby.

3.2 Summary of results of basic tests

The basic tests yielded the following conclusions:

(1) The inclusion of an intermediate support along each line-boring bar is beneficial with respect to manufacturing quality.

(2) The same intermediate support is also beneficial with respect to machining form deviation with a composite material.

Nevertheless, it was determined that measures to improve accuracy further were necessary to ensure consistent accuracy on the production line.

4. Basic structure and other features of production machinery

4.1 Overview of main body

The line-boring machine developed for the production line in accordance with the results of the basic tests is shown in Fig. 5. At the right-hand side is a two-spindle line-boring unit that uses an alternating-current (AC) motor to drive the spindles via a timing belt. The use of a timing belt for power transmission allows the two line-boring bars' cutting-tool tips to be aligned in the same direction at all times and thus allows offset insertion of the line-boring bars into the camshaft holes in the cylinder head.

The line-boring unit has a mechanical feed unit employing an AC servo motor. This arrangement allows the feed speed to be varied easily. At the opposite side of the machine is a support unit that supports the ends of both line-boring bars during the machining

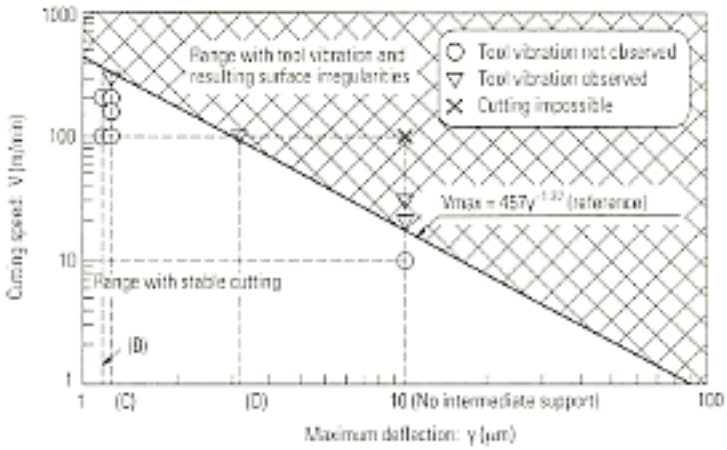

Fig. 3 Relationship between cutting speed and maximum deflection for each line-boring-bar support location

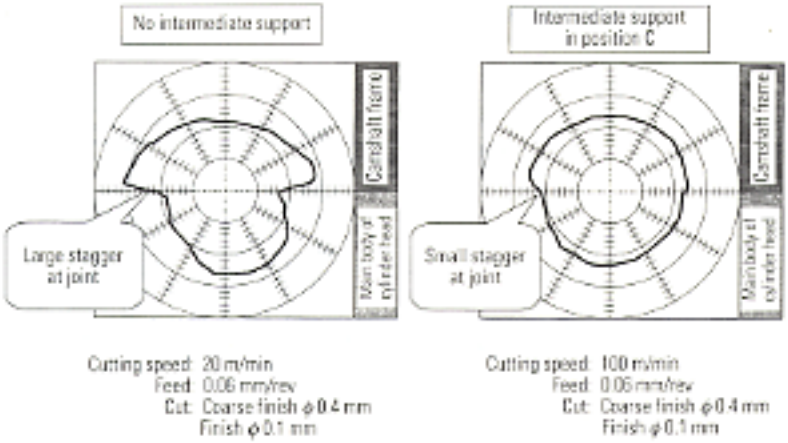

Fig. 4 Roundness of a journal hole drilled in composite material (aluminum casting + ferrum casting)

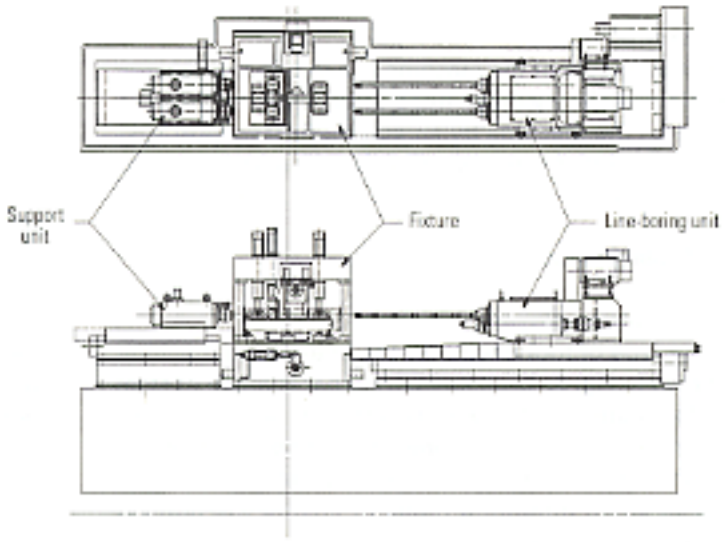

Fig. 5 Top and side views of line-boring machine

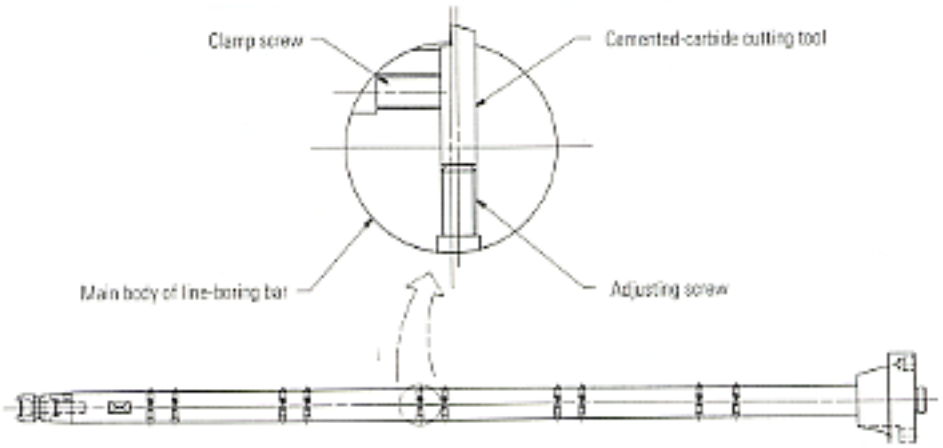

Fig. 6 Line-boring bar

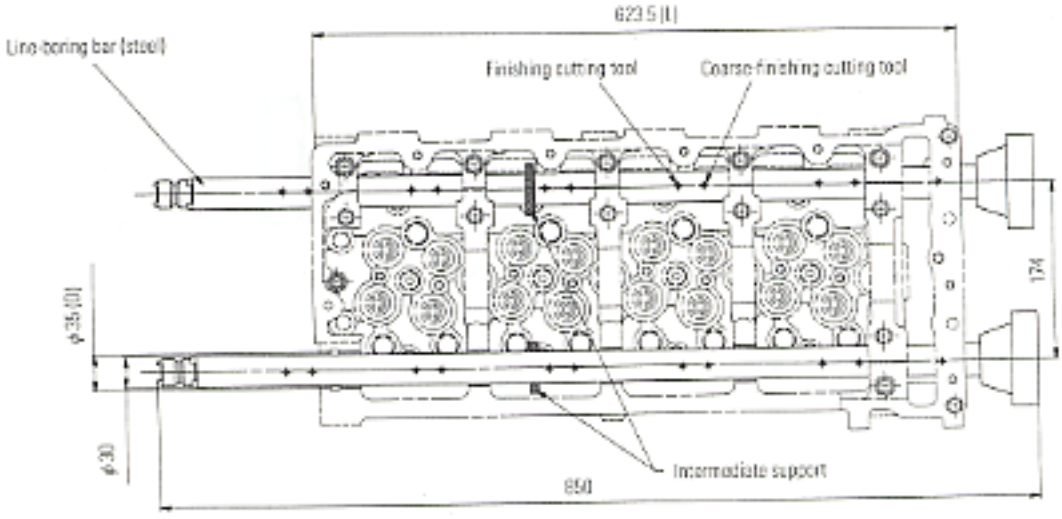

Fig. 7 Tooling layout

process.

In the middle of the machine is a fixture that locates and clamps the cylinder head (each cylinder head is placed on the machine by an automatic transport system) and is fitted with a support for the middle of each line-boring bar.

4.2 Tooling layout

4.2.1 Tools employed

The type of tool used with the line-boring machine is shown in **Fig. 6**. Each line-boring bar is made of steel (SCM415) and is fitted with two round, cemented-carbide (HTi10) cutting tools (one each for coarse finishing and finishing) for each journal. The cutting tools are fixed to small mounting holes to ensure the highest possible bar rigidity.

4.2.2 Tooling layout

Fig. 7 shows the machine just before it begins cutting material after inserting the line-boring bars into the camshaft holes in a cylinder head. The intermediate supports (one for each line-boring bar) are made of ceramic and are 8.5 mm thick. They were positioned in accordance with the results of the basic tests to ensure that they would give the greatest possible benefit without interfering with the workpiece and cutting tools during the machining process.

4.3 Tensioning mechanism for line-boring bars

The effectiveness of an intermediate support in reducing the line-boring-bar deflection that accompanies a high L/D ratio and in increasing the roundness of holes bored in a composite material was confirmed through the basic tests. However, further improvements in shape deviation and surface roughness were required before the machine could be used on the production line. The machine was thus provided with a mechanism that increases line-boring-bar rigidity by applying tension to the line-boring bars throughout the machining process. By further reducing line-boring-bar deflection, this mechanism further increases the roundness of the camshaft holes.

The tensioning mechanism is shown in **Fig. 8**. It operates as follows:

① The main-spindle head is moved forward by the

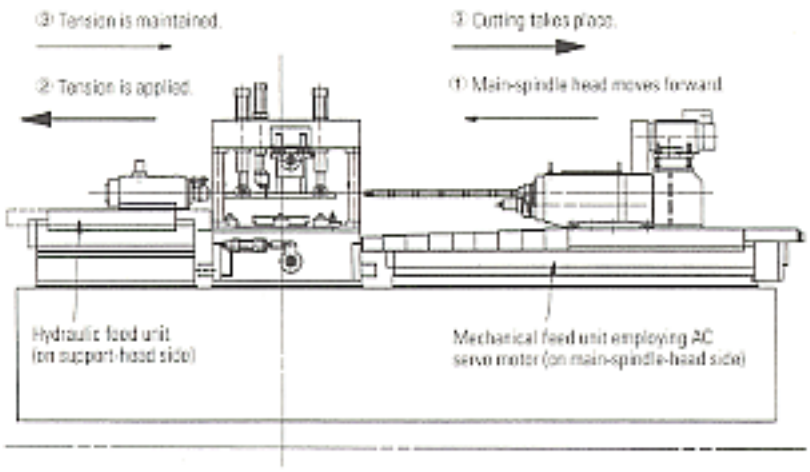

Fig. 8 Tensioning mechanism for line-boring bars

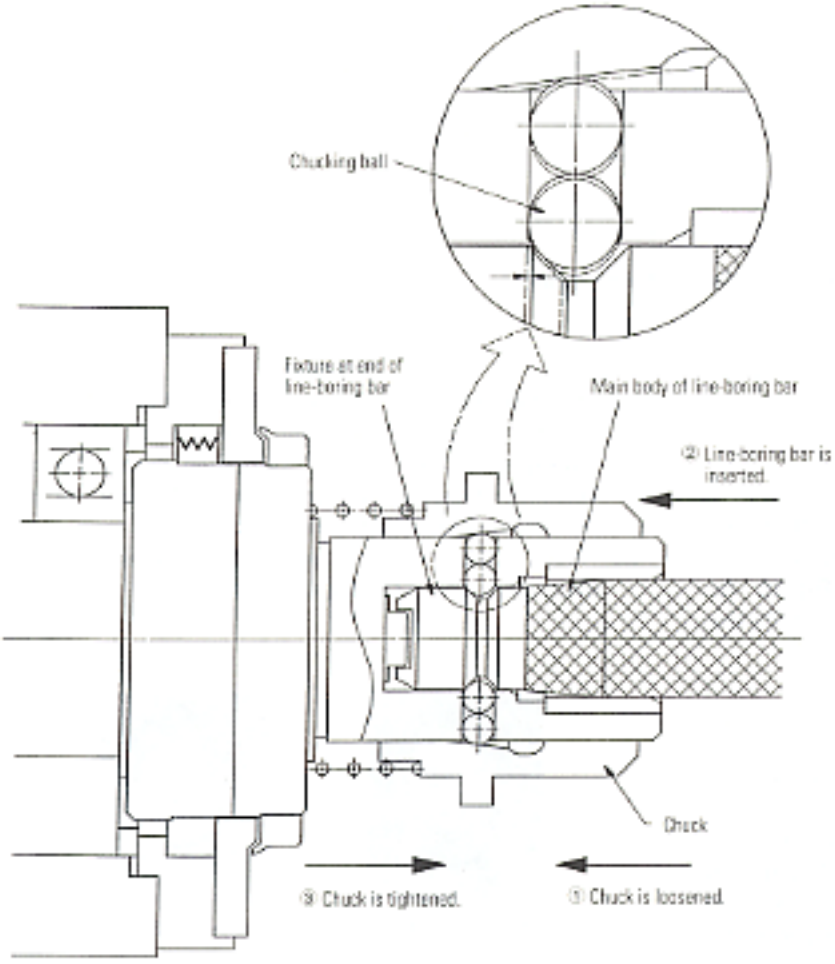

Fig. 9 Cross-sectional view of chucking mechanism

mechanical feed unit. Thus, the line-boring bars pass through the camshaft holes in the cylinder head and their ends enter the support head, where they are retained by a chucking mechanism.

② Before the main spindle turns, the hydraulic feed unit starts pulling the support head in the reverse direction, thereby applying tension to the line-boring bars.

③ With the hydraulic feed unit still pulling the support head in the reverse direction, the main spindle turns such that the mechanical feed unit moves in the reverse direction. Thus, the line-boring bars bore the camshaft holes under consistent tension.

The tension applied to the line-boring bars is optimized by adjustment of the hydraulic pressure applied to the hydraulic feed unit.

4.4 Support head

The cylinder head of the 4M5 engine contains a double-overhead-camshaft valve system and thus incorporates camshaft holes for two camshafts (an intake camshaft and an exhaust camshaft). To maximize the positional accuracy of the two sets of camshaft holes, the line-boring machine bores the two sets of camshaft holes simultaneously.

When two line-boring bars of the same type are produced, they typically differ slightly in terms of length owing to inconsistent factors in the production process. To enable the two line-boring bars to be used for machining under identical tension, it is necessary to compensate for the length difference while retaining both line-boring bars with the same force. To overcome this problem, a new type of chucking mechanism was employed in the support head.

Fig. 9 shows the new chucking mechanism in detail. The mechanism operates as follows: ① The chuck is loosened. ② The line-boring bars are inserted into the support head. ③ The balls in the chucking mechanism enter the groove in the fitting at the end of each line-boring bar as the chuck is tightened and are clamped in their respective grooves by the wedging action of tapered surfaces. The length difference between the two line-boring bars causes the balls to press against the two line-boring bars' respective grooves at different depths. The length difference is thus absorbed by the mechanism. This mechanism enables both line-boring bars to be retained without mechanical complexity. Further, the wedging action of the tapered surfaces ensures that the retaining force applied to the two line-boring bars is both consistent and adequate.

Continuous contact between the chucking balls and the fitting at the end of each line-boring bar makes wear and other problems conceivable. To facilitate maintenance during production and keep costs to a minimum,

Cutting conditions		Coarse finish	Finish
Cutting speed	(m/min)	152	
Feed	(mm/rev)	0.08	0.03
Cut	(mm)	0.5	0.2
Cutting tools		Material: cemented carbide, nose radius: 0.4 mm	

Manufacturing quality		
Roundness	(μm)	2.0
Straightness	(mm)	φ 0.02
Surface roughness	(μm)	6.05

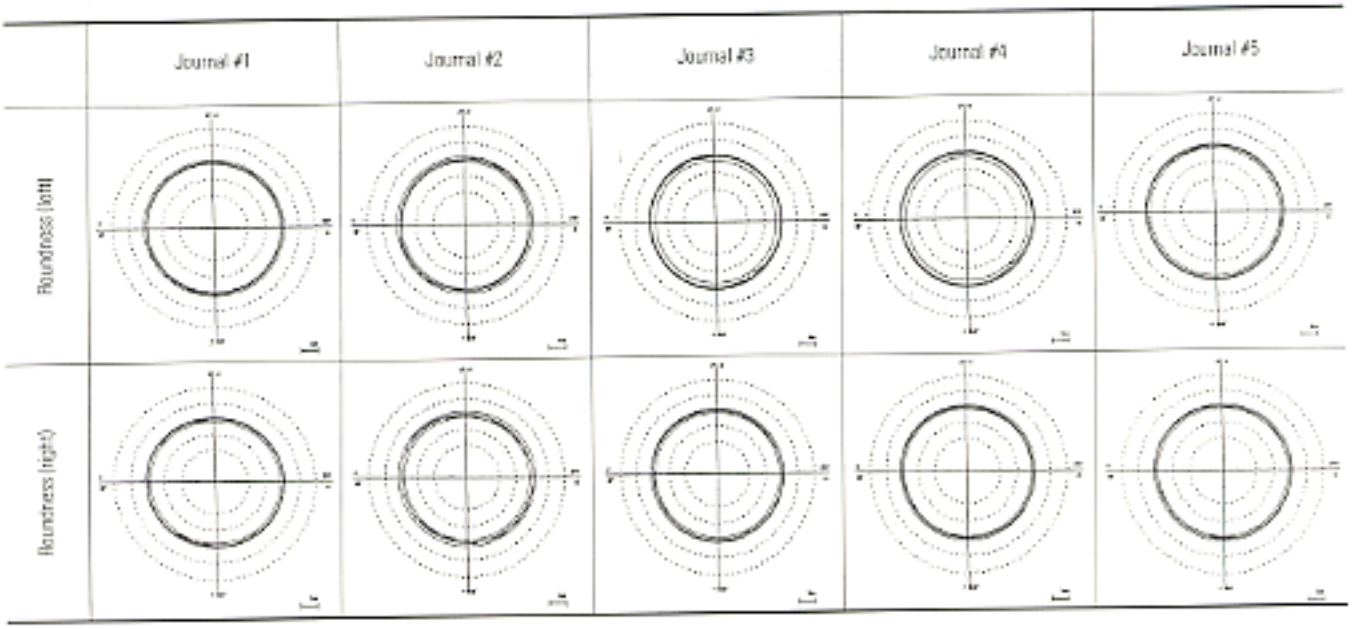

Fig. 10 Manufacturing quality

therefore, the fitting at the end of each line-boring bar is removable.

5. Manufacturing quality

The manufacturing quality of camshaft holes machined with the small-bore line-boring machine described in part 4 of this paper is shown in **Fig. 10.** As shown, the machine yields excellent results despite the high L/D ratio and composite material.

6. Closing comments

The testing, planning, designing, and fabrication tasks necessary for development of the line-boring machine took approximately one year. During this period, the authors enjoyed the cooperation of Mitsubishi Materials Corporation and various other parties. The authors wish to express their gratitude to everyone who helped make the project a success.

References

(1) "Ana Kakou Kaiden" (The Art of Boring), Sessaku Gijutsu Kenkyuu Kai (Society for Cutting Oil Research), 1994, p. 135
(2) "Nakaguri Ni Okeru Bibiri" (Vibration during Boring), Technical Research Institute, Japan Society for the Promotion of Machine Industry 50, 3A, 00
(3) "Kikai Kakou Bibiri Genshou" (Vibration during Machining), Kogyo Chosakai Publishing Co.

Misao NAKAMURA

Hitoshi KAZUMI

NEW TECHNOLOGIES

New Technologies for CVT Production Line

Katsuya FUJIWARA* Yoichiro DATE* Masaru ARIYASU*

Abstract

Mitsubishi Motors started production of its first continuously-variable-transmission (CVT) in a specially-established plant, and for use in this plant, the company has recently developed a high-temperature-carburizing continuous furnace and a multi-grinder for the production of those sheaves which are exclusive to the CVT. The high-temperature carburizing continuous furnace allowed the carburizing of materials at temperatures of up to 1050 °C – a world's first. Furthermore, the multi-grinder can efficiently cut sheaves of complicated shapes, and it can do this with an extremely high degree of accuracy and without the need for additional machinery.

Key words: *Carburizing, Multi-Grinder, Sheaves, Internal Groove*

1. Introduction

Mitsubishi Motors recently constructed in Yagi-cho, Kyoto Prefecture, Japan, a plant specially for production of its first continuously variable transmission (CVT), which is fitted in the LANCER CEDIA. The CVT combines smooth acceleration with low fuel consumption. A variety of new technologies were adopted in production processes for functional parts that enable the CVT to realize these superior characteristics.

Among them are new heat-treatment and grinding processes for power-transmission sheaves, which are important parts of the CVT. This paper gives an overview of these two technologies.

2. High-temperature (1050 °C) carburizing furnace

2.1 Issues related to heat treatment of sheaves

A CVT is a power-transmission mechanism in which the power is transmitted from a driving element to a driven element by means of a metal belt that is pinched in two hydraulically operated pairs of sheaves (one pair each on the driving and driven elements) (**Fig. 1**). Since the CVT has a simple structure and permits stepless shifts, it offers the advantages of zero shift shock and high transmission efficiency.

Relative slippage between the belt and sheaves during shifts makes the contact surfaces of the belt and sheaves prone to wear and surface separation. Thus, the sheaves are carburized at a temperature in excess of 900 °C then case hardened. To give the sheaves sufficient wear resistance, the carbon-permeation depth must be at least twice that realized with typical carburization. The time required for carburization is proportional to the square of the carbon-permeation depth. The sheaves therefore require four times the typical carburization time. The required time is approximately 10 hours.

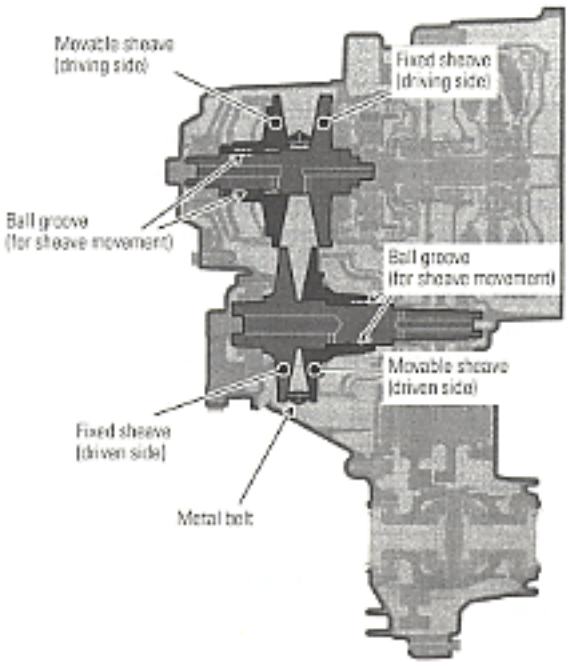

Fig. 1 CVT sectional view

2.2 Reduction of carburization time

To shorten the carburization time, a plan to perform carburization at 1050 °C was devised; it was recognized that the higher carburization temperature would activate the carbon, causing it to diffuse into the material more quickly. This technique had been used previously with certain vacuum furnaces. With continuous ambient-pressure carburizing furnaces, however, slower technological development meant that the highest carburization temperature previously achieved was 950 °C. Obstacles to the adoption of 1050 °C carburization and steps taken to overcome them were as follows:

(1) High-temperature durability of carburizing furnace

The high-temperature strength of materials used in the construction of furnaces typically decreases sharply when the temperature exceeds 950 °C. Bricks and

* Car Production Headquarters, Kyoto Plant

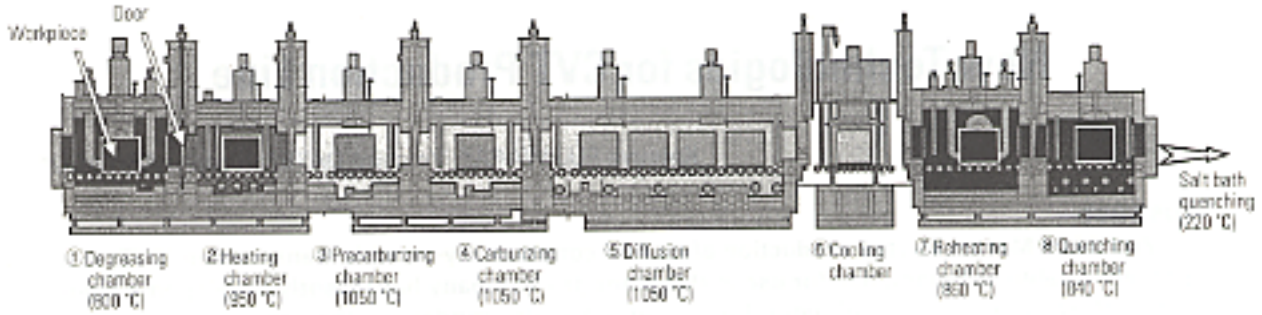

Fig. 2 High-temperature carburizing continuous furnace

heaters capable of withstanding a temperature of 1400 °C were thus specified for use in the new furnace. Also, rollers made of ultra-heat-resistant steel were specified.

(2) High-temperature deterioration in material strength (grain growth coarsening)

Keeping the temperature of a workpiece as high as 1050 °C for a long period can lead to deterioration in material strength (grain growth coarsening). The conventional countermeasure is to make enlarged crystal grains smaller by quenching them again. However, this technique entails the energy losses of two temperature increases and makes the process complex. To avoid these conventional problems, a type of steel whose crystal grains do not grow at high temperatures was developed in conjunction with a steel manufacturer[1].

(3) Control of furnace atmosphere

Higher temperatures necessitate a higher degree of accuracy in analysis of the furnace atmosphere; the accuracy required at 1050 °C is 10 times that required at 900 °C. For continuous measurement of CO, CO_2, and CH_4, therefore, high-precision infrared analysis equipment was specified.

2.3 Development of high-temperature carburizing furnace

Key specifications of the new high-temperature carburizing furnace are as follows.

- Carburization temperature: 1050 °C
- Furnace type : Roller-hearth continuous carburizing furnace
- Quenching process : Salt bath quenching
- Furnace gases : Gases denatured in furnace (butane + air)
- Atmosphere control : CO/CO_2 control

The furnace structure was a particularly important consideration in the development effort. As shown in **Fig. 2**, the furnace was designed with eight individually isolated chambers, allowing the atmosphere to be established on a zone-by-zone basis. In the degreasing chamber ①, cutting oil on the workpieces is burned off and the temperature of the workpieces is increased to 600 °C. In the heating chamber ②, the temperature of the workpieces is further increased to 950 °C. In the precarburizing chamber ③, the temperature of the workpieces is increased to 1050 °C and the workpieces' surface carbon concentration is increased. In the carburizing chamber ④, the workpieces' surface carbon concentration is further increased, thus increasing the carbon concentration gradient between the surface and interior of the workpieces such that the carbon is enabled to diffuse more forcefully into the material. In the diffusion chamber ⑤, the carbon is caused to diffuse from the surface to a depth of almost 2 mm. When carburization is finished, the workpieces pass through the cooling chamber ⑥ and reheating chamber ⑦. The workpieces then enter the quenching chamber ⑧, where they are kept at a temperature of 840 °C before being rapidly cooled to 200 °C in a salt solution outside the furnace.

CO, H_2, and N_2 gases are produced through the reaction of butane and air in catalysts fitted on the furnace floor, and a small amount of butane is added to them. The resulting mixture of gases is fed into the furnace. The gases undergo chemical reactions on the surface of the steel, causing the carbon to penetrate from the surface. The carbon's penetration power is calculated from the gas composition indicated by the aforementioned high-precision infrared analysis equipment, and it is controlled by concomitant adjustment of the amount of added butane. A high degree of accuracy is required in gas measurements taken at high temperatures; any inaccuracy in the measurements could lead to inadequate carburization and cause the inside of the furnace to become covered with soot.

Critical factors in addition to the gas control process include the gas feed positions and the gas sampling mechanism. Through improvement of these and other factors, carburization at 1050 °C on the production line was achieved for the first time. Carburization time was thus cut to one quarter of that previously required, resulting in a dramatic improvement in productivity.

3. Development of high-precision multi-grinder

3.1 Machining of CVT sheaves

The movable sheaves of a CVT are important functional parts. They are mated with their corresponding fixed sheaves and realize shifts by moving relative to the fixed sheaves under hydraulic control. Movement of the movable sheaves is permitted by hardened balls that run in grooves between the movable and fixed sheaves in the manner of linear-movement ball bearings (**Fig. 1**). Datum faces related to the movement of each movable sheave are the inside diameter, the ball

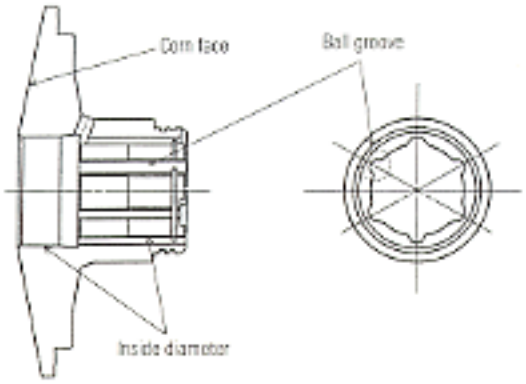

Fig. 3 Movable sheave

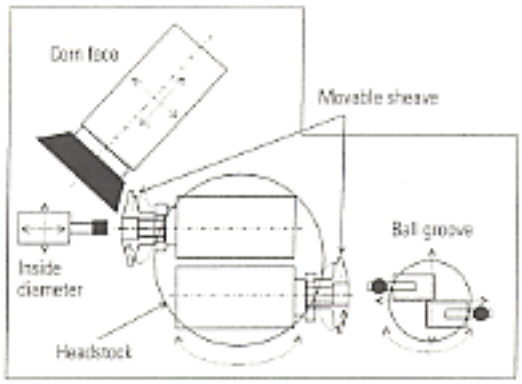

Fig. 4 Multi-grinder layout

grooves, and the corn face that makes contact with the steel belt (**Fig. 3**). The dimensional accuracy of these three faces is critical, so grinding is necessary after hardening.

3.2 Selection of production method

With a line configuration employing conventional general-purpose machine tools, the oblique face, inside diameter, and ball grooves must be machined in separate processes. Since each workpiece must be moved from one machine tool to the next, consistent coaxiality is difficult to achieve. A multi-grinder capable of machining all three faces simultaneously without requiring the workpiece to be unclamped was thus specified.

3.3 Development of multi-grinder

At the center of the multi-grinder is a 180°-rotatable headstock carrying two clamps. Facing the headstock on the left-hand side is a machining unit for the corn face and inside diameter, and facing the headstock on the right-hand side is a machining unit for the ball grooves (**Fig. 4**). This configuration was selected for high precision and high productivity.

The ball grooves are specified in terms of shape, inner ball diameter, and tolerable matching error, but machining of the inside diameter in accordance with the specifications is extremely difficult owing to restrictions on the grinding-wheel diameter and wheel-spindle length. To ensure consistent machining accuracy, therefore, various refinements, none of which had been seen among machine tools made by other companies for similar purposes, were incorporated into the multi-grinder (**Fig. 5**).

Key technological features are as follows:

(1) The wheel spindles are made of a tungsten alloy, and the spindle-to-workpiece clearance is minimized. This arrangement maximizes rigidity.

(2) Ultra-high-speed wheel spindles driven by a high-speed motor and belt realize an appropriate machining speed even with small-diameter grinding wheels. Also, high-pressure coolant is sprayed from the wheel spindles to enhance machinability.

(3) To realize consistent accuracy and a long grinding-wheel life, the extent of machining necessary for finishing is minimized by the use of two spindles (one for coarse grinding and one for finishing).

(4) To minimize thermal deformation of the machine, a coolant-temperature regulator is provided, allowing the coolant to be supplied at a temperature consistent with the head temperature.

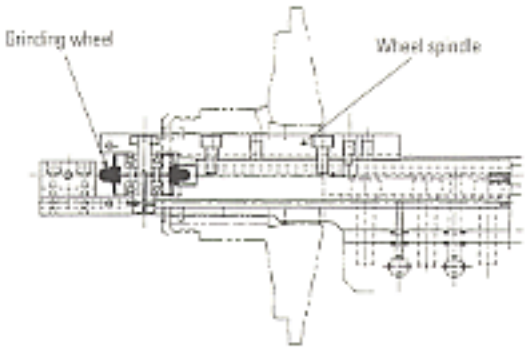

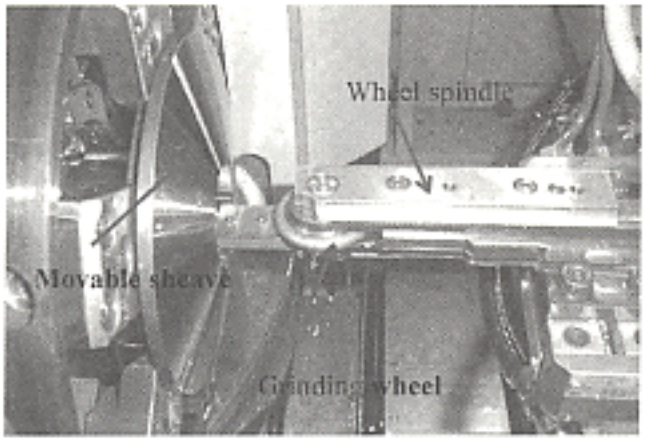

Fig. 5 Internally grooved wheel spindle

The above mentioned refinements made it possible to machine the ball grooves with levels of inner-ball-diameter tolerance and matching error that were superior both to the guaranteed performance of other, similar machines and to the levels achieved in test machining. Further, the target process capability of Cpk 1.0 was achieved. Consistent machining accuracy on the production line was thus realized.

4. Conclusion

Although this paper deals primarily with new technologies for the production of CVT sheaves, the new CVT plant where they are used also incorporates advanced environmental technologies intended to realize clean, environment-friendly operation. In terms of both its production line and its environmental compatibility, the new CVT plant offers state-of-the-art benefits.

Reference

(1) Noritsune Harada, Yuuichi Yamada, Kazuhiko Kato: "Development of a New Alloy Steel for High Temperature Carburizing", Mitsubishi Motors Technical Review, NO. 12, p. 47 – 53, 2000


Katsuya FUJIWARA


Yoichiro DATE


Masaru ARIYASU

A Challenge to 24-hour Travel Distance Record of EV

Tomiji OWADA*

An electric vehicle (EV), a MMC's FTO-EV, covered a distance of 2142 km in a 24 hour continuous run on December 19 through 20, 1999. The distance was officially recognized and accepted as a new world record by the editors and compilers of the Guinness Book of Records. The venture was carried out to demonstrate how far the EV can run in 24 hours by employing a rapid charging system and repetition of run and charging. An original target exceeding 2000 km was set in commemoration of the coming new millenium.

Certificate of World Records

Principal factors which supported the achievement of this world record were a manganese-lithium ion battery, a new product quickly rechargeable by using a large charging current and a reduction of running resistance of the vehicle. The lithium ion battery used in the run was developed through joint collaboration between Japan Storage Battery Co. and MMC and produced in December 1999. Special features of the battery is its smaller internal resistance and ability to accept a quite large charging current of 240 A.

A reduction in the vehicle's running resistance was mostly achieved by reducing the air resistance. Cd value was ultimately improved to 0.22 and the running distance was extended by about 200 km by this reduction.

Newly developed lithium ion battery

Performance of batteries installed on FTO-EV (at quick charge)

		Lithium ion battery	Nickel-metal hydride battery*	Lead acid battery*
Capacity	(kWh)	27	26	17
Max. charging current	(A)	240	100	240
Standard voltage	(V)	14.8 x 23	12 x 24	
Charging time	(hs)	1.2	3.3	1.5
Mass	(kN)	3.5	4.3	4.8

*Ref. data

After repeating a number of test runs by employing various different times and intervals of recharging and cruising speeds, an optimum condition was set at "cruise at 130 km/hr for 50 min. and charge for 20 min".

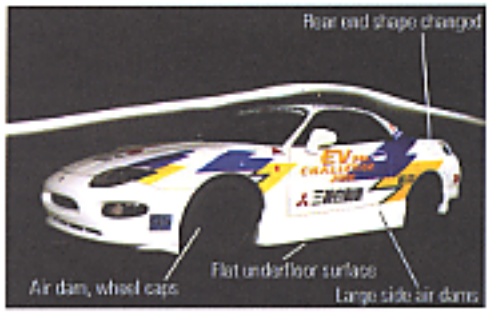

Improvement of aerodynamic performance

The final run of FTO-EV was commenced on December 19, 1999 on the oval test course at MMC's Car Research and Development Center in Okazaki city. This run finished early in the morning of the 20th after registering 2142 km by circling the course for 899 turns. The distance easily exceeded the existing world record of 1700 km, recorded in 1996.

The motor vehicle industry is required to introduce measures to protect the environment such as improved fuel economy, reduced exhaust gas emissions and others. At the same time the industry has to meet demands for the development of a new next generation power-train independent from the conventional internal combustion engine. One such power-train is the electric vehicle. We are convinced that development of a high performance electric vehicle will itself present an effective contribution to environmental protection. As such we are firmly determined to continue our research and study for enhancing and promoting the performance of electric motor vehicle.

* Electronics Engineering Dept., Car Research & Dev. Office

NEW PRODUCTS

New LANCER CEDIA and LANCER CEDIA WAGON

A new model of LANCER was introduced to the domestic market in May, 2000 with the sub-model name of CEDIA. It embodies "a spacious cabin, a sophisticated appearance and riding comfort", all features which will meet growing demands in the domestic car market. Although the CEDIA is one notch above ordinary popular small cars, it falls within the cost saving range of car registration category number 5. A sporty looking LANCER CEDIA WAGON was added to the line in November of the same year to enhance the line-up. All are mounted with GDI engines and INVECS-III CVT (continuously variable transmission) and are introduced as the forerunner of the GDI SIGMA series.

Fig. 1 LANCER CEDIA

Fig. 2 LANCER CEDIA WAGON

1. Target

As the life style of people changes, the number of those customers who demand high grade performance and comfortable riding even in sedans slated for the sale in the common mass market, is getting bigger and bigger. Those customers tend to strongly demand an improvement in spaciousness of a cabin along with sophisticated appearance of vehicles, yet an affordable price. To cope with such demands, we adopted the theme "a pleasant and high quality compact sedan" and the development work commenced with the following targets in mind.

- Sophisticated appearance exceeding the level of ordinary vehicles
- Roomy interior space
- Smooth running and improved fuel economy

Special features embodied in the sedan were applied to the wagon exactly in the form as they were. In addition to an assignment of sporty features to the wagon, an excellent cargo loading feature was incorporated.

The sedan version is principally targeted at the 40s and above age group who usually look for high quality and riding comfort, while the wagon is mainly designed to appeal to a younger generation made up of those in their 20s and 30s wanting an active touring wagon. Several configurations are offered in the wagon to satisfy a wider range of customers' needs.

2. Features

(1) Sophisticated appearance exceeding that of ordinary class vehicles

The vehicle has an attractive silhouette enhanced by a short overhang and long wheelbase. By placing large 4 lamp headlights and a grille consolidated with the engine hood, the front of the vehicle offers an exciting, sophisticated appearance. Rear combination lamps of the sedan are in a new sensual look, giving a feeling of transparency. The wagon features a distinctively longitudinal form well asserting its individualistic character. (Figs. 1 and 2)

An ornamental wood grain pattern giving a broader appearance to the dashboard, a center panel equipped with a large dial for handy operation of the air conditioner, meters of high contrast providing good visibility and large wraparound, comfortable seats, the furnishings normally appointed to a vehicle one grade above, are incorporated in the CEDIA. (Fig. 3)

(2) Roomy interior

By extending the wheelbase (additional 100 mm to the previous model) a rear section having plentiful excess room has resulted. Also the adoption of a forward deck has brought about a spacious cabin.

The seating position of occupants is raised, making it easier to get in and out of the vehicle. An upright seating position with a lower set dashboard and belt line will allow a wider view and provide a more relaxed feeling to the driver.

A large arm rest fitted to the sedan's rear seat is col-

lapsible and also offers access to the trunk compartment. A 6/4 splitting and retractable rear reclining seat in the wagon will add extra space to the baggage compartment.

(3) Smooth running and improved fuel economy

All vehicles are installed with GDI engines complying with the emission control regulations enforced in the year 2000 (12th year of Heisei in Japan) along with newly developed INVECS-III CVT and are capable of demonstrating smooth and safe running entirely free from gear shifting jerk. INVECS-III SPORTS MODE CVT with highly-sensitive 6-speed manual shift is fitted in the 1.8 L sporty model so a driver can enjoy quick response and extremely smoother gear shifting, not available with a conventional 4-speed automatic transmission.

Fig. 3

The front suspension is a combination of a strut type with flat frame crossmember and for the rear suspension, a long arm multilinkage system is adopted. Assisted by a wider tire tread, reduced friction and extended stroke rebound of the shock absorber, driving stability has been improved remarkably and flat and well-dampened cruising is now assured.

All vehicles are also equipped with the ABS (antilock brake system) and the EBD (electronically controlled braking force distribution system) which assure balanced and reliable braking.

(4) Safety and ecology

All vehicles incorporate MMC's unique collision safety reinforced body construction called "RISE" which will protect the occupants by greatly reducing offset collision and lateral impacts and possible impacts to their heads in case of an accident.

Needless to say, regarding the purification of exhaust emission gas, the combination of GDI and CVT has achieved compliance with the fuel economy standards to be enforced in Japan in 2010. It will also contribute to the reduction of CO_2 emission considerably.

3. Major specifications

The model configuration and main specifications are shown in the table below.

Specifications \ Model				LANCER CEDIA			LANCER CEDIA WAGON	
				GH-CS2A	GH-CS5A		GH-CS5W	
				MX, MX-E, MX-S	SE-G, SE-R	Touring	TS, EXCEED	Touring
				INVECS-III CVT		INVECS-III SPORTS MODE 6-CVT	INVECS-III CVT	INVECS-III SPORTS MODE 6-CVT
Seating capacity				5				
Dimensions	Overall length		(mm)	4,360	4,480		4,415	4,425
	Overall width		(mm)	1,695				
	Overall height		(mm)	1,430 (4WD: 1,435)			1,465 (4WD: 1,470)	
	Wheelbase		(mm)	2,600				
	Tread	Front	(mm)	1,470				
		Rear	(mm)	1,470				
	Minimum ground clearance		(mm)	150 (4WD: 155)				
Engine	Model			4G15	4G93			
	Displacement		(cc)	1,468	1,834			
	Valve mechanism, cylinders			DOHC 16 valves, 4 cylinders				
	Maximum output	(kW (PS)/min^{-1} Net)		74 (100)/6,000	96 (130)/6,000			
	Maximum torque	(Nm (kgf·m)/min^{-1} Net)		137 (14.0)/3,500	177 (18.0)/3,750			
	Fuel supply system			GDI (gasoline direct injection)				
Running equipment	Steering			Rack and pinion type (with power steering)				
	Suspension	Front		McPherson strut				
		Rear		Multi-link				
	Brakes	Front		Ventilated disc				
		Rear		Leading and trailing drum				
	Tires			175/70R14 (4WD: 185/65R14)	185/65R14	195/55R15	185/65R14	195/55R15

(Car Research & Dev./Marketing Headquaters: Tsujimura, Murasaki, Aiba)

NEW PRODUCTS

New LANCER EVOLUTION VII

LANCER EVOLUTION was originally introduced to the market in 1992 mainly to provide a basic model for participation in many motor sports events to begin with WRC. After being upgraded to EVOLUTION II and III through various modifications and refinements, the second generation models IV through VI were introduced and now finally the third generation LANCER EVOLUTION VII entered the market in February, 2001 as an outstanding machine truly worthy of commemorating the start of the 21st century.

1. Target

The target set up for the development of LANCER EVOLUTION VII was an attainment of further improvement of the vehicle's sporty performance by utilizing precious knowhow and technical data accumulated through participations in many past sports events and the creation of a super quality image, that of a high performing sporty sedan to represent a new generation.

2. Features

(1) New generation sedan of sophisticated appearance manifesting excellent quality and rugged high performance capability

Even though originally based on LANCER CEDIA, the completion of a totally new super-performing sedan which is packaged in a form manifesting a high quality as well as rugged capability was the objective of the development. The vehicle features multi-eyed headlamps and attractive rear combination lamps, a wide air inlet assuring abundant supply of cooling air, a large rear air spoiler implying an excellent aerodynamic performance and a consolidated blister fender suggesting smooth cruising. These all contribute to creating an image of harmony between the vehicle's high-performing function and a feeling of super quality.

The interior of vehicle has a sporty appearance through the use of well laid out instruments, a steering wheel designed and produced by MOMO, Recaro seats, exclusively for this vehicle and other fittings of advanced design.

(2) Vehicle in package emphasizing crisply responsive driving

The wheelbase has been lengthened by 115 mm and the front tread width by 5 mm and the rear by 10 mm over and above former LANCER EVOLUTION specifications to assure a higher level driving stability. The driving height is 30 mm lower than that of LANCER CEDIA, resulting in a lower center of gravity.

(3) MMC's unique control on all wheels

The vehicle's dynamics will always be maintained in the best condition by efficient control of all four wheels through the introduction of a new full-time advanced 4WD system developed by MMC. An ACD (active center differential) consisting of an electronically controlled multiplate hydraulic clutch as an alternative to the VCU type limited differential system and a finely tuned AYC make up this 4WD system. It maintains optimum control in all driving conditions including acceleration, deceleration, cornering, etc. In addition to the EBD system which controls distribution of braking power to the front and rear wheels, a new sports type ABS is installed to optimally suit prevailing driving conditions. This unit when activated will control brake power distribution to left and right wheels to maintain braking stability when a vehicle is in a cornering operation and in other situations. These new 4WD controls along with improved braking work together to optimize the vehicle dynamics in acceleration, deceleration and cornering.

(4) Refined motive power and underbody structure

The proven and extensively used 2 L DOHC turbocharged engine was chosen for the vehicle. The max-

imum torque was increased by modifying the characteristics of the turbocharger and an output in the range between 3,000 to 6,000 rpm has been attained, outstanding in this class.

Suspension in its original form has been retained in the vehicle. However, critical cornering performance and maneuverability are much more enhanced by modifications to the front frame crossmember resulting in greater rigidity and by increasing bouncing stroke by 15 mm in front and 10 mm in the rear. The size of tire has been increased from 225/45ZR17 to 235/45ZR17 and this in coordination with the suspension characteristics provides excellent vehicular performance, critical for safe driving.

(5) Carefully applied weight reduction and highly rigid body structure

The introduction of an aluminum engine hood and front fenders and adoption of this metal for various chassis component parts have brought about a reduction in vehicle weight. Further reduction has been achieved by using magnesium for the rocker cover, adopting a hollow camshaft, reducing weight of engine component parts and using aluminum engine brackets.

For increased body rigidity against torsion and bending special reinforcement has been applied throughout.

(6) Excellent cooling effect supporting high performance

An intercooler spray system which automatically injects a coolant in an engine depending on vehicle's cruising condition, large oil cooler and intercooler and a large front under-cover devised for cooling of brakes and the drivetrain system as well as reduced lift are equipped to provide a better cooling effect and maintain a high performance even under severe cruising conditions.

3. Major specifications

Major specifications are shown in the following table.

Specifications \ Model				LANCER EVOLUTION VII
				Mitsubishi GH-CT9A
				Full time 4WD
				5 M/T
Seating capacity				5
Dimensions	Overall length		(mm)	4,455
	Overall width		(mm)	1,770
	Overall height		(mm)	1,450
	Wheelbase		(mm)	2,625
	Tread	Front	(mm)	1,515 (GSR)/1,500 (RS)
		Rear	(mm)	1,515 (GSR)/1,500 (RS)
	Minimum ground clearance		(mm)	140 (When equipped with brake cooling air guide: 110)
Engine	Model			4G63 turbocharger
	Displacement		(cc)	1,997
	Valve mechanism, cylinders			DOHC 16 valves, 4-cylinder
	Maximum output		(kW (PS)/min^{-1} Net)	206 (280)/6,500
	Maximum torque		(Nm (kgf·m)/min^{-1} Net)	383 (39.0)/3,500
	Fuel supply system			ECI-MULTI (Electronically controlled fuel injection)
Running equipment	Steering			Rack and pinion type (with power steering)
	Suspension	Front		MacPherson strut
		Rear		Multi-link
	Brakes	Front		Ventilated disc (17 in. (GSR)/15 in. (RS))
		Rear		Ventilated disc (16 in. (GSR)/15 in. (RS))
	Tires			235/45ZR17 (GSR)/205/65R15 (RS)

(Car Research & Dev./Marketing Headquarters: Fujii, Yamamoto, Ueyanagi)

NEW PRODUCTS

6M7 Series Diesel Engine for Heavy-Duty Trucks and Buses

Due to the fast growing environmental concern worldwide, there is an urgent need for a ready supply of diesel engines delivering smaller exhaust emission gas and lower noise level. Diesel engines have been extensively used on trucks and buses mainly because of their superior thermal efficiency, but now there is a growing demand by fleet operators for a reduction in fuel consumption to help reduce their operating costs as well as allow them to play a part in the prevention of global warming.

Placing these demands foremost, MMC developed a new series of diesel engine, the 6M7, for use on heavy-duty trucks and buses. These engines employ a new basic structure and advanced technologies applied to each individual section. The engine first appeared in February, 2000 in the SUPER GREAT 2000 model. Following this it was mounted on AEROSTAR, a large city transit-type bus and marketing began in May. Finally, the 6M70T5 turbocharged engine appeared on a fuel-efficient high-speed truck tractor for semitrailers in September of the same year.

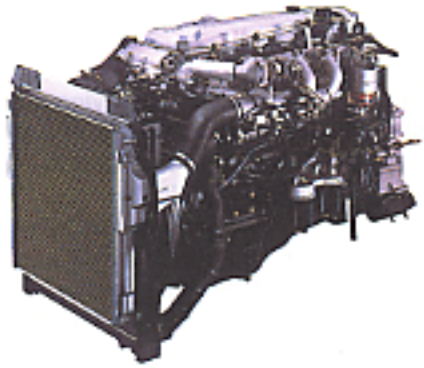

6M70T

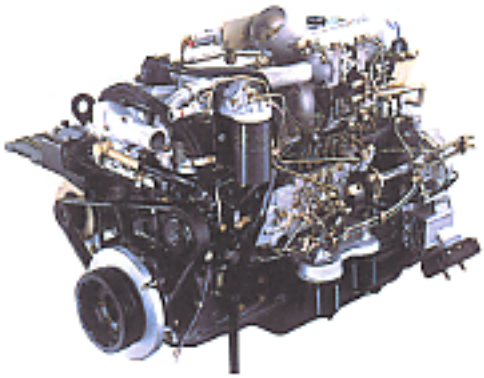

6M70

1. Target

The development targets for the 6M7 series engine were set for the attainment of lower exhaust emission as required in diesel engines of the next generation, reduced fuel consumption, enhanced reliability, larger output power, lower noise level, and significant weight reduction. In addition to the above, the realization of a harmonious balance of engine and vehicle characteristics was added to the target for improvement in drivability and auxiliary brake performance.

2. Features

(1) Performance and exhaust emission gas

While the initial model had already cleared the exhaust emission gas regulations enforced in the 11th year of Heisei (1999) by the adoption of a full electronic control high pressure fuel injection system, EGR system and VG (variable geometry) turbocharger, the latest model boasts an increase in output power and torque of 5 to 20 % and reduced fuel consumption of 2 to 5 %. In order to economize fuel consumption and enhance the torque of 6M70T5 engine, the mean effective cylinder pressure at a torque point was raised up to 2,160 Nm, the largest value current in Japan. When the engine is combined with INOMAT (mechanical automatic transmission), a further big reduction in fuel consumption in a range of 7.5 to 11.5 % during high speed operation is possible.

(2) Fuel and injection system

A full electronic pre-stroke control type fuel injection

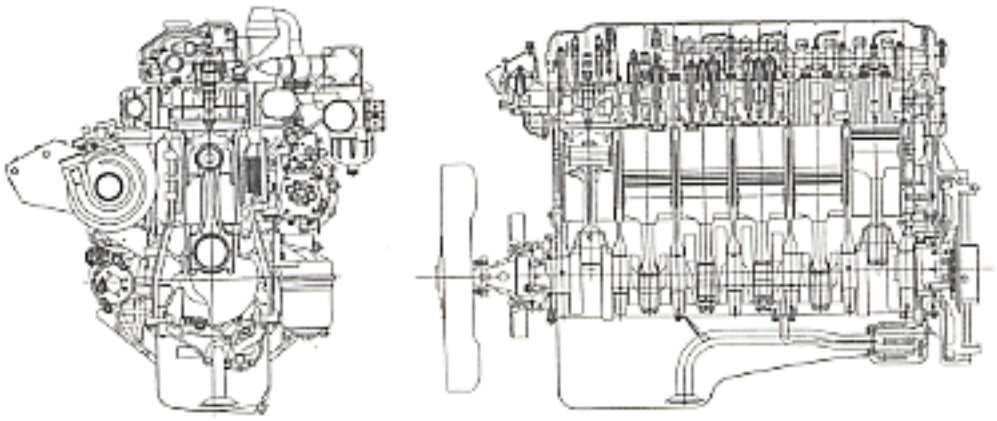

Sectional views of 6M70T engine

pump is mounted on non-supercharged engines and output of black smoke has been substantially reduced by using high injection pressure attained by minimizing the hole size of the injector as well as modifying the shape of the combustion chamber.

A common rail type fuel injection system is applied to turbocharged engines and in combination with MIQCS (Mitsubishi Innovative Quiescent Combustion System), a combustion system where fuel and air are optimally mixed by means of the coherent energy carried by injected fuel, less exhaust gas emission and reduced fuel consumption result.

(3) Structure of valve drive and main movement systems

Weight reduction is achieved by an adoption of an OHC 4 valve mechanism and an assembled type camshaft. Lobes on the camshaft are made of sintered metal for maximum resistance against severe abrasion. Reduction of friction in the system is attained by the adoption of a rocker arm fitted with double rollers.

In order to enhance resistance to very high pressures created in the cylinders of the 6M70T5 engine, reinforcements of major parts directly associated with combustion and cycling have been carried out, such as high pressure forging of the FRM pistons with built-in pin bushing, plus rolling processing applied to the curve of the crankshaft fillet, heightening the rigidity of the connecting rods, and adopting a bearing metal of strong resistance to high pressure.

(4) EGR system by electronic control

An electronically-controlled EGR system is fitted to all engines to achieve reduction of NOx gas and fuel consumption in an extremely practical way.

An intake air choke control system is attached to non-turbocharged engines for optimum control of the flow in the EGR system. An EGR, controlled by the nozzle vane of the VG turbo, a unique system developed by MMC, is installed on turbocharged engines with the EGR functioning when the vehicle is operating under a heavy load. This has resulted in normally hard to attain performance in which NOx gas is reduced satisfactorily, with little black smoke produced, plus greater fuel economy.

(5) Engine brake system

A new type powertard brake system is built in the cylinder head to act as an auxiliary brake system. Pressure in the powertard system is increased through turbocharging, supplemented by energy from released compression pressure and then recovered by the VG turbo system to increase the braking force.

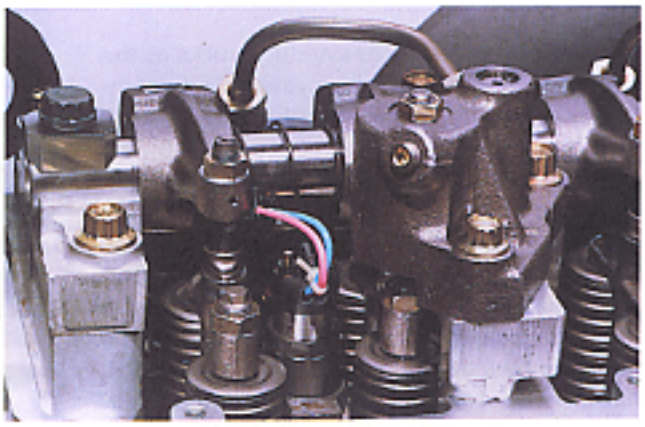

New powertard system

A braking force greatly exceeding that when using conventional exhaust brake systems is now possible with this new system.

(6) Low noise level

Reduction of noise levels by 1 dB(A) during idling and by 2 dB(A) during normal operation has been realized. This was achieved by adding reinforcement to the crankcase skirt, improving precision of the timing gear system, adopting a floating system for the rocker cover and air intake manifold and applying optimum tuning to the fuel injection system for such items as injection pressure, timing and pilot injection.

(7) Weight reduction

A reduction of weight by 65 kg from that of the 6D40 engine has been achieved by a thorough review on the total structure and the decision to adopt OHC construction, shortened crankcase length, consolidated cylinder head, a new powertard system, and the use of a thinner cylinder head gasket.

3. Major specifications

Major specifications are shown in the following table.

Specifications \ Model		Non-turbocharged	Turbocharged with intercooler				
		6M70	6M70T1	6M70T2	6M70T3	6M70T4	6M70T5
Type		Diesel 4 cycle					
No. of cylinders		6					
Combustion chamber type		Direct injection type					
Valve mechanism		OHC 4 valves (two intake valves and two exhaust valves)					
I.D. x stroke	(mm)	φ135 x 150					
Total displacement	(L)	12.882					
Compression ratio		19.5	17.5				
Intake system		Natural aspiration	VG turbocharged (with intercooler)				
Maximum output	(kW/min^{-1})	184/2,200	235/2,200	257/2,200	279/2,200	302/2,200	
Maximum torque	(Nm/min^{-1})	883/1,400	1,275/1,200	1,520/1,200	1,618/1,200	1,765/1,200	2,160/1,200
Injection system		Prestroke controlled	Common rail				

(Engine Design Dept., Truck & Bus Div. Office: Okada)

2001 Year Model Heavy-Duty Truck "SUPER GREAT"

The role played by heavy-duty trucks as the core of freight distribution systems is becoming increasingly larger. SUPER GREAT 2000 year model introduced in February, 2000 with minor modifications has already gained favorable acceptance by many fleet operators because of its superb merchantability. It is now taking a leading position in the domestic market. The vehicle is built with a short cabin for maximum exploitation of loading space and powered by a V8 non-supercharged engine. It has a short turning radius ideal for tight cornering, a feature particularly necessary for special purpose vehicles such as dump trucks, concrete mixer trucks, tank lorries, etc. Effective with 2001 year model introduced in February, 2001 a large and powerful 6M70T 6 cylinder in-line turbocharged engine is added to the SUPER GREAT series. It is a short cabin model providing a high loading capability, as well as retaining special characteristics of low fuel consumption and operation efficiency with plenty of power reserve.

1. Target

The reason behind the development of SUPER GREAT 2000 year model was to create variations which will contribute greatly to fleet operators engaged in regular long distance haulage who are eager to reduce their operating costs particularly by taking advantage of the following features.

- Larger loading space and capacity
- High output power and low fuel consumption which can be rated highest among competitive models.

2. Features

(1) Longer cargo platform and larger cargo carrying capacity among vehicles in the same class

In order to create a vehicle with a longest cargo body now available in Japan, where an overall length of truck is legally limited to 12 m, a cabin shortened by 350 mm from the standard by sacrificing driver's berth space first introduced in the 2000 year model was carried over to this vehicle. To eliminate a bulge at the rear of the cabin, an engine of shorter length is installed further ahead. The cabin has been raised up to furnish installation space for the engine in the new position. As the result of these modifications, the longest van body available (10,075 mm) is now possible. This body can accommodate 18 fully loaded T11 pallets, the type most popular now in Japan, stacked in 9 rows, offering one row more than possible in conventional standard van bodies. The loading capacity has also been expanded by an increase in the interior height gained by minimizing the protrusion of exhaust pipe and transmission above the top chassis frame. The platform height above ground of the FS 4-axle low platform truck, a vehicle produced to meet special demands for a larger load capacity, is further lowered by changing the engine installation angle and resultantly, a van body with a 2,750 mm interior height can be fitted. Therefore, a vehicle with a 67 cubic meter capacity van body, the largest available in Japan at present, can now be provided. In order to retain ample space between the snorkel duct and a corner post located in the front of a winged-type van body, a type most popularly used by local transportation operators, the duct has been relocated to the inside and as a result, a body length of 10,030 mm, the longest available in Japan, is now possible. Any increase of chassis weight of this vehicle is curtailed by a reduction of cabin length and shortening of wheelbase (for FS and FU trucks) and a load of a weight equivalent to that which can be handled by a vehicle fitted with a standard size cabin can be hauled. The front end of loading platform has been moved forward reducing the burden on the rear wheels. This change allows the vehicle to carry an additional 500 kg load over a standard vehicle.

(2) High output power and low fuel consumption engine (6M70T)

There are 5 varieties in the 6M70T engine series and 3 types of engine, delivering 320, 350 and 380 PS respectively which can be fitted, making the vehicle the most powerful in the class. Major engine components such as the MIQCS combustion system, common rail, EGR, etc. are exactly the same as 2000 year model; however, the overall length of the engine is shortened by 84 mm by the use of a shorter fan coupling and minimized gap between the radiator and intercooler. The power steering pump mounted on the rear end of engine has been shifted to almost completely eliminate the protrusion above the upper level of the chassis frame.

(3) Cabin appearance

To cover a gap created by the raising up of the cabin, a new lower grille has been fitted to the chassis frame. The Three Diamond trade mark normally fitted to the front panel of the cabin has now been relocated to the new grille. Another climbing step has been added in concordance with the higher cabin position and the front fender wheel arch has been extended accordingly. Headlamps are now positioned to the

lower grille to comply with the traffic regulations regarding their height above ground.

Despite the fact that the shortened cabin format introduced with 2000 year model has been carried over to the new model, it now has a more refined style, with its rounded cube look, giving a more powerful and rugged appearance appropriate to a heavy-duty truck.

(4) Excellent comfort

The high driving position created by the raising up of the cabin will provide the driver a much broader and wider view and allow accurate observation of the surrounding situation and, therefore, he will be able to endure a prolonged driving with a more relaxed mental condition. Riding comfort of 2000 year model has been carried over to the new vehicle by the employment of the cabin and chassis suspension system developed and built for that model. Interior appointments in the cabin are like those found in the 2000 year model, including a highly functional air conditioning unit and audio set. A very quiet ambience just like in a passenger car is ensured in the cabin. Seating in 2000 year model was arranged mainly for local short runs. However, to provide more comfort to a driver engaged in prolonged driving, an arm rest, lumbar support and longitudinal seat sliding mechanism have been added. A seat which can be slid forward up to 180 mm is installed just as in a standard size cabin. The seatback can be reclined up to 45 degrees when the seat is slid to the most forward position. The front side of the headrestraint has been flattened to give a better feeling.

A wire transmission control system has been fitted to the vehicle because the installation of a linkage type control was not feasible due to limited space in the cabin. But a gear shift feeling equal to or even better than that of the system used in a standard cabin has been attained through reduced friction resistance of the control wire and the addition of a counterweight for good balancing.

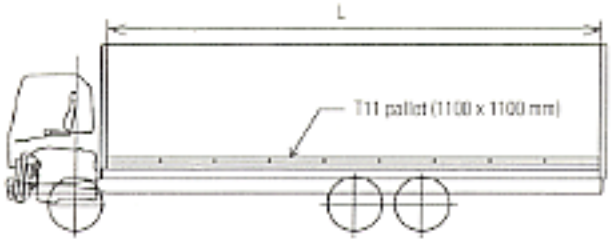

Table 1 Comparison of loadable pallets

	Short cab vehicle	Standard cab vehicle
Body internal length (Max)	10,075 mm	9,600 mm
Number of loadable pallets	9 x 2 = 18	8 x 2 = 16

(5) Variations of vehicle

Model variations of vehicles mounted with the short cabin and powered by the 6 cylinder in-line engine are increased in number this time to include FS, FT and FU series cargo trucks of longer overall length mostly used in regular long distance haulage. An air suspension system for the rear wheels, which has become quite popular recently, is now available for FS and FT series trucks. Air suspension on all wheels, as available for the 2000 year model, can be applied to vehicles for fleet operators having a need for low loading platform trucks which will improve the quality of transportation and offer trouble-free loading. An INOMAT system (mechanical automatic transmission), a unit enjoying a fast growing market, is now available as an option on all trucks of the 25 ton GVW rating. These technically advanced systems, being promoted by MMC, are finding considerable acceptance in these model variations.

3. Major specifications

The model configurations and main specifications are shown in the table below.

Specifications \ Model				Leaf spring suspension type cargo truck, 6 x 2, front tandem axle	Air suspension type cargo truck, 6 x 2, rear tandem axle	Cargo truck, low deck, 8 x 4	
						Air suspension type	All axles air suspended
				FT50JVX2S	FU54JYZ3S	FS54JUZ3S	FS55JUZ3S
Dimensions	Overall length		(mm)	11,990			
	Overall width		(mm)	2,490			
	Overall height		(mm)	3,100	3,080	2,960	2,930
	Wheelbase		(mm)	7,550	7,100	7,300	
	Tread	Front	(mm)	2,050		2,060	
		Rear	(mm)	1,845		1,855	
Weight	Vehicle weight		(kg)	8,040	8,530	8,630	8,800
	Minimum payload		(kg)	11,700	16,200	16,100	15,900
	Gross vehicle weight		(kg)	19,850	24,840		24,810
Engine	Model			6M70T2	6M70T3		
	Displacement		(L)	12.882			
	Maximum output		(kW [PS]/min^{-1} Net)	257 (350)/2,200	279 (380)/2,200		
	Maximum torque		(N·m {kgf·m}/min^{-1} Net)	1,520 (155)/1,200	1,618 (165)/1,200		
Running equipment	Suspension	Front		Long tapered leaf springs			Air spring
		Rear		Long tapered leaf springs	Air spring		
	Brakes			Wedge type, fully air-controlled drum brakes			
	Tires	Front		11R22.5-14PR	295/80R22.5	245/70R19.5	
		Rear		11R22.5-14PR		245/70R19.5	

(Vehicle Dev. Design Dept., Truck & Bus Dev. Office: Yoshikawa, Noguchi)

NEW PRODUCTS

Medium-Size City Bus "AERO NOSTEP MIDI"

The "AERO MIDI ONE STEP", a low floor transit type medium size bus, which was originally put in the market in July, 1999 has already acquired very favorable acceptance among many fleet operators, likely helped by the trend currently taking place in the public transport business of downsizing from large to medium size buses as well as the introduction of bus services operated by community groups.

With an awareness of the impending increase of aged people in the society and in order to comply with the newly introduced "barrier free" public vehicle legislation enacted in November, 2000, the "AERO NOSTEP MIDI" bus was built and introduced in December, 2000. The bus is built with a floor set at a lower level than the ONE STEP model, so there is virtually no stepping up or down required by passengers when entering or exiting the vehicle at a bus stop. The aim of development and special features of this new bus are described in the following.

1. Target

In order to create an ideal medium non-step bus, the following targets were set for its development.

(1) An interior space offering an open feeling through the use of a lower floor and the provision of a wide space in the non-step zones.

(2) Easy entry and exit for passengers by lowering floor level while maintaining running through performance appropriate for transit type operation, and insurance of good turning-circle characteristics.

(3) Compliance with the "barrier free" public vehicle legislation.

2. Features

(1) Low floor

The floor height above ground in the 7 m long conventional one-step medium transit bus MJ with a transversely mounted engine, "T drive" and the 9 m long MK with longitudinally mounted engine is 530 mm. On the other hand, the floor height above ground of the AERO NOSTEP MIDI bus at the front entrance door is 340 mm and the step height is 300 mm. The non-step construction of the floor between the front and middle doors is accomplished by using a center drop type front axle of new design and a 5-link air suspension system in front and for the rear, a trailing arm type air suspension, a system extensively used on MMC's medium sightseeing type buses, but modified to suit transit type operation. Thanks to the installation of air suspension, vibration and noise of the vehicle are dampened remarkably. A kneeling system which will lower the vehicle height by discharging air from the bellows of the air suspension system is fitted to all 4 wheels as standard equipment. With this system the height of the entrance and exit level can be lowered by 50 mm (the ground clearance by 250 mm).

(2) Basic layout

In order to secure a broader non-step floor space, engines are mounted transversely in vehicles of both the two wheelbase categories namely, F (overall length of 7 m), and L (overall length of 9 m) and are coupled with "T drive", a system well proven in conventional MJ buses. The rear overhang of the body is shortened by this arrangement. The difference between the F and L models lies simply in the wheelbase. The layout of the body and the equipment mounted on the underside of the front and rear body overhang sections is identical in these two models.

The wheelbase of the L model is 5,260 mm, a dimension which has never been seen in a medium-size bus before and, therefore, the steering angle is widened and, as a result, the width of the area occupied on a road during a 90 degree turn is now almost identical with that required by an MK transit bus of 9 m overall length. Consequently, satisfactory turning-circle characteristics have been attained.

(3) Interior layout

To furnish a bright and open space in the inside, the cabin height is now increased to 2,285 mm by lowering the floor level by 85 mm while retaining the ceiling height of a one-step bus. Side windows are also widened vertically by 210 mm in the downward direction in balance with the lowered floor.

Since the body overhang of F model is the same as that of the L model, the front door opening is now widened by 90 mm to 695 mm which is greater than that of the MJ one-step bus. The width of the middle door of the L model has been increased to 1,005 mm, the

same as that of MMC's large transit buses, allowing a wider space for entry and exit of passengers.

Taking an advantage of the long wheelbase and spacious non-step floor (the most spacious among medium size buses), the seat layout is arranged to accommodate a maximum permissible number of seated and standing passengers in this space.

In order to eliminate equipment mounted under the seats in the non-step area of both F and L models, direct drive air conditioning units are now installed on the roof. All 6 air reservoirs for brake and air suspension systems are now situated in the front and rear body overhang sections.

(4) Functional improvement

The body skelton and frame structure construction has been modified to create the non-step floor. Additional reinforcement has been given to the body construction resulting in remarkably improved rigidity and reliability.

Although general concern exists over possible deterioration in running through performance in a low floor bus because of its body construction, this bus, even under a fully loaded condition, will have running through performance which is equal to or even better than that of the MK one-step because of the following: Installation of fuel tank and batteries to a mid-wheelbase section, with structural components specially produced for such purpose, a shortening of body front overhang and a provision of body lifting mechanism, as standard equipment by which a body can be lifted up by 50 mm when the gear is shifted to 1st or reverse position.

A 6M61-3 diesel engine which has been certified in compliance with the exhaust emission regulations, enforced in 1988, is installed in this bus just as in the MK model. An "Idling stop and start system" (ISS) is equipped as standard equipment and will contribute to a further reduction of emission gas.

A "Finger-touch control" 5-speed transmission is installed as standard equipment, but a 5-speed automatic transmission is also available as an option for those people who may prefer easy driving.

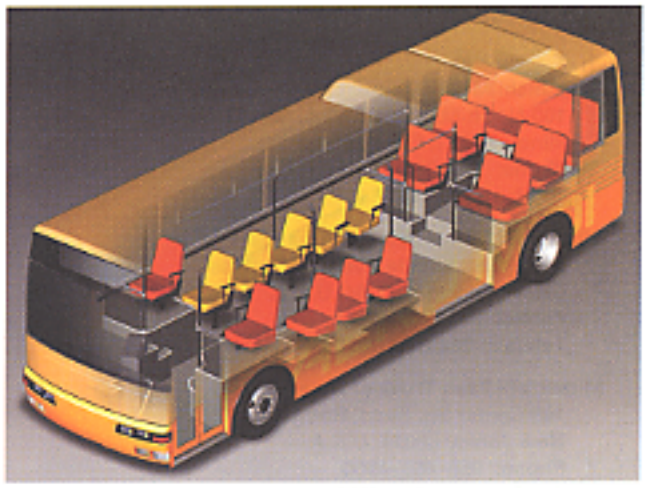

(5) Facilities to cope with "Barrier Free" public vehicle legislation

Facilities provided on the bus for complying with the new "Barrier Free" public vehicle legislation are as follows.

- A retractable board for loading and unloading a person on a wheel chair is provided for the middle door.
- A mechanism to fasten a wheelchair is provided on the floor. (Just for one wheel chair only)
- A space for stowage of a wheelchair is reserved with a mark indicated by a sticker label.
- A public address system for an announcement of bus stop and a LED type display system indicating the coming bus stop.
- A vertical steel stanchion for passenger's grip is fitted to each seat every 3rd row.

3. Major specifications

Major specifications are shown in the following table.

Specifications \ Model				MJ26HF (NLF) L model (overall length 9 m class)	MJ26HF (NFF) F model (overall length 7 m class)
Rated riding capacity (Seated passengers + standing passengers + driver)				61 (23 + 37 + 1)	45 (19 + 25 + 1)
Dimensions	Overall length		(mm)	8,690	6,990
	Overall width		(mm)	2,300	
	Overall height		(mm)	2,900	2,990
	Wheelbase		(mm)	5,250	3,560
	Tread	Front	(mm)	1,915	
		Rear	(mm)	1,665	
	Minimum turning radius		(m)	8.0	5.6
	Width of area occupied on road during a 90 degree turn		(m)	5.3	4.5
	Minimum ground clearance		(mm)	150	
Engine	Model			6M61-3	
	Total displacement		(L)	8.2	
	Maximum output		(kW (PS)/min^{-1} Net)	165 (225)/2,900	
	Maximum torque		(Nm (kgf m)/min^{-1} Net)	588 (60)/1,700	
Running equipment	Steering			Ball and nut type integral power steering	
	Suspension	Front		Axle type air suspension	
		Rear		Axle type air suspension	
	Brakes	Front/rear		Dual airover hydraulic	
	Tires	Front/rear		245/70R19.5	

(Vehicle Dev. & Design Dept., Truck & Bus Dev. Office: Takaoka, Yamaguchi)

INTERNATIONAL NETWORK

Mitsubishi Motor Manufacturing of America, Inc.
100 North Mitsubishi Motorway, Normal
Illinois 61761, U.S.A.
Phone: 309-888-8000
Telefax: 309-888-8154

Mitsubishi Motor Sales of America, Inc.
6400 West Katella Avenue, Cypress
California 90630-0064, U.S.A.
Phone: 714-372-6000
Telefax: 714-373-1020

Mitsubishi Fuso Truck of America, Inc.
100 Center Sq. Road, Bridgeport
New Jersey 08014, U.S.A.
Phone: 856-467-4500
Telefax: 856-467-4695

Mitsubishi Motors America, Inc.
6400 West Katella Avenue, Cypress
California 90630-0064, U.S.A
Phone: 714-372-6000
Telefax: 714-373-1020

Mitsubishi Motors R & D of America, Inc.
3735 Varsity Drive Ann Arbor
MI 48108, U.S.A.
Phone: 734-971-0900
Telefax: 734-971-0901

Mitsubishi Motor Sales of Caribbean, Inc.
Carretera No. 2, Km 20.1 Barrio
Candelaria Toa Baja, PUERTO RICO
Phone: 787-251-8715
Telefax: 787-251-8700

Netherlands Car B.V.
Dr. Hub van Doorneweg 1,
6121 RD Born, THE NETHERLANDS
Phone: 31-46-489-5316
Telefax: 31-46-489-5488

Mitsubishi Motors Europe B.V.
Douglassingel 1
1119 MB Schiphol-Rijk
THE NETHERLANDS
Phone: 31-20-4468111
Telefax: 31-20-4468741

Mitsubishi Trucks Europe - Sociedade
Europeia de Automoveis, S.A.
Apartado 7, 2206-906 Tramagal, PORTUGAL
Phone: 241-899800
Telefax: 241-899877

Mitsubishi Motor Sales Europe B.V.
Douglassingel 1
1119 MB Schiphol-Rijk
THE NETHERLANDS
Phone: 31-20-4468111
Telefax: 31-20-4468135

Mitsubishi Motors Sales Nederland B.V.
Diamantlaan 29
2132 WV Hoofddorp, THE NETHERLANDS
Phone: 31-23-5555222
Telefax: 31-23-5540620

Mitsubishi Motor Sales Sweden AB
Box 8144 s-163 08 Spanga, SWEDEN
Phone: 46-8-474-5400
Telefax: 46-8-621-1794

MMC Automotive Espana S.A.
Trvesia de Costa Brava no. 6-5a planta
28034 Madrid, SPAIN
Phone: 34-91-3877400
Telefax: 34-91-3877458

Mitsubishi Motor Marketing Research Europe GmbH
Schieferstein 11A
65439 Floersheim/Main
GERMANY
Phone: 49-6145-808-00
Telefax: 49-6145-808-164

Mitsubishi Motor R & D Europe GmbH
Diamant-strass
D-65468 Trebur
GERMANY
Phone: 49-6147-9141-0
Telefax: 49-6147-3312

Mitsubishi Motor Sales Danmark A.S.
Provestensvej 50 DK 3000
Helsingor, DENMARK
Phone: 45-4926-6700
Telefax: 45-4926-6767

Mitsubishi Motors de Portugal, S.A.
Povos 2600-997 Vila Franca de Xira codex,
PORTUGAL
Phone: 351-263-286100
Telefax: 351-263-286232

Mitsubishi Motors Australia, Ltd.
1284 South Road, Clovelly Park
South Australia, 5042, AUSTRALIA
Phone: 8-8275-7111
Telefax: 8-8275-6841

Mitsubishi Motors New Zealand, Ltd.
Private Bag, 50914, Porirua, NEW ZEALAND
Phone: 4-237-0109
Telefax: 4-237-4495

MMC Sittipol Company, Ltd.
69-69/1-3 Mu 11 Phaholyothin Road,
Tambol Klongneung, Ampur Klongluang,
Phathumthanee, 12120, THAILAND
Phone: 2-908-8000
Telefax: 2-908-8280

Mitsubishi Motors Philippines Corporation
Ortigas Avenue Extention,
Cainta, Rizal, Manila, PHILIPPINES
Phone: 2-658-0109
Telefax: 2-658-0006

P.T. Mitsubishi Krama Yudha Motors and Manufacturing
Petukangan 3, J1 Raya Bekasi
Km-21 Pulo Gadung, Jakarta Timur
Jakarta, INDONESIA
Phone: 021-460-2908
Telefax: 021-460-2915

MITSUBISHI MOTORS CORPORATION

- **Head Office**
  33-8, Shiba 5-chome, Minato-ku, Tokyo 108-8410, Japan
  Phone: +81-3-3456-1111
  Telefax: +81-3-5232-7731
  Telex: J26639, J26839

- **Design Center**
  Tama Design Center
  1-16-1, Karakida, Tama-shi, Tokyo 206-0035, Japan
  Phone: +81-423-89-7307

- **Engineering Offices**
  Car Research & Development Office
  1, Nakashinkiri, Hashime-cho, Okazaki-shi, Aichi Pref. 444-8501, Japan
  Phone: +81-564-31-3100
  (Tokachi Proving Ground)
  22-1, Osarushi, Otofuke-cho, Kato-gun, Hokkaido 080-0271, Japan
  Phone: +81-155-32-7111
  Truck & Bus Development Office
  10, Ohkura-cho, Nakahara-ku, Kawasaki-shi 211-8522, Japan
  Phone: +81-44-587-2000
  (Kitsuregawa Proving Ground)
  4300, Washijuku, Kitsuregawa-machi, Shioya-gun, Tochigi Pref. 329-1411, Japan
  Phone: +81-28-686-4711

- **Plants**
  Nagoya Plant
  (Nagoya Plant - Oye)
  2, Oye-cho, Minato-ku, Nagoya-shi, Aichi Pref. 455-8501, Japan
  Phone: +81-52-611-9100
  (Nagoya Plant - Okazaki)
  1, Nakashinkiri, Hashime-cho, Okazaki-shi, Aichi Pref. 444-8501, Japan
  Phone: +81-564-31-3100
  Kyoto Plant
  (Kyoto Plant - Kyoto)
  1, Uzumasa Tatsumi-cho, Ukyo-ku, Kyoto-shi 616-8501, Japan
  Phone: +81-75-864-6000
  (Kyoto Plant - Shiga)
  2-1, Kosunacho, Kosei-cho, Koga-gun, Shiga Pref. 520-3212, Japan
  Phone: +81-748-75-3131
  Mizushima Plant
  1-1, Mizushima Kaigandori, Kurashiki-shi, Okayama Pref. 712-8501, Japan
  Phone: +81-86-444-4114
  Tokyo Plant
  (Tokyo Plant - Kawasaki)
  10, Ohkura-cho, Nakahara-ku, Kawasaki-shi 211-8522, Japan
  Phone: +81-44-587-2000
  (Tokyo Plant - Nakatsu)
  4001, Nakatsu Aza Sakuradai, Aikawa-cho, Aikou-gun, Kanagawa Pref. 243-0303, Japan
  Phone: +81-462-86-8111

Printed in Japan

MITSUBISHI MOTORS CORPORATION
TOKYO, JAPAN

ISSN 0915-3802